2015

INKJET PRINTING: FACING CHALLENGES AND ITS NEW APPLICATIONS IN COATING INDUSTRY

Sadegh Poozesh
University of Kentucky, sadegh.poozesh@gmail.com

STUDENT AGREEMENT:

I represent that my thesis or dissertation and abstract are my original work. Proper attribution has been given to all outside sources. I understand that I am solely responsible for obtaining any needed copyright permissions. I have obtained needed written permission statement(s) from the owner(s) of each third-party copyrighted matter to be included in my work, allowing electronic distribution (if such use is not permitted by the fair use doctrine) which will be submitted to UKnowledge as Additional File.

I hereby grant to The University of Kentucky and its agents the irrevocable, non-exclusive, and royalty-free license to archive and make accessible my work in whole or in part in all forms of media, now or hereafter known. I agree that the document mentioned above may be made available immediately for worldwide access unless an embargo applies.

I retain all other ownership rights to the copyright of my work. I also retain the right to use in future works (such as articles or books) all or part of my work. I understand that I am free to register the copyright to my work.

REVIEW, APPROVAL AND ACCEPTANCE

The document mentioned above has been reviewed and accepted by the student's advisor, on behalf of the advisory committee, and by the Director of Graduate Studies (DGS), on behalf of the program; we verify that this is the final, approved version of the student's thesis including all changes required by the advisory committee. The undersigned agree to abide by the statements above.

Sadegh Poozesh, Student

Dr. Kozo Saito, Major Professor

Dr. Haluk E. Karaca, Director of Graduate Studies

INKJET PRINTING: FACING CHALLENGES AND ITS NEW APPLICATIONS IN COATING INDUSTRY

DISSERTATION

A dissertation submitted in partial fulfillment of the requirements for the degree of Doctor of Philosophy in the College of Engineering at the University of Kentucky

By

Sadegh Poozesh

Lexington, Kentucky

Co-Directors: Dr. Kozo Saito, Professor of

and Dr. Nelson Akafuah, Assistant Research Professor of

Mechanical Engineering

Lexington, Kentucky

2015

ABSTRACT OF DISSERTATION

INKJET PRINTING: FACING CHALLENGES AND ITS NEW APPLICATIONS IN COATING INDUSTRY

This study is devoted to some of the most important issues for advancing inkjet printing for possible application in the coating industry with a focus on piezoelectric droplet on demand (DOD) inkjet technology. Current problems, as embodied in liquid filament breakup along with satellite droplet formation and reduction in droplet sizes, are discussed and then potential solutions identified. For satellite droplets, it is shown that liquid filament break-up behavior can be predicted by using a combination of two pi-numbers, including the Weber number, *We* and the Ohnesorge number, *Oh*, or the Reynolds number, *Re*, and the Weber number, *We*. All of these are dependent only on the ejected liquid properties and the velocity waveform at the print-head inlet. These new criteria are shown to have merit in comparison to currently used criteria for identifying filament physical features such as length and diameter that control the formation of subsequent droplets. In addition, this study performs scaling analyses for the design and operation of inkjet printing heads. Because droplet sizes from inkjet nozzles are typically on the order of nozzle dimensions, a numerical simulation is carried out to provide insight into how to reduce droplet sizes by employing a novel input waveform impressed on the print-head liquid inflow without changing the nozzle geometry. A regime map for characterizing the generation of small droplets based on *We* and a non-dimensional frequency, Ω is proposed and discussed. In an attempt to advance inkjet printing technology for coating purposes, a prototype was designed and then tested numerically. The numerical simulation successfully proved that the proposed prototype could be useful for coating purposes by repeatedly producing mono-dispersed droplets with controllable size and spacing. Finally, the influences of two independent piezoelectric characteristics - the maximum head displacement and corresponding frequency, was investigated to examine the quality of filament breakup quality and favorable piezoelectric displacements and frequencies were identified.

KEYWORDS: Inkjet printing, CFD modeling, Filament breakup, Small droplet generation

INKJET PRINTING: FACING CHALLENGES AND ITS NEW APPLICATIONS IN COATING INDUSTRY

By

Sadegh Poozesh

Prof. Kozo Saito
Director of Dissertation

Dr. Nelson Akafuah
Co-Director of Dissertation

Prof. Haluk E. Karaca
Director of Graduate Studies

November 23, 2015

Acknowledgments

It has been a long journey to complete this dissertation, and fortunately a great many people have provided help. I wish to express my gratitude to all of them. I have greatly benefited from their kind help and support, and they have made my graduate study experience one that I will cherish forever.

First, I would like to thank my advisor Dr. Kozo Saito for enabling me to study and perform my PhD dissertation at the University of Kentucky. His patience, insightful instructions, encouragement and continued support helped me overcome many difficulties and provided guidance for completing this dissertation.

Second, I am thankful to Dr. John M. Stencel, who gave numerous comments and great technical support for writing my dissertation.

Third, I would like to thank my committee members, Dr. Nelson, Dr. Yang-Tse Cheng, Dr. Tim Wu and Dr. Alberto Corso for reviewing my dissertation, for their alternative ideas and explanations which have undoubtedly augmented this work, and for their timely flexibility.

Forth, I am also grateful to people who have helped to make this dissertation better. Special thanks to Dr. Tianxiang Li, Dr. Zhengchang Song, Dr. Nelson K. Akafuah, Dr. Ahmad Salaimeh, Dr. Liangyong Chen, Dr. Zhen Fan, Dr. Guojie Qi, Dr. Dazhi E, Dr. Harisawa and Dr. Fuchihata who gave insightful comments and constructive criticism on how to improve the dissertation.

And finally, and most importantly, I would like to thank my wife, Kiandokht Bashiri, for her love, understanding and dedication to me. I am also indebted to my parents for their encouragement and support.

Table of Contents

List of Tables

List of Figures

CHAPTER 1

1 INTRODUCTION

1.1 Background and motivation

The concept of inkjet printing originated in the 19th century, and the technology was first extensively developed in the early 1950s. Inkjet printing recreates digital images by producing and then transporting tiny ink droplets to printed surfaces. In recent years, inkjet printing has gone beyond just a computer printing process, and the prospect of it in various high-tech processes is very promising. For example, already versatile applications have been demonstrated in material coating, electronic circuits, drug delivery, printing of electronics and biomaterials, DNA arranging, fabricating Micro-Electro-Mechanical Systems (MEMS) components, manufacturing of particles and microcapsules, and spraying processes (Basaran, 2002, Burr et al., 1996, Wijshoff, 2010, Poozesh et al., 2015b). Although a large range of inkjet technologies exist, two predominate in contemporary industrial applications: continuous inkjet (CIJ) and drop-on-demand (DOD). In the former, a liquid inkjet is produced and forced to breakup into an endless stream of drops by pressure modulation; this technology is used commercially for marking and coding of products and packages. In CIJ technology, a high-pressure pump directs liquid ink from a reservoir through a gun body and a microscopic nozzle, creating a continuous stream of ink droplets via the Plateau-Rayleigh instability (Chuang, 2009). A piezoelectric crystal creates an acoustic wave as it vibrates within the print-head and causes the stream of liquid to break into droplets at regular intervals at repetition rates even upwards of 64,000 to 165,000 droplets per second.

After forming, ink droplets are subjected to an electrostatic field created by a charging electrode; the field varies according to the degree of drop deflection desired and results in a controlled, variable electrostatic charge on each droplet. Charged droplets are separated by one or more uncharged "guard droplets" to minimize electrostatic repulsion between adjacent droplets. The charged droplets are deflected by the electrostatic deflection plates to print on a receptor material (substrate); if insufficient deflection occurs, the droplets are directed toward a collector for recirculation and re-use. Generally, only a small fraction of the droplets is used to print whereas the majority is recycled.

CIJ is one of the oldest ink jet technologies in use and is fairly mature. Its major advantages are the very high velocity (~50 m/s) of the ink droplets, allowing for a relatively long distance between print head and substrate, and a very high droplet ejection frequency, allowing for very high speed printing. Another advantage of CIJ is a lower probability of nozzle clogging because the jet is always in use; this advantage enables inks with volatile solvents such as ketones and alcohols to be used which promote quick drying upon delivery to the substrate. The main disadvantages of CIJ technology are the difficulties in controlling droplet sizes, producing satellite droplets (undesired droplets), and splashing of the droplets on the target as a result of the droplets high speed.

In DOD, droplets are formed intermittently by the action of piezoelectric elements or thermal heaters in response to discrete pressure pulses or heat fluxes, respectively. Unlike in CIJ, no droplet deflection system is used to eliminate undesired droplets from depositing on a target. Hence, DOD nozzles are placed close to a target surface. For commercial inkjet printing applications, multiple nozzles are employed for printing one or a few lines (depending on the print configuration). Because individual nozzles are fired independent

of the other nozzles, with up to hundreds of nozzles in a commercial printhead, the nozzles are inactive for much of the time which can lead to nozzle clogging and decreased print quality. In order to overcome this problem, various mitigation strategies are used, like specialized ink formulations and intermittent purging steps. In general, no special materials of construction are required for DOD print heads, generally making them cheaper and less complex to produce than CIJ print heads.

Figure 1 illustrates the mechanisms and configurations of both CIJ and DOD printing methods. In CIJ, Figure 1(a), a continuous jet of ink released from a nozzle travels downward and progressively breaks into droplets; favorable droplet sizes are directed to the target whilst unfavorable ones are recycled to be used again. In DOD, Figure 1(b), ink droplets also travel downward but are separated uniformly because their characteristics, like velocity and trajectory, can be controlled by manipulating input driving forces that could be either thermal or pressure activated.

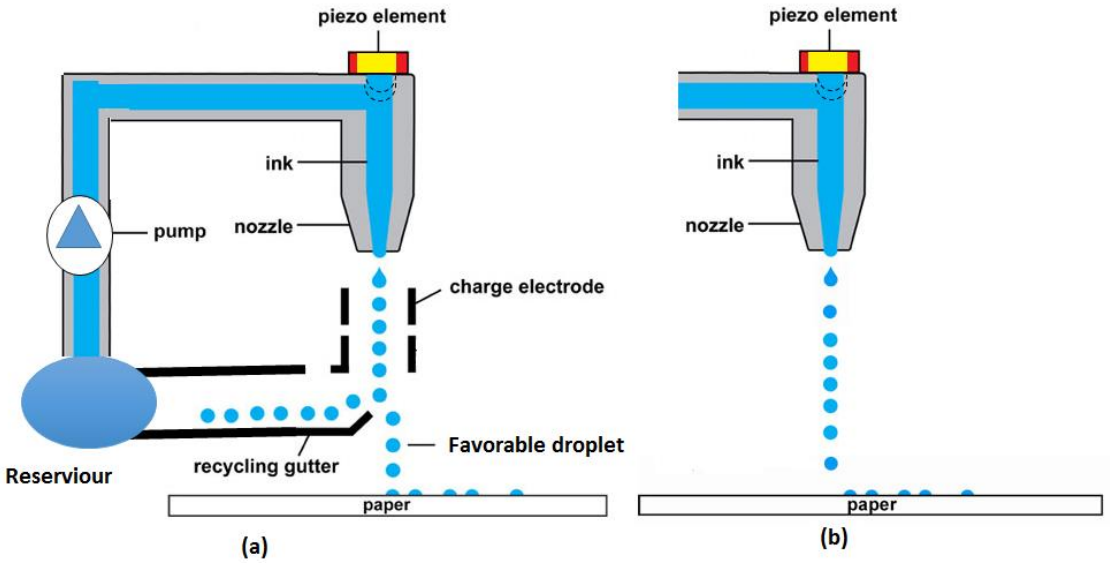

Figure 1. CIJ (a) and DOD (b) technologies.

In thermal DOD, the print cartridges consist of a series of tiny chambers, each of which contains a heater and all of which are constructed by photolithography. To eject a droplet from each chamber, a pulse of current is passed through a heating element to cause rapid vaporization of the ink in the chamber and the formation of a bubble; vaporization causes a large pressure increase and propels a droplet of ink onto a target. Hence, for thermal DOD the inks must have a volatile component that promotes formation of vapor bubbles, otherwise droplet ejection cannot take place.

Most commercial and industrial inkjet printers and some consumer printers (those produced by Epson and Brother Industries) place a piezoelectric material in an ink-filled chamber behind each nozzle instead of a heating element. When a voltage is applied, the piezoelectric material changes shape, generating a pressure pulse in the fluid and forcing a droplet of ink from the nozzle. Piezoelectric (also called Piezo) inkjets allow a wider variety of inks to be used in comparison to thermal inkjets because no volatile component is needed within the ink formulation; also, with Piezo inkjets no issues arise from kogation or buildup of ink residue in the nozzle. However, Piezo print-heads are usually more expensive to manufacture due to the use of the piezoelectric material.

During printing using Piezo DOD, integrated software controls the heads to apply between zero-to-eight droplets of ink per dot, only where needed. This flexibility is important when it is used in production lines to mark products; for instance, the "expiration date" on containers is often applied with this technique and is accomplished by keeping the head stationary while the product moves past. Requirements of this application are high speed, long service life and a relatively large gap between the print-head and the substrate. Figure

2 shows the two most widely used Piezo DOD printing methods, and their corresponding droplet ejection mechanism.

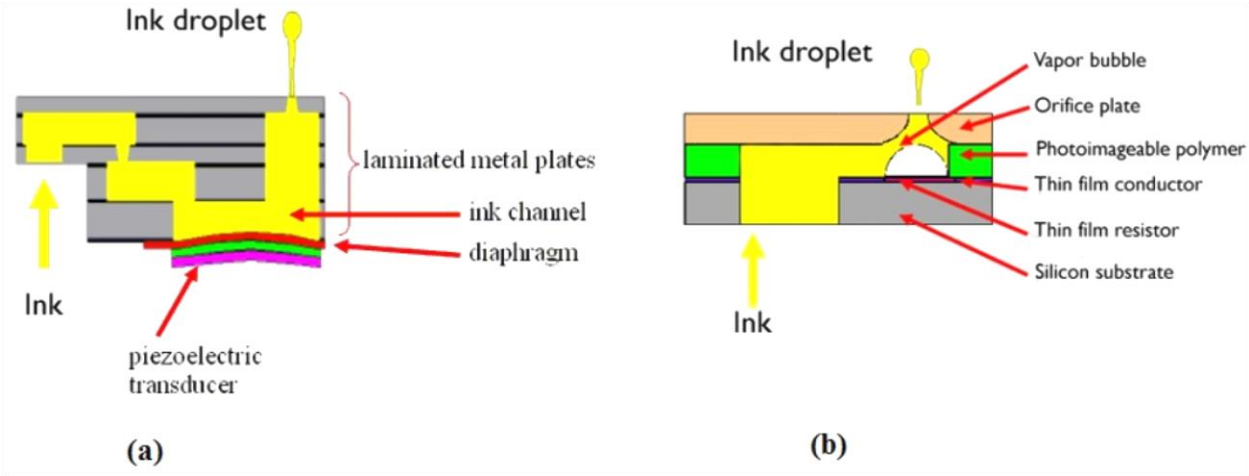

Figure 2. Piezoelectric (a), and thermal inkjets (b)

Inkjet printing technology provides a process to produce individual or multiple droplets of liquid, then directs them toward the target surface under digital control. A wide range of materials with versatile properties and functionalities can be coated by this method. Basically a digital fabrication technique, inkjet printing technology offers the possibility to print or create materials even at a microscopic level, and place the materials exactly where they are required with exactly the right properties. Furthermore, as a coating method, DOD technology could be a possible way to paint materials. Hence, the current study focuses on DOD technology because of its potential for broader applicability and high efficiency, especially for painting. In this application arena, the need for controlling paint droplets is discussed hereafter, and then a deterministic or digital spray painting method is proposed and assessed.

The fundamental dynamics of DOD inkjet droplet formation and impaction on substrates are not yet fully understood because the key stages during formation and impaction take

less than 100 μs for micron-sized droplets. It is worthy to note that the droplet sizes consider herein are of the order of 40–50 μm in diameter, and these diameters are considered micron size or micron scale. Normal high-speed photography cannot capture the details of such processes because even if a 10,000 frame per second camera was used, it would capture only one or two images during the transit time of the droplets from the inkjet nozzle to a target. Furthermore, illumination requirements are demanding because sufficient illumination within a very small field of view over very short exposure periods is needed, thus requiring an intense light source which must not generate excessive heat to change the fluid temperature. In contrast, the current study uses numerical simulation as the prominent tool to visualize micron-sized motions involved in DOD inkjet drop formation. Accurate simulations offer an inexpensive and efficient means to seek optimal operational conditions that could improve printing and painting applications.

For piezoelectric DOD inkjets, the two main issues influencing application efficiencies are: droplet sizes and satellite droplets (Castrejón-Pita et al., 2012b). A summary of each issue, affecting parameters and arising consequences will be given in the following sections; then, alleviating approaches and methods will be introduced and developed.

1.2 Filament breakup and satellite droplets

When a contracted piezoelectric transducer expands, liquid in the nozzle is accelerated and released from the nozzle orifice. Initially, a meniscus quickly extends outward until a liquid column with a round leading edge is formed; then, the column elongates into thread-like structure which forms a tapered column of liquid; after which the thread-like structure thins until it breaks to form individual droplets of fluid (Figure. 3). The physical reason behind

these phenomena can be explained by the amount of kinetic energy confined in the thread-like or filament surface area. If more surface area is present than the minimum required to contain the volume of fluid, the system has an excess of surface energy. Thereby, a minimum energy state is sought which causes deformation of the filament, and breakup of the filament into smaller pieces or droplets that minimize surface energy by reducing surface area. The resultant breakup process is dependent on the surface tension, viscosity, density and diameter of the filament undergoing breakup.

Besides the main droplets, satellite droplets are also formed. Once formed, these satellites can easily lose directionality and deteriorate printing or painting quality; such quality is critical during the generation of very fine patterns. In spite of this importance, it is hard to quantitatively define the degree of satellite formation because it is affected by many processing and physical parameters such as the imposed pulse shape from the transducer and its frequency, and the liquid viscosity, surface tension and density. For instance, decreasing liquid velocity facilities satellite formation whereas increasing liquid velocity lowers the possibility of satellite droplet. However, increasing the liquid velocity depends on increasing the pressure drop which actually contributes to reducing the velocities of the main droplets. Hence, finding optimum ranges of input signal parameters like shape, amplitude and frequency, and understanding influences of liquid physical characteristics like viscosity, surface tension and density, are required to eliminate or at least minimize satellite droplets.

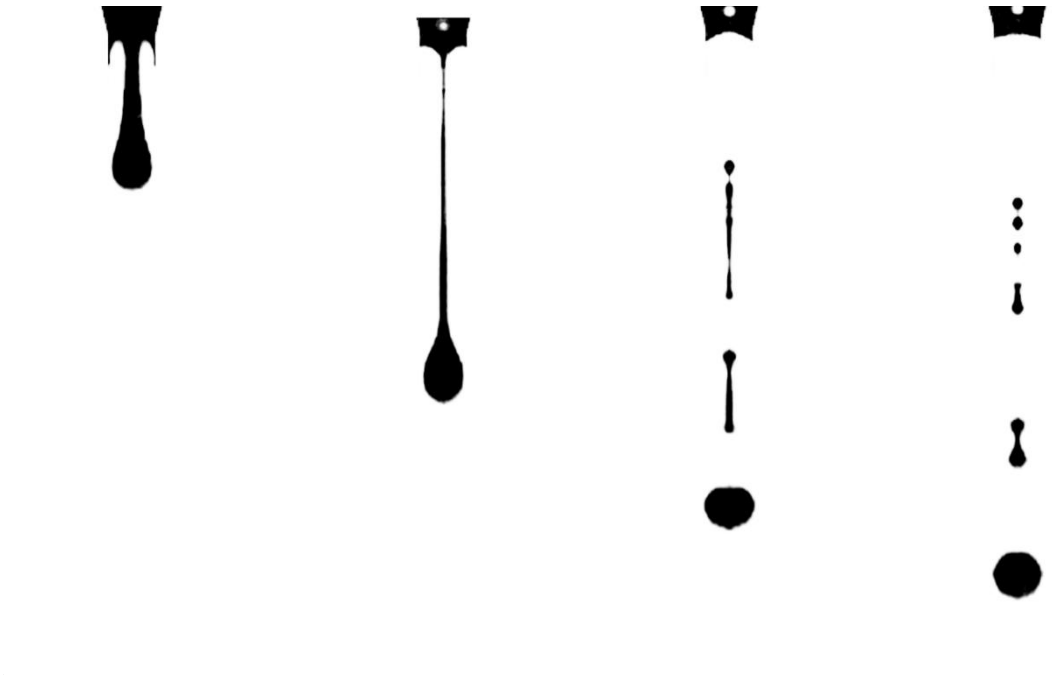

Figure 3. Evolution of a typical filament emanating from an inkjet printer.

1.3 Droplet sizes

DOD inkjet printing applications are increasing in many industries ranging from gene chip manufacturing to microbiology to marking products. Unique features like producing desired droplets with desired size, speed and frequency have made this technology versatile as well as economical. The extreme needs of these diverse industrial applications necessitates understanding the fundamentals and parameters that are involved during droplet and satellite formation, characteristics of which include size, speed, orientation, and generation frequency. In many of abovementioned applications like gene chip arraying devices, an initial coating task must be accomplished with a particular nozzle size which then needs to be changed for high precision applications when the droplet radius should be below 2 μm. However, examination of professional literature on DOD drop generation (Table 1) reveals that the typical radius of the generated droplets is nearly the same as the

radius of nozzles. As such, producing 2 μm droplets from a DOD inkjet printer demands an extremely small nozzle size with the maximum radius near 2 μm. Such nozzles are susceptible to plugging, breaking and produce high pressure drops.

To address the issue of lowering the droplet size without manipulating nozzle size, researchers have come up with the idea of using specialized input electrical control signals to the print-head (Gan et al., 2009). For instance, several new DOD systems employ an input signal with a single polarity whilst others use input signals with double polarity such as a full square wave (Gan et al., 2009). These input signals depend on the employed amplifier and input signal configurations or the time interval limitations of some amplifiers. In these situations, the generation of small droplets may also be accompanied by the generation of undesired satellite droplets.

Another way of producing small droplets from a given nozzle is to impose oscillating conditions onto the protruded meniscus as it is exiting the nozzle. These conditions can cause meniscus separation before its diameter reaches that of the nozzle diameter; in fact, the imposed oscillations usually don't provide enough time for the meniscus to reach the nozzle size. A main disadvantage of this method is that the resultant droplet is completely dependent on the imposed oscillation frequency and is significantly influenced by manufacturing defects within the nozzle orifice.

But how does a droplet with at least the same size as the nozzle emanate from a nozzle orifice? Generally, for a normal input pulse which consists first of a pushing stage and then a pulling stage, the droplet size is equal to or larger than the nozzle orifice because during the pushing stage a large meniscus forms at the exterior of and protrudes from the orifice; then, in the pulling stage, the meniscus separates from the orifice's walls. Thus, the size of

the meniscus produced by normal input pulses is dependent on the boundary conditions imposed by the orifice's walls. Figure 4 shows the ejection of a large droplet that is the consequence of exerting a normal push-pull input voltage (a); its corresponding pressure pulses are presented in (b).

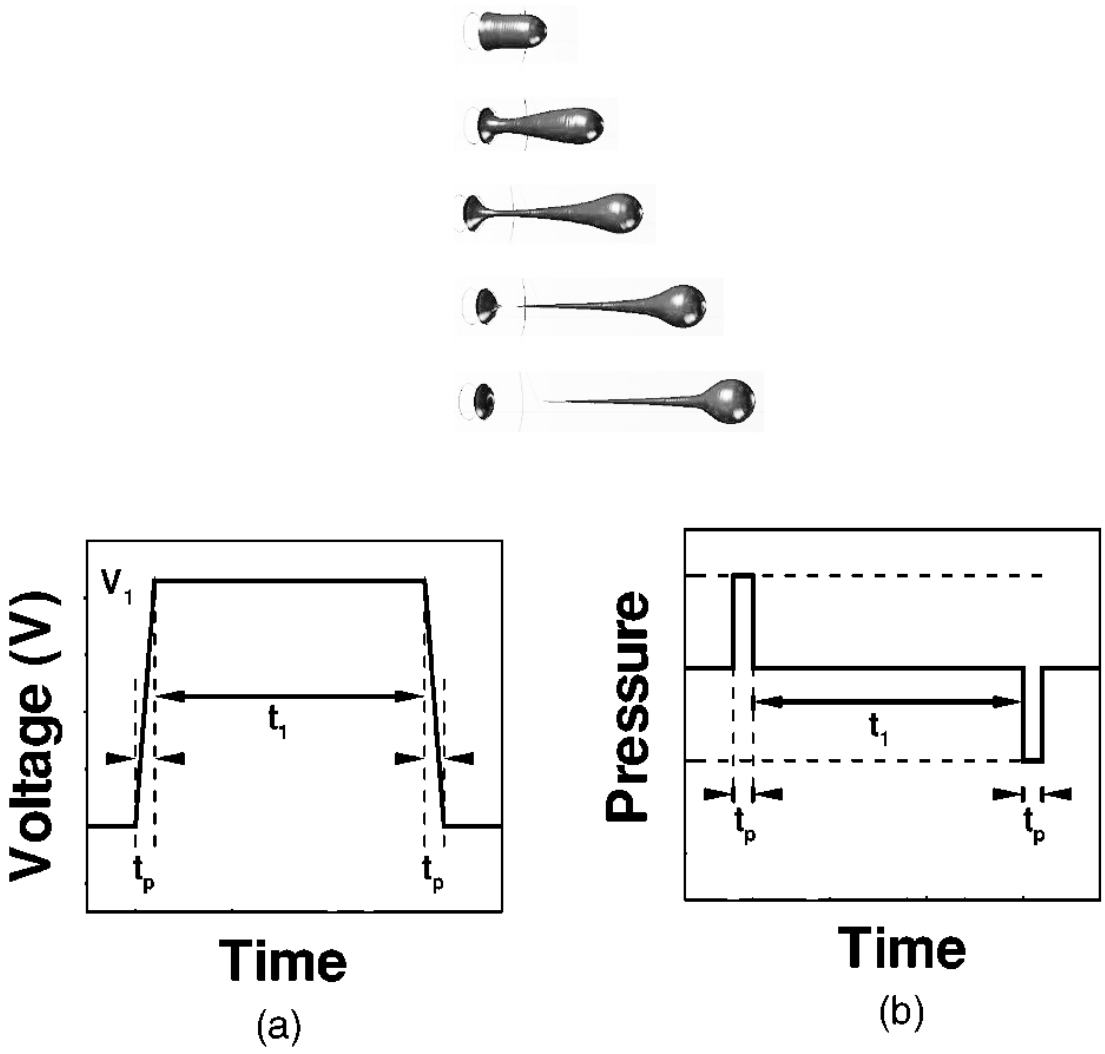

Figure 4. Time evolution of filament separation with imposed waveform depicted in (a) and its corresponding pressure pulse, (b).

In the current study, a new mechanism will be introduced and then examined that ejects lower-sized droplets from a nozzle. The mechanism consists of four stages: first, a negative pulse is applied to pull the liquid inside, toward the internal passage of the nozzle orifice; then, a positive pulse is applied to create a "tongue-like" structure protruding out of the pulled liquid column; this positive pulse is followed by another negative pulse to separate the resultant tongue; finally a refilling process is initiated by applying another positive pulse. These four stages require appropriate time sequencing to promote wanted liquid flows and droplet sizes. For example, after generation of each droplet, a specific time interval is introduced, called the quiescent time, during which the disturbed liquid column can return to its initial shape. Accordingly, a key point within these four stages is creating and extending a protruding "tongue" from the primary liquid column, and then appropriately separating it from the principal liquid column.

Figure 5 gives a schematic view of the mechanism of propelling one small droplet from a nozzle with the mechanism described in the previous paragraph; one complete time period is represented in the figure. This dissertation focuses on finding optimized values of parameters involved in this process and examines and then discusses the variation and extent of these parameters which provide an understanding of droplet sizes that can be produced. The influences of parameters are investigated and presented using numerical simulation based on Computational Fluid Dynamics (CFD).

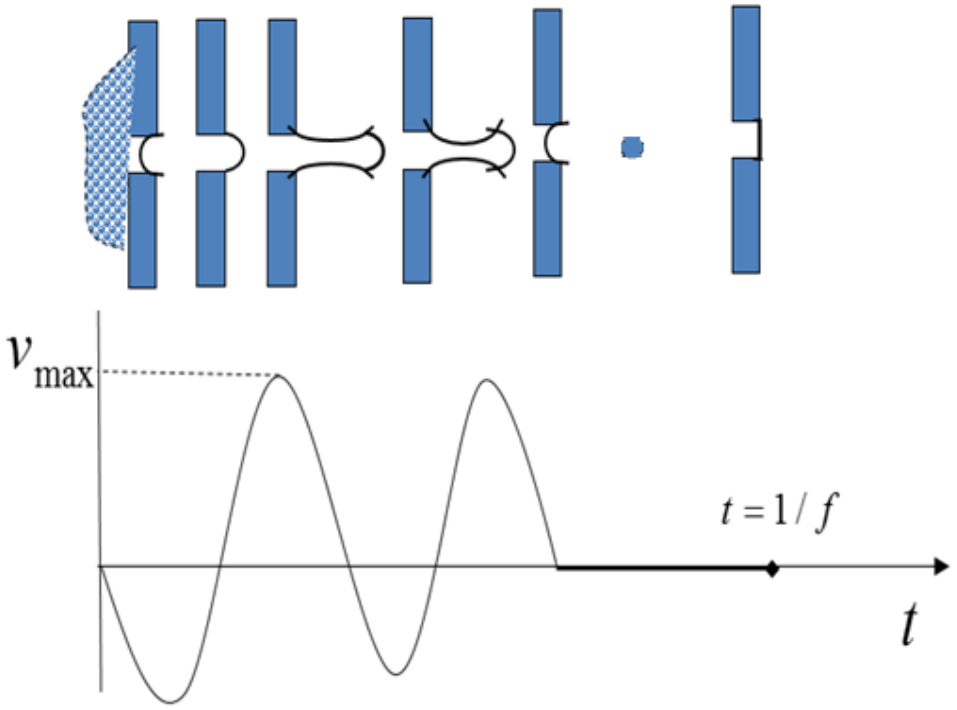

Figure 5. Proposed mechanism for producing a small droplet out of a given nozzle.

1.4 Issues with the Current Automotive Spray Coating Technologies

Automobile painting starts with the spraying of paints toward a car surface. No matter which spray technology is used, broad and important issues associated with automotive painting include: paint transfer efficiency (TE); coating deposition; energy consumption and efficiency; inspection of the quality of finished surfaces; and environmental and work place safety.

After paint is atomized by the spray guns, only a portion of the paint droplets actually coats a vehicle surface because of overspray. The paint not deposited on an automobile surface

constitutes a waste of material and energy, and must be managed with additional processes to circumvent process, worker and environmental problems. Issues of finish quality are alternative to overspray, and can be analyzed in terms of atomizer designs, paint formulation and composition, and surface modification.

The TE of paint can be defined as the ratio of the amount of paint that coats a surface relative to the amount that is supplied to an atomizer. Although automotive spray painting is among the most sophisticated and controlled industrial painting operations currently performed, only 50% to 60% of the spray supplied to a paint atomizer is actually reaches and remains on a vehicle (Fettis, 1995, Toda, 2013). This relatively low TE remains the most important, fundamental problem within automobile painting; finding ways to increase the TE while maintaining a high quality surface finish is a challenging task that has attracted the attention of researchers for many years.

Hence, another focus in this research is on the combined issues of TE and surface finish. Although, these two issues have an interactive relationship to the process, and worker and environmental problems, increasing the TE to use less material and energy and to decrease the level of effort in handling the overspray does not necessarily mean a better quality surface finish. A one percent improvement in TE can save millions of dollars per year in the cost of paint-shop bulk material usage, and a higher TE reduces the amount of volatile organic compound (VOCs) emissions, the amount of paint sludge produced and associated after-treatment costs, and over spray paint capturing hardware. Furthermore, decreased amounts of over-spray allow a reduction in the booth airflow requirements, creating significant energy and cost savings. Simultaneously, it is necessary to maintain or improve

the quality of the surface finish if vehicle sales and owner satisfaction are to continue or expand.

The following items are well documented factors that affect TE (Lee et al., 2012):

- Target surface characteristics (composition, geometry and position)
- Finishing spray technologies
- Operating parameters
- Spray booth air conditions (relative humidity and temperature)
- Liquid coating characteristics

A direct implication of 50–60 % TE is that the remaining 40–50 % oversprayed paint must be captured because of environmental emission regulations. Due to the substantial amount of paint used, water washing or wet scrubbing has been a preferred capturing method. The ratio of the amount of overspray captured to the amount entering the capturing system is defined as the overspray capturing efficiency. Capturing more overspray while using less energy is fundamentally important because of both environmental and operational cost issues. Recently-enacted environmental regulations strengthen the strong demand for efficient overspray capturing technologies (Alloo et al., 2005). Because different spray technologies are known to produce different amounts of overspray, the following discussion presents a brief description of current spray technologies, primarily in terms of TE.

During paint spraying, the liquid must be broken into fine droplets by forcing it under pressure through a small orifice, after which the paint droplets are to be deposited onto a

car body. In general, most spray guns have a common design structure consisting of a fluid needle attached to a trigger which acts as a liquid flow controller, a pathway for the liquid paint and another one for the air, plus an atomization head known as an air cap after which the air is turbulently mixed with the paint to atomize it (Haruch, 2001). However, the mechanisms of atomization differ substantially depending on whether fluid/liquid instabilities are caused by the interaction of inertial, viscous, surface tension, buoyancy or electrostatic forces during the interaction of air with the liquid.

Some spray guns, like those considered to be airless sprayers (Greer Jr and Tryon, 2001), operate like high-powered pistols that discharge high velocity paint streams and produce less fluid instability than when air and the liquid are turbulently mixed; generally, such airless sprayers have relatively little atomization. Other technologies, like conventional air spray (Haruch, 2001), use a small amount of paint mixed with a large volume of air, much like a conventional aerosol spray or a spray can of household paint; in these kinds of atomizers, the main forces responsible for atomization are inertial and drag forces. Introducing new forces like electrostatic and pulsating forces from ultrasonic transducers have also been introduced into the spray painting technology toolbox. In many cases the use of modern engineering tools like computer-aided design (CAD), 3D modeling and CFD simulations have enabled the design of more effective sprays guns and the ability to simulate their performance before constructing prototypes or devices for testing and use.

The main desired characteristics of paint applicators in automotive coating can be summarized as follows (Fettis, 1995, Haruch, 2001):

1) Maximized paint TE without impairing film appearance and processing,

2) Fast, flexible, reliable and robust method of spray paint application while applying a specified film thickness in the limited time available, i.e. a high production rate, and
3) An ultra-clean air environment avoiding painted surface defects, including mottle (orange peel), solvent ‘popping’, sags and craters.

Optimizing the spray technology would lead to more efficient conversion of the liquid paint into fine droplets and the creation of a smooth and uniform film with the highest TE, least overspray and maximum production rate. Importantly, the droplet size distribution has a prominent effect on TE and finish quality (Brosseau et al., 1992). Qualitatively, small droplets produce a good finish but low TE due to the relatively larger air drag forces which can disrupt paint droplet trajectories toward and onto target surfaces. Plus, small droplets have high surface-to-mass ratios which can lead to the evaporation of paint solvents more quickly than with larger diameter droplets; very fine droplets are prone to becoming a ‘dry’ spray when the paint particles reach target surfaces, and dry particles will no longer wet a surface to produce a smooth finish. On the other hand, large diameter droplets are known to create a rough and uneven film thickness but produce a high TE due to their large momentum and the relatively smaller drag forces. These effects can be more understood by looking at Figure 6 which shows TE versus droplet diameter for both an ideal and an actual spray. For an ideal inertial spray, the TE transitions from 0-to-100% at a critical value of droplet size, d_p; in other words, all of the droplets at and above d_p will be deposited on the target surface. However, a real spray creates a TE curve that contains a "S" shape. Depending on the application, an optimized paint droplet size distribution exists in which both TE and finish quality are improved.

In general, the size distribution of droplet sizes is known as a function of both the spray technique and its operational conditions. Larger diameter droplets will be created using a lower air pressure condition and smaller diameter droplets will be created using a higher air pressure condition, if the liquid flow rates are identical. The droplet size distribution is a function of atomization performance which, in turn, is characterized by the finish quality as well as the TE (Kwok, 1991). The narrower the droplet size distribution, the higher the atomization performance (Lee et al., 2012). Thereby, it has been proposed that the ultimate objective of paint atomizer technology development should be to achieve mono-dispersed droplets (Toda, 2013). The mono-dispersion criterion is achieved in inkjet printing technology both during generation of the droplets and their transport to a target in a mono-dispersed manner that avoids droplet-droplet collation; furthermore, inkjet technology deposits droplets exactly where they must be. Therefore, the current research aims to introduce a new coating applicator based on inkjet technology with a goal of achieving both high TE and finish quality.

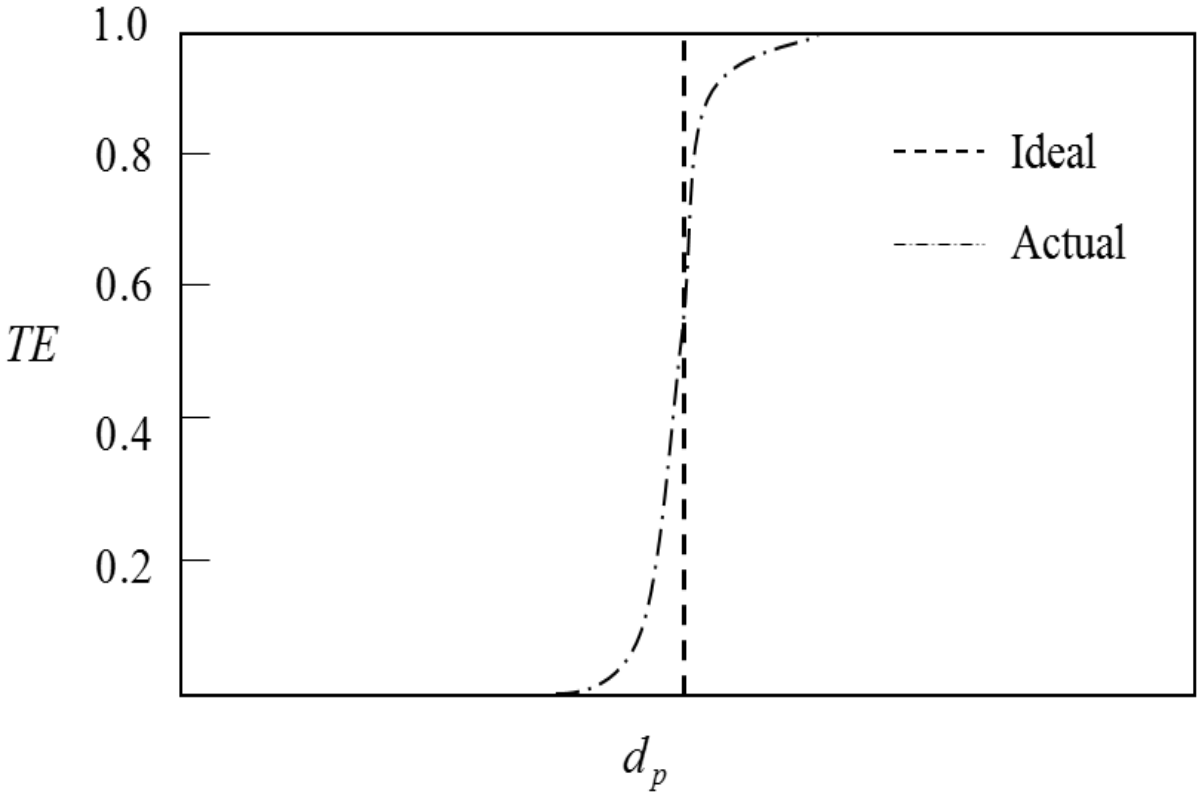

Figure 6. Ideal and actual TE Curves for an inertial spray (Kwok, 1991).

1.5 Overview

The following is a summary of the remainder of this dissertation. Chapter 2 provides a comprehensive literature review on previous research in inkjet printing technology with an emphasis on DOD. The status of research for liquid filament breakup, droplet size and current spray technologies will be evaluated and discussed in detail. Then, approaches for each issue will be introduced and elucidated.

Chapter 3 provides a comprehensive description of the creation of targeted droplet sizes and the numerical methods used in tracking interfaces and liquid disintegration process for each issue. The models are validated against experimental conditions and other previous

research. Also, the governing equations and the scaling parameters that control droplet breakup behavior are examined.

Chapter 4 is devoted to developing and describing the numerical results of filament breakup and satellite droplet formation. A new mechanism for the generation of droplet sizes smaller than the nozzle orifice diameter is presented and discussed. Numerical simulation results will be shown and influential parameters will be investigated. Results will be shown and discussed in detail; they will be compared with results from research literature. Finally a CFD simulation in combination with a paint rheology model will be used to estimate the operational performance of the proposed digital atomizer. A numerical methodology will be used to capture the dynamics of the free boundary between the liquid and air, and atomization mechanisms for the optimum design parameters of the digital atomizer are shown.

Chapter 5 provides concluding remarks and future directions for complementary research of the current results. It also highlights the current dissertation contributions.

1.6 Objectives

The three main objectives of this research are:

1. To gain valuable insight into breakup phenomena of filaments ejected from a nozzle and obtain the influential parameters on liquid filament breakup.

2. To seek an approach that leads to droplets smaller than nozzle orifice diameters and investigate the effects of parameters controlling droplet diameters and promoting their minimization.

3. To develop and test a prototype model for painting applications that is based on digital printing technology.

CHAPTER 2

2 LITERATURE REVIEW

2.1 Introduction

A multitude of processes such as spray combustion, spray drying, spray cooling, spray deposition and aerosol generation require distinct droplet characteristics having specific droplet sizes and spatial distribution characteristics. It would be ideal to establish a spray technique that enables user complete control of droplet diameters and other droplet characteristics of critical importance to their application. Inkjet printing technology offers significant possibilities to achieve this ideal scenario, to produce controllable droplets with pre-determined sizes, speed and orientation. However, significant issues need to be resolved before its benefits can be realized within an automobile manufacturing facility.

The beginnings of inkjet printing began with Felix Savart who, in 1833, showed that the breakup of liquid jets into a chain of droplets is governed by the laws of fluid dynamics (Savart, 1833). Although reported earlier by both Young (1805) and Laplace (de Laplace, 1806), Savart neglected the role that surface tension played in the formation of drops. In 1856, Plateau published an article about the formation of jets from circular nozzles (Plateau, 1856) and later obtained a relationship between nozzle orifice diameter and droplet size. In 1878 Strutt and Lord Rayleigh published an article that is the benchmark for follow up studies on the instability of jets, where they described the breaking up of inviscid liquid jets into streams of droplets by the application of a transient pressure pulse to the nozzle (Strutt and Rayleigh, 1878). The formation of droplets from the breakup of viscous liquid jets was later explained by Weber (1931). These benchmark studies then led to the first

inkjet printer in 1951 by Rune (Rune, 1951) in form of a mingograph for medical applications.

Two principal physical properties of the injected liquid are most important during breakup phenomena: viscosity and surface tension. Also, one imposed effect on the liquid is important: inertia. Generally, the surface tension of a liquid shows that molecules at a free surface have a higher energy than those in the bulk. Because of this difference, liquid filaments contract and form thick and thin regions to increase the surface area. As a consequence, disturbances to the shape of the cylinder will grow and the jet will eventually break up. This tendency of liquids to form a shape with the lowest total energy causes the liquid surface to become spherical. Therefore, a continuous stream of liquid ejected from a circular nozzle, that is initially cylindrical in shape, will gradually become a sphere and will be mostly stable. The liquids employed for inkjet printing have surface tension, σ, of the order of tens of mNm^{-1}. As a tangible example, water at $20^{0}C$ has $\sigma=72\ mNm^{-1}$.

In addition to surface tension which contributes to breakup, the two other forces tend to prevent contraction of the liquid jet, i.e. viscosity and the inertial of the liquid. Viscous forces are a result of liquid molecules sliding against each other; these forces act on and affect adjacent layers of the liquid. Typical liquids that are used for inkjet printing purposes have viscosities, μ, in the range of 2-50 cP (it is worthy to note that water at 20 ^{0}C has $\mu=1cP$. Furthermore, droplet diameters ejected from an inkjet printer are typically in the range of 10-100µm; and droplet velocities immediately before hitting a substrate are ~5-8 ms^{-1}.

In the following sections, a detailed literature review on filament breakup in DOD inkjet printing,on reducing droplet sizes, and on current problems with spray coating technology will be given.

2.2 Filament break-up in DOD inkjet printing

A challenging issue prevalent in inkjet printing is the creation of undesired droplets which are called satellites. Satellites result from the collapse of the liquid filament by surface tension, and normally form when the conditions for the ligament or continuous jet to contract into one single, independent droplet are not fully met. A large number of studies have been dedicated to satellite formation; the corresponding liquid filament breakup regimens will be discussed herein.

Several experimental studies have investigated problems of droplet formation in which the pioneering studies of Hauser et al. (1936) and Edgerton et al. (1937) have remained among the most illuminating observations about droplets and their satellites that are formed during liquid flow from a nozzle. Their research used a high-speed filming at rates up to 1200 frames per second to visualize both primary drops and satellites using a drop weight method for surface tension measurements with a main focus on determining the number of satellites that would form. More than fifty years later, Peregrine et al. (1990) reinvestigated the subject of filament breakup and interface tracking with photography that showed the dynamics shortly before and after pinch-off of both the primary drops and satellites for water dripping from a capillary. However, they only reported the shapes of satellites during the early stages of their evolution. Furthermore, pictures depicting the time evolution or dynamics of the droplets were not from a single same droplet but were

from different droplets at different stages of their dynamics. Consequently, only relative times of droplet breakup were able to be estimated from their data.

Zhang & Basaran (1995) used high-speed visualization to study the effects of physical properties, flow rate, tube radius, tube wall thickness and the presence of surfactants on the primary drop volume, limiting drop length at breakup, and the fate of satellites for drops of glycerol/water solutions forming from a capillary tube. However, they were not able to study the details of the satellite dynamics due to the insufficient time resolution of their imaging system. Shi et al. (1994) revealed the interesting effect of increasing drop viscosity on the shape of a drop near the point of pinch-off. They showed that, for concentrated glycerol/water solutions, a micro-thread or possibly a series of micro-threads were created with each succeeding micro-thread significantly thinner than the one from which it was spawned; also, their data concluded that the main thread would reconnect with the about-to-form primary drop.

Henderson et al. (1997) experimentally studied both pinch-off of the primary drop from the main thread and the pinch-off of the main thread from the fluid pendant from a capillary tube using highly viscous liquids. They noted that, although one or more micro-threads formed where the main thread connected to the primary drop, no micro-threads formed when the main thread connected to the fluid in the capillary. They also compared the recoil speed of the main filament after it separated from either the primary drop or from the fluid in the capillary to that predicted by scaling analysis.

The problem of filament breakup has been examined in theoretical and numerical investigations as well. In a benchmark study, Fromm's pioneering numerical simulation

research (Fromm, 1981) used the marker-and-cell (MAC) method to analyze the axisymmetric dynamics of drop formation from a DOD nozzle.

Schulkes (1994) used the boundary element method (BEM) to solve for the potential flow inside a growing droplet to theoretically predict the dynamics of formation and breakup of an inviscid liquid from a capillary into droplets. Among other things, he showed that the interface of the primary droplet at the incipience of breakup was overcome near the pinch-point.

Eggers and Dupont (1994) studied the breakup of liquid droplets by solving one-dimensional slender-jet equations. They also investigated the asymptotic behavior of interfacial rupture for low-viscosity fluids and compared their results with those for an inviscid fluid. Shi et al. (1994) solved one-dimensional equations to predict cascades of micro-threads that could form for concentrated glycerol/water solutions shortly before the primary droplet detached from the main thread. They showed that, while one micro-thread formed naturally, an external source of noise was necessary to trigger the formation of subsequent micro-threads. Brenner et al. (1997) also studied the formation and pinch-off of low viscosity drops by solving one-dimensional equations and authors paid particular attention to the dynamics shortly before and after the point of filament pinch-off. Zhang and Stone (1997) used the boundary element method (BEM) to theoretically study the formation of droplets in Stokes flow into a viscous ambient fluid also undergoing Stokes flow. Among other things, these authors concluded that the length of the drops at breakup increased significantly while the primary drop volume varied only slightly as the ratio of the drop's viscosity to the external fluid's viscosity increased.

Wilkes et al. (1999) studied the formation and pinch-off from a tube of Newtonian liquid drops using a three-dimensional axisymmetric or two-dimensional algorithm employing the Galerkin finite element method (G/FEM). They illustrated the high-accuracy of their computations by showing that their computed results agreed with new and old experimental measurements within an error of about a percent, and were in excellent agreement with results obtained using an inviscid code when viscous force was small compared to inertial force. These authors also showed for the first time that the interface of a liquid droplet having finite viscosity can overturn prior to breakup. Before this work, interface overturning prior to pinch-off had been thought to occur only in the absence of viscosity as the phenomenon had only been observed in inviscid flows (Mansour and Lundgren, 1990).

Zhang (1999) used the volume-of-fluid (VOF) method to predict the formation of several droplets of liquid in sequence into air. He reported a correlation for the critical flow rate beyond which satellites did not form as a function of fluid properties. Gueyffier et al. (1999) used a fully three-dimensional VOF algorithm to predict the dynamics of droplet formation, including the dynamics and formation of satellites. However, the calculations by both Zhang (1999) and Gueyffier et al. (1999) for droplet shape at the incipience of breakup and subsequent satellite dynamics were too coarse and hence did not capture the fine details of existing experimental observations very well (Notz et al., 2001).

Fuchikami et al. (1999) have also used experiments and one-dimensional equations to explore the dynamics of the so-called leaky faucet problem; their research using computational techniques and experimental verification elucidated a number of

interesting nonlinear, dynamical phenomena including period doubling, hysteresis and chaotic dripping.

Chen et al. (2002) studied computationally the formation of an incompressible Newtonian liquid from a tube at constant flowrate by solving the NS equations using (G/FEM) with elliptic mesh generation employing a finite element algorithm; they showed a change of scaling from one scaling regime to another as pinch-off neared; e.g., distinct forces were shown to control the breakup process when pinch-off of the liquid filament was about to occur if it was surrounded by a dynamically inactive fluid, depending on the regimen. They further showed for the first time that the computed value of the minimum neck radius of a forming droplet followed Eggers's so-called universal solution (Eggers and Dupont, 1994) until it becomes unstable. Ambravaneswaran et al. (2002) recently compared the predictions of droplet formation based on one-dimensional equations with those based on three-dimensional axisymmetric Navier–Stokes equations to assess the accuracy of the one-dimensional method under different operating conditions. As part of the same study, these authors used the one-dimensional method to show that a critical flow rate existed beyond which satellites no longer formed if the fluid and tube radius were fixed but the flow rate was varied.

The former discussion highlighted a general literature review on satellite droplet formation and liquid filament rupture. In the following, the subject of emphasis is on the determinant parameters for producing a free cylindrical filament and, then, for a filament ejected from an inkjet printing; also considered are the influential factors influencing on the breakup procedure.

Schulkes (1996) predicted that a filament for which Oh ≥ $O(1)$ will contract into a droplet regardless of its initial aspect ratio, L_0, while a sufficiently long filament with Oh ≤ $O(0.01)$ will form bulges separated by thinner filaments and ultimately break up into separate droplets. Moreover, Schulkes predicted that critical Oh lies within the range of $0.005 < Oh < 0.01$ for $8 \leq L_0 \leq 15$.

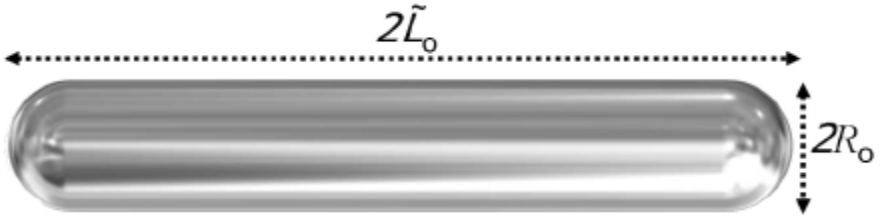

Figure 7. Geometry of a free cylindrical liquid filament with spherical end caps as assumed in the models of Schulkes (1996).

Notz and Basaran (2004) went further by concluding that, for low Ohnesorge numbers Oh ≤ $O(0.1)$, the final breakup is governed by both a Oh critical value, Oh_c and a critical initial aspect ratio, $L_{0,c}$ in which a filament with $L_0 > L_{0,c}$ and $Oh > Oh_c$ will break up whereas it will not with $L_0 < L_{0,c}$ and $Oh < Oh_c$.. They established explicit values for the critical Ohnesorge number and aspect ratio by computational modelling; however, experimental data are not available for the (L_0, Oh) parameter space.

Dong *et al.(2006)*, in an experimental study on the dynamics of DOD droplet formation, employed a piezoelectrical actuated inkjet print-head over a wide range of viscosity and surface tension. They observed the effects of the driving signal and liquid properties on DOD stages including ejection and stretching of the liquid, pinch-off of liquid thread from a nozzle, contraction of the liquid thread, breakup of the liquid thread into a primary drop and satellites, and recombination of the primary drop and satellites. Their study showed that, after the liquid thread had pinched off from the nozzle, two modes of

breakup occurred: single droplet formation occurred where the liquid thread formed an almost spherical droplet without breakup, and multiple breakups occurred where the primary droplet was followed with one or more satellite droplets. By investigating the effects of liquid and system parameters, a necessary condition for each mode was proposed.

Xu and Basaran (2007) applied the method of lines coupled with the Galerkin/finite element method for spatial discretization and an adaptive finite difference method for time integration to solve transient equations for incompressible Newtonian fluid from a simple capillary tube. Imposing a time-periodic inflow rate, they provided a regimen map with three regions describing three modes of breakup based on the three non-dimensional parameters, including *We*, *Oh* and a droplet size parameter, and on the inlet flow rate frequency.

In another study, Castrejon-Pita et al. (2011) developed a simple experimental device to produce droplets on demand and a large-scale model for a real inkjet printing system.They visualized droplet shapes and positions with a shadow-graph technique and conducted a numerical study to simulate the experimental results employing a Lagrangian finite-element method. Good agreement between the numerical simulation and experimental results validated their numerical model and its capability to predict the creation and evolution of droplets from Newtonian liquids. Note, however, that the large-scale model had a much larger nozzle diameter (2 *mm* in diameter) than those used in practical applications. They kept the jetting parameters (*Oh* and *We*) nearly constant at values between that for a generic commercial DOD print-head (nozzle diameter, $50\mu m$ and droplet speed 6 ms^{-1}) and their large-scale model. The gravity effect became

important for larger diameter drops than for smaller diameter drops, while the gravity effect was not included in the scaling. Hence, the large-scale model did not exactly match the dynamic behavior of a commercial print head but showed good qualitative agreement. Employing the same model with the same dimensions as (Castrejón-Pita et al., 2011), and using the volume of fluid (VOF) model, Kim and Baek (Kim and Baek, 2012) obtained a regime map describing different liquid filament breakup mechanisms based on the three non-dimensional parameters *Oh*, *We*, and Capillary (*Ca*). Castrejon-Pita et al. (2012a), based on the experimental data from a liquid jet generator capable of producing free cylindrical liquid filament, determined the conditions under which a liquid filament will break up into droplets using a wide range of two dimensionless quantities, including the aspect ratio of the filament and the *Oh* number. Ignoring the relative motion of a massive head and trail, Hoath et al.(2013) predicted the behavior of an asymmetric, single-ended filament (observable in inkjet applications) of length *l* attached to a large drop by comparing it to a free cylindrical filament studied by Castrejón-Pita *et al* (2012a), but with a length twice as great as a single-ended one. They used print-head drive waveforms to produce jets with only a small initial relative speed between their two ends to find the critical transition line above which the ejected liquid filament would break into more than one droplet.

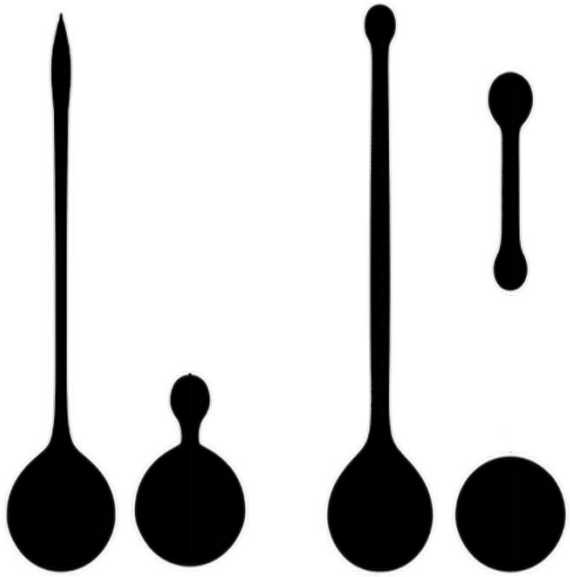

Figure 8. Two modes of the secondary breakup: (a) single droplet formation where the liquid thread form an almost spherical droplet without breakup, and (b) multiple breakups due to capillary waves.

It is difficult to control a satellite droplet's speed and diameter and, therefore, precise control of the liquid droplet onto a target becomes difficult. As such, avoidance of satellite droplet is of the utmost importance for DOD applications like high-quality printing and micro-devices. Two different modes of creating satellite droplets are shown in Figure 8: (a) the liquid thread ejected from the nozzle contracts into a single drop without breaking up, and (b) the liquid thread ejected from the nozzle breaks up, and form two or more independent droplets. Obviously (a) is favorable condition for operation of inkjet printing and applications, while (b) is not. Therefore, one focus of the current research is to determine if a transition line between these two different modes can be established based on *Oh* and *We*.

2.3 Review on Droplet Sizes

In the piezoelectric DOD inkjet field, two issues of importance are reducing droplet sizes preventing satellite droplet formation (Castrejón-Pita et al., 2012b). In general, during DOD droplet generation utilizing normal input waveforms to the print-head the radius of the generated droplets is nearly the same as the radius of nozzle from which it is generated (Chen and Basaran, 2002). Hence, in the following an overview is presented on studies emphasizing the reduction of droplet sizes for DOD droplet generation.

In 1989, Kimura et al., presented a novel enzyme immobilization method (Kimura et al., 1989) which used an inkjet nozzle, originally developed for printing equipment, as a tool for precise enzyme deposition onto a silicon on sapphire (SOS) device. They asserted that, with this approach, a great conservation in enzyme usage was seen and expensive enzymes could be used efficiently in biosensor applications. Additionally, by employing computer selections it was easier to select an appropriate enzyme from among several enzymes and to determine the enzyme emission position, a result of which was that many kinds of multi-biosensors having different enzyme combinations could be realized on one wafer. The nozzle they used has a 50 μm diameter hole and a normal pressure pulse which first pushed the liquid column outside and then pulled it inside to detach the released filament from the liquid column. Therefore, when chamber contraction was induced by increasing pressure within the pressure chamber, the enzyme solution filling the pressure chamber was pushed into the air and created an enzyme solution drop. After an enzyme drop exited the chamber the chamber pressure returned to its initial value. They reported enzyme droplets to be about 48 μm in diameter.

Bernardini et al. (1991) was the first to use piezoelectric inkjet printing technology for dispensing fluids in neurobiological research. They performed two types of experiments; in one experiment, 50 μm droplets of a histochemical reagent were jetted from a 52 μm onto discrete targets of frozen tissue sections, and qualitative and quantitative histochemical studies were done on the small (170 μm) diameter circle of tissue wet by the droplets. In the other experiment, 50 μm droplets of neuroactive drugs were jetted onto brain tissue slices while recording single neurons extracellularly in vitro, and the effects of the drugs were found to vary systematically as a function of the number of drops and the distance between drop application and the recorded neuron. Their results indicated that piezoelectric inkjet printing could have wide application for dispensing fluids in neurobiological research.

Sziele et al. (1994) signified reduction of droplet size for a reliable analysis in capillary electrophoresis, an electrokinetic separation method performed in submillimeter diameter capillaries and in micro- and nanofluidic channels. Emphasizing the disadvantages of current separation methods such as sensitive laser fluorescence detection method, electrochemical detection method and a combination of both of these methods, introduced a reliable and elegant solution to the problem of micro injection in capillary electrophoresis. A commercially available ink-jet system, originally used in an ink-jet printer, had been adapted for a contact-free shooting of sub-nanolitre sample droplets into the capillary of a standard capillary electrophoresis system. By employing the inkjet printer they were able to generate extremely small sample volumes with great precision and good reproducibility.

Sakai (2000) applied a sequence of negative and positive pulses to modulate the actuating mode to create droplets with a diameter of about 70% of nozzle diameter, when a nozzle of 32 μm in diameter was used. A very interesting aspect of his study was the introduction of a model called "equivalent circuit" that related input voltage to the piezoelectric actuator and pressure or the velocity at the print-head inlet. This aspect is important because a velocity or pressure at the inflow to the nozzle is required to numerically simulate the ejection of ink droplets. Since only the input voltage to the piezoelectric actuator is known, the "equivalent circuit" method included the effect of ink cartridge, supply channel, vibration plate and piezoelectric actuator to simulate the ink velocity and pressure at the nozzle inflow over a range of given dynamic voltages. Thereby, a real ink jet could be simulated by solving the "equivalent circuit" and corresponding flow equations.

Chen and Basaran (2002) investigated formation of small water–glycerin droplets and observed a tongue of liquid moving at a higher velocity than the nearby liquid when successive negative and positive driving waves were applied. In their experiments, ink droplets were produced from a "squeeze mode" DOD nozzle In which the inkjet nozzle consisted of a piezoelectric transducer or sleeve that was bonded outside of and concentric with a glass capillary tube having an outlet orifice radius of 35 mm. The piezoelectric DOD dispenser was actuated by a piezo driver (A. A. Labs A-303) which amplified an appropriate voltage signal synthesized by an arbitrary waveform generator. They also benefited from an ultrahigh speed digital imaging system that included a Cordin camera which can capture images at a rate of 100 million frames per second, and a Questar lens which can resolve images between 1.1 mm from 15cm in size. This system

was able to capture the generation and transport of small droplets (diameter smaller than 90 mm) from a DOD nozzle having flight times as small as tens of microseconds. They claimed that the droplet sizes and entire formation dynamics of drops ejected from the DOD nozzle were extremely consistent beyond the first few drops, and that from the tenth and beyond the drops were indistinguishable from each other.

Chen and Basaran (2002) did experiments with several forms of voltage signals applied to the amplifier to assess their influence on droplet size. They pointed to "waveform 2" and "waveform 3", shown in Figure 9 (a) and (b), respectively that could promote small droplets. They also found that, by imposing "waveform 3", ultra-small droplets about 40% smaller than the nozzle size could be produced. Figure 10 shows the droplet generation process over time for the waveforms shown in Figure 9.

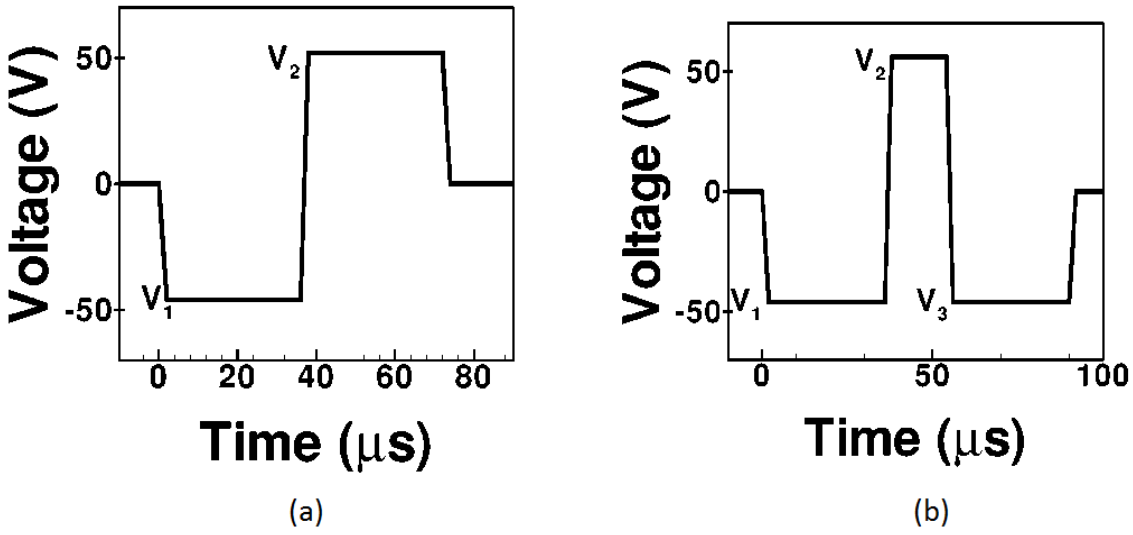

Figure 9. Voltage waveforms used in experiments done by Chen and Basaran (2002) (a) "waveform 2" voltage signal; and (b) "waveform 3" voltage signal.

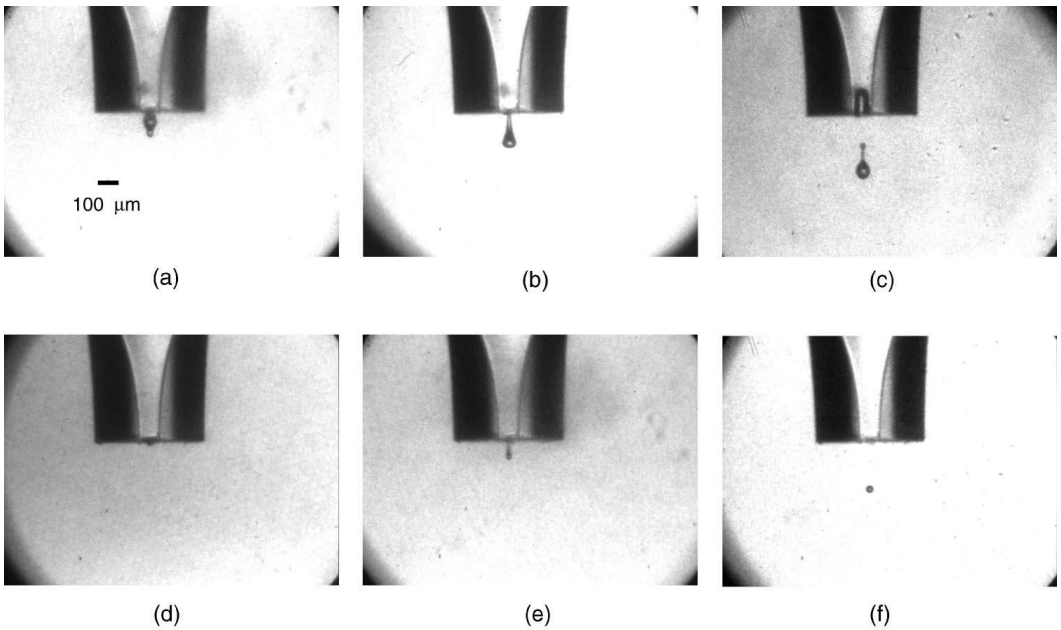

Figure 10. (a)- (c) Images are showing appearance and disappearance of a tongue and formation of a droplet upon application of "waveform 2". The times of photographs shown were 84, 104 and 144 ms for (a), (b) and (c) respectively. (d)- (f) Images are showing formation of an ultra-small drop upon application of "waveform 3". The times of photographs shown were 60, 80, and 200 ms for (d), (f), and (e) respectively (Chen and Basaran, 2002).

Gan et al. (2009) applied different types of waveforms, including a unipolar, bipolar, M-shaped and W-shaped waveforms, on an inkjet system with a nozzle driven by a circular piezoelectric element. They also considered the effects of the amplitude and pulse duration of each waveform on the jetting process with an ultimate goal was to minimize droplet sizes ejected from a typical inkjet system (Jetlab II, Microfab Technologies Inc.) containing a special kind of ink called Poly (3, 4-ethylenedioxythiophene) (PEDOT, Sigma Aldrich). Their experiments were accomplished using a constant actuator frequency of 550 Hz. The different types of their waveforms are shown in Figure 11, and the PEDOT droplets ejected onto a silicon wafer while using four different waveforms are illustrated in Figure 12. Their effective reduction of droplet volume was near 50–

80%, values for which were compared to the unipolar waveform which gave the highest droplet volume. For Newtonian inks, the bipolar waveform was recommended because to its relative simplicity and the quality of the inkjet; for non-Newtonian inks, the M- or W- shaped waveforms with optimal pulse parameters were recommended because of the significant reduction in droplet volume.

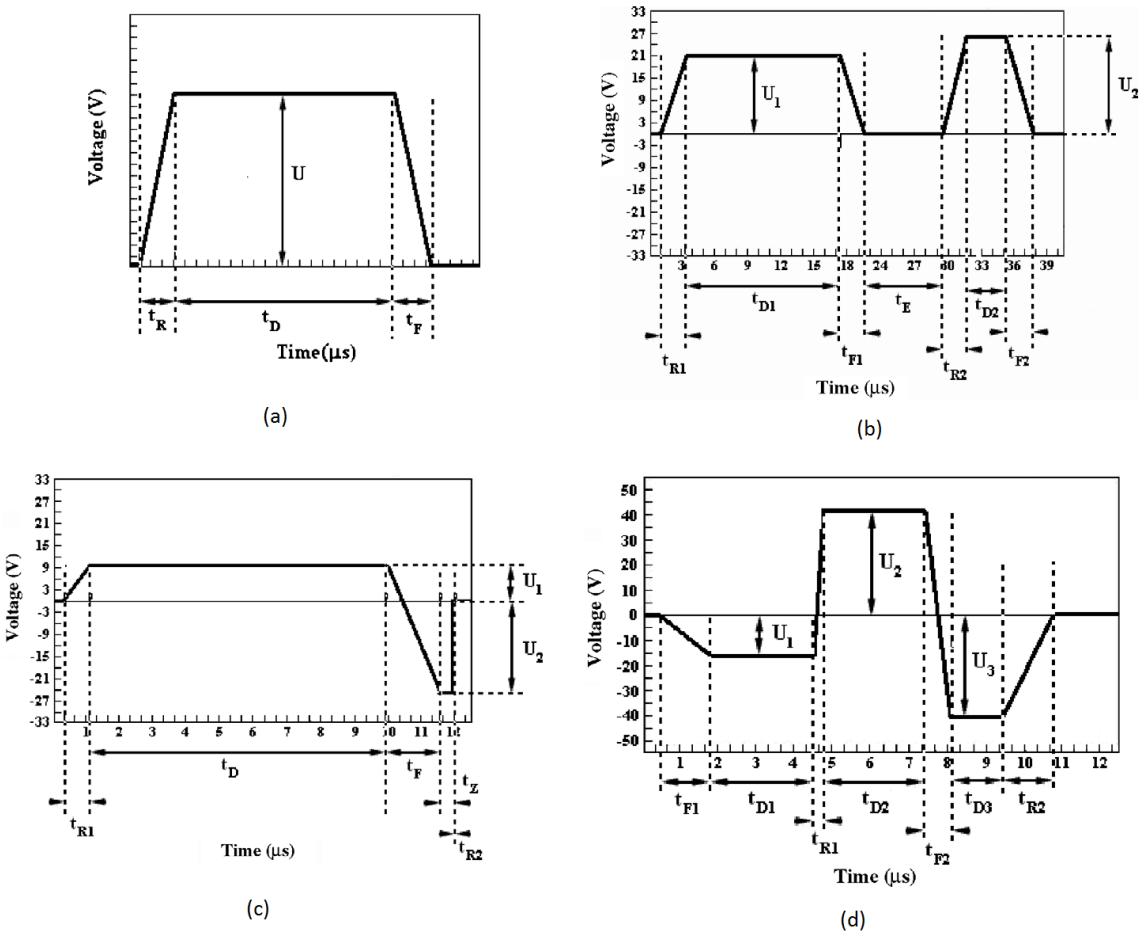

Figure 11. Voltage waveforms types applied on actuator by Gan et al. (2009). The types are unipolar, M-shaped, bipolar and W-shaped shown in (a)-(d) respectively.

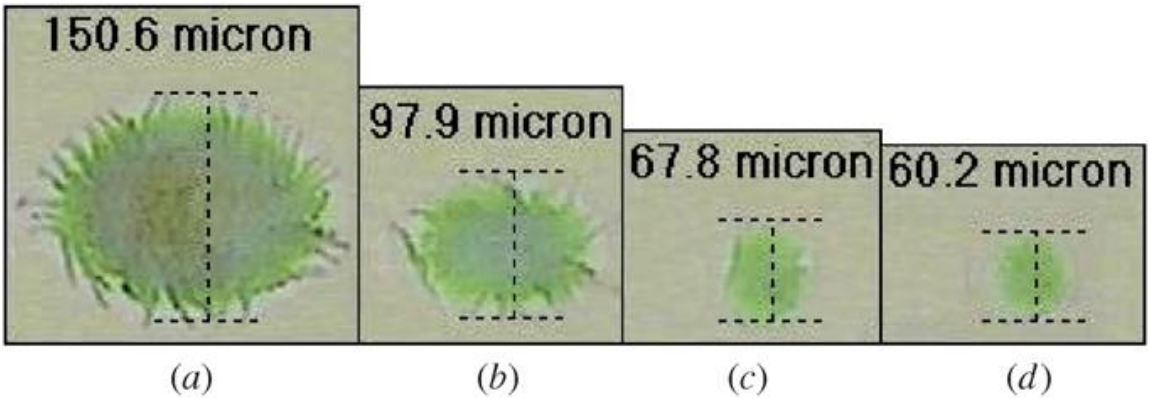

Figure 12. Comparison of PEDOT droplet sizes (a) By unipolar waveform, (b) by bipolar waveform, (c) by M-shaped waveform and (d) by W-shaped waveform (Gan et al., 2009).

For high precision applications, the droplet radius may need to be smaller than 2μm, a value which demands a nozzle with the maximum radius near 2μm. However, such nozzles are highly susceptible to plugging and breaking, and are difficult to manufacture (Chen and Basaran, 2002). Hence, a significant amount of researches has examined how to decrease discharged droplet size without decreasing nozzle size (Chen and Basaran, 2002, Castrejón-Pita et al., 2012b).

One approach, as described in the foregoing, has been to adjust the applied waveform to the inkjet. This approach can generate drops with diameters smaller than the nozzle by control of the capillary, inertial, and viscous timescales that govern the flow inside the nozzle, and can be performed by applying a pull-push-pull-push waveform into a "squeeze-mode" nozzle. The second "pull" pulse suppresses the formation of the large primary drop (obtained by conventional pull-push waveforms) and a small drop is produced instead. The last pulling stage enables the print-head to be refilled and the liquid column is returned to its initial position.

Other methods of producing droplets of decreased size exist but their application in industrial processes has been limited by one or more of the following factors: operating frequency, material compatibility, size and speed of printed droplets, and miniaturization/mass production capability. An example of one such method is called acoustic focusing, which was used commercially by Hon et al. (Hon et al., 2010). These print-heads can be nozzle-less systems that produce relatively small drops (down to 140μm but commonly millimeter size) but have not been widely used in industry because they require large and complex transducers. Although alternative methods can produce droplets down to the nanometer scale, such as in electrospraying (Taylor cone), the production of these extremely small drops is difficult to control; furthermore, control of the droplet directionality is an issue and important limitations exist on the number and type of fluids for which this technique can be applied. Recently, Castrejón-Pita et al. (2012b) did experiments with four droplet generator prototypes that demonstrated the capabilities of the mechanism given by Chen and Basaran (2002). The prototypes included: a "large-scale system" with nozzles from to 4mm down to 1 mm in diameter; two "small scale systems" with nozzle diameters in the range from 60 μm to 400 μm; and a "micro-scale" version in which a nozzle of 60μm diameter was tested. They reported a reduction of droplet size of about 40% for the jetting prototypes.

An overall listing of studies performed in this area along with corresponding applications, and nozzle and resultant droplet sizes, is given in Table 1.

Table 1. Typical nozzle and produced droplet diameter in DOD drop production.

Reference	**Application**	**Nozzle diameter**	**Droplet diameter**
Kimura et al. (1989)	Enzyme deposition and immobilization	50 µm	48 µm
Lloyd and Taub (1988)	Inkjet printing	40 µm	78 µm
(Bernardini et al., 1991)	Dispensing liquids in neurobiological research	50 µm	52 µm
(Brennan, 1999)	Arraying of biologically active materials	40 µm	50 µm
(Sziele et al., 1994)	Injection of sample drops in capillary electrophoresis	60 µm	60 µm
(Perçin et al., 1998)	Dispensing (a) water (b) photoresist	(a) 60 µm (b) 110 µm	(a) 50 µm (b) 94 µm
(Laurell et al., 1999)	Chromatography	60 µm	50 µm
(Sakai, 2000)	DOD inkjet printing	32 µm	23 µm
(Chen and Basaran, 2002)	DOD inkjet printing	70 µm	32 µm
(Gan et al., 2009)	Polymeric inkjet printing (a) DI water (b) PEDOT	50 µm	(a) 28 µm (b) 62 µm
(Castrejón-Pita et al., 2012b)	DOD inkjet printing	100 µm	38 µm

All of the referenced research in the foregoing was experimental in nature and focused on reducing droplet sizes below that of the nozzle. To the author's knowledge, no numerical simulations have been reported on this issue whereas such studies are inexpensive and can be an efficient approach for examining the dynamics of DOD droplet formation. Numerical simulation can also be employed to investigate the so called pull-push-pull-push mechanism in a more comprehensive way. Therefore, an important part of this dissertation is the numerical simulation based on computational fluid dynamics (CFD) to attempt finding optimized controlling parameters for the pull-push-pull-push mechanism as a way for reducing droplet sizes below the nozzle size.

During pull-push-pull-push, the first negative imposed pressure creates a cavity, then the positive pressure transfers energy to a narrow jet that emerges rapidly from the center of the collapsing cavity. The following negative pressure contributes to breakup and avoids releasing a big droplet. Finally, the last pushing stage is for refilling and accelerating produced droplet as well (Figure 5).

2.4 Review on current spray technologies

In this section a brief summary of the current coating sprayers and associated studies will be presented. Generally, automotive spray painting technologies consist of three main approaches: conventional, electrostatic, and effervescent spray applicators. Conventional spray applicators consists of air spray guns, airless guns, high volume low pressure (HVLP) guns, air-assisted airless guns, and high speed rotary atomizers. Electrostatic spray painting can be coupled with any of the conventional spray methods. However, the

most commonly used as well as the most efficient spray method for current automotive applications is electrostatic rotary bell (ESRB) applicators (Corbeels et al., 1992).

2.4.1 Conventional Air Spray Devices

Generally, conventional atomizers include air spray, airless spray, air-assisted airless spray, HVLP spray and rotary sprayers. The atomization of paints using conventional air spray devices was first used in the early 1900s to apply paint to limited areas of cars and other items on a production basis (Fettis, 1995). For many years conventional air spray was the most prominent method of applying paint onto automobiles and is still used in various parts of the world, particularly in smaller paint shops. Although offering an acceptable level of film appearance, it provides poor TE and consequently a high rate of paint usage.

Extensive research has been conducted to identify the parameters and mechanisms controlling atomization for conventional air spray devices (Kim and Marshall, 1971, Kumar and Lakshmi Prasod, 1971). An important focus has been on measuring droplet sizes and size distributions, and on the spatial distribution of the spray, because it is known that small droplets deposited on an automobile body provide a high finish quality if the spray distribution is acceptable; however, small droplets also lead to rather low TE's.

Early and important contributions on the study of conventional spray devices were described by Nukiyama and Tanasawa (Nukiyama and Tanasawa, 1939, Nukiyama and Tanasawa, 1940) who proposed an empirical expression to relate droplet sizes with the gas and liquid rates and liquid properties. Their research showed that the most

influential parameters affecting droplet sizes were the liquid and gas viscosities, their densities, the liquid surface tension, and the velocity and flow rates of the liquid and gas. These conclusions have been mostly confirmed in more recently published research (for example Corber (2010)) although design variables like the needle diameter and nozzle cone angle are also currently known to affect droplet sizes.

It has been found that full cone nozzles produce the largest droplet sizes followed by flat spray and hollow cone nozzles if the liquid and air rates, and pressures, are the same independent of the type of cone nozzle used (Andrade et al., 2012). An increase in flow rate will typically increase the droplet sizes and a decrease in flow rate will decrease the droplet sizes (Masters, 1979, Schick, 2006). Air pressure has, in general, an inverse relationship with droplet sizes. An increase in air pressure results in smaller droplet size and a decrease in pressure results in larger droplet size. Similarly, the spray angle has an inverse relationship effect on droplet sizes. Typically, larger spray angle results in smaller droplet size and a decrease in spray angle causes an increase in droplet size (Lefebvre, 1989, Schick, 2006).

Specific liquid properties that affect droplet sizes are the viscosity, liquid density and surface tension. An increase in viscosity will typically increase the spray droplet's Sauter Mean Diameter (SMD) and also contributes to a reduction in liquid flow rate if the pressure is not changed; hence, with an increase in viscosity, the pressure also has to be increased to maintain adequate spray angle and coverage (Lefebvre, 1989, Schick, 2006). However, the influence of liquid density on SMD is fairly small in comparison to the other parameters (Lefebvre, 1989, Rizkalla and Lefebvre, 1975). Lefebvre (1989) suggested that for pre-filming nozzles, the SMD was proportional to the air density to

the -0.6 power. For conventional air spray devices, air velocity is undoubtedly the most important factor influencing the droplet SMD values. For low-viscosity liquids, the SMD is approximately inversely proportional to the air velocity; this dependency underlines the importance of using the highest possible air velocities that are consistent with available pressure drop (Lefebvre, 1989). The effects of increasing air pressure and decreasing air temperature are a reduction in the SMD.

An issue which may cause differences in results when investigating individual spray parameters that affect droplet size distribution is the interactive nature of these parameters. Each of the above-mentioned parameters, like liquid density, can influence liquid viscosity and even surface tension (Schonhorn, 1967). Hence, to achieve repeatable and comprehensive conclusions from research on conventional air spray devices it is recommended that interactions between influential parameters should also be taken into consideration. This fact raises another issue: droplet size distributions are highly influenced by interactions between the design of the spray device and environmental factors like temperature and humidity. In other words, besides the interactions between the design of the spray device and inherent parameters associated with the liquid, operational velocities and pressures, the interrelationships between the spray device and external parameters like ambient temperature and humidity also have to be considered when attempting to understand or develop a new and efficient spray devices.

2.4.2 Twin-Fluid Atomizer Air Spray Devices

A typical cap for an air spray atomizer is shown in Figure 13 that illustrates its main component functions. Generally, air spray devices have a central paint orifice,

primary and secondary atomization air orifices, cleaning air orifices which help to prevent clogging of the paint nozzle, and shaping air orifices which can substantially affect the paint atomization mechanism (Hicks, 1995).

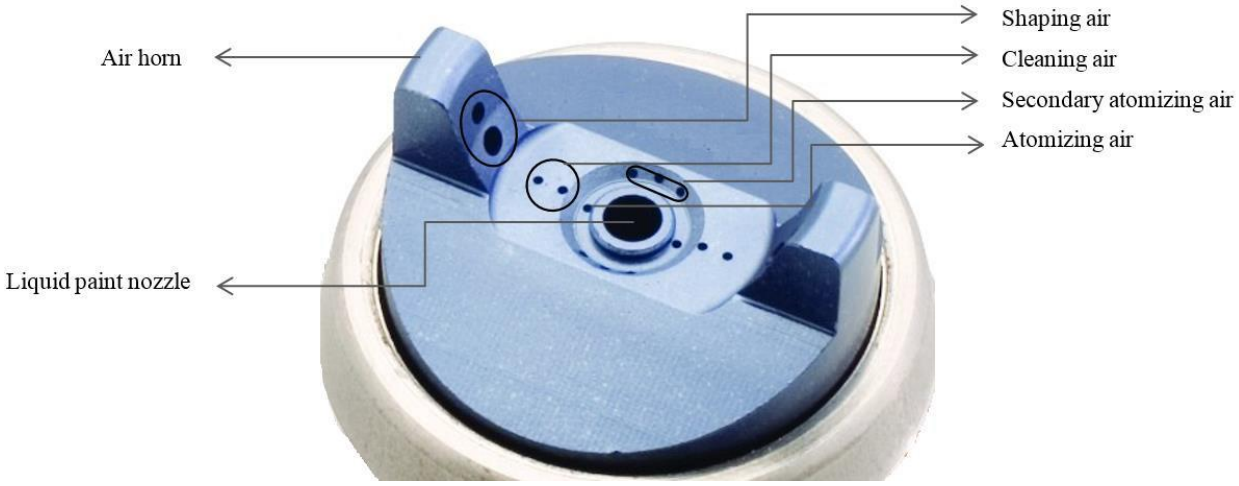

Figure 13. Structure of a typical air spray cap.

Liquid exiting the paint nozzle at a low velocity (about 5 *m/s*) is atomized by a high velocity annular air flow from the primary air spray orifices. Because the orientation of the secondary air orifices is distinct from the primary air orifices, secondary atomization occurs after primary atomization, i.e. droplet generation occurs twice. These spray guns normally operate at a high liquid pressure of up to 0.5 MPa and moderate air pressure up to 0.3 MPa. Overspray from this type of spray device is generated within a shear layer near and on the target surface which prevents small droplets to impact and adhere onto the surface; the shear layer's influence on the trajectories of the small droplets is large because small droplets have small axial momentum. Employing this type of air spray device contributes to a smooth, even finish but also produces a low TE (typically 15 to 20%) in comparison with other spray devices

(Plesniak et al., 2004).

Kim and Marshal (1971) were among the first to obtain droplet size correlations using curve fitting techniques to analyze experimental data. They studied a twin-fluid atomizer type of device for spraying molten wax and melts of wax-polyethylene mixtures. Droplet size correlations relative to air and liquid velocities, air density, ratios of mass flow rates for air and liquid, nozzle design and liquid properties were developed, but their final correlations were limited to small ranges of the investigated variables.

To estimate TE of an air spray device, Hicks *et al.(1995)* and Hicks and Senser (1995) developed a model to simulate paint droplet transport and deposition based upon some key assumptions that resulted from their experimental research. In their simulations that employed a stochastic, separated flow approach, the effects of turbulent air velocity on paint droplets' trajectories were assessed and the TE was evaluated. The droplet TE information detailed the efficiency with which the air spray device operated for droplets having different diameters, i.e. it characterized the droplet size dependence with respect to TE. They concluded that the TE was 100% for droplets of diameter larger than120 μm; for smaller diameter droplets, the TE was less and depended on whether a spray induced turbulent airflow was or was not adjacent to the work piece. Interestingly, without a turbulent airflow induced by the spray, very small droplets did not deposit onto the target surface.

Additional disintegration to smaller droplets or coalescence to bigger droplets can and does occur after formation of a spray droplet and during its flight to a target. This dynamic situation has not yet been addressed to an adequate degree in spray and painting research, but could be important for advancing the science and technology

of spray painting. Lacking this information and a comprehensive, practical theory for air spray paint atomization has provided impetus for researchers to seek other tools of analyses, like CFD (see Domnick *et al.(2005)*; Morikita and Taylor(1998); Flynn and Sills (Flynn and Sills, 2001, Flynn, 2000); Yousefifard et al. (2015) and (Shim et al., 2008)). These studies have used basic methods to predict diameters and velocities, including magnitudes and trajectories, of droplets derived mainly from experimental data. In general, curve fitting methods were employed to assess data that had been obtained under various conditions of nozzle operation. This experimental procedure is the basis for distributions like those described by the terms Rosin-Rambler, Nukiyama-Tanasawa or log- kernel (Movahednejad et al., 2010). Other attempts to measure and understand droplet size distributions and velocities have been accomplished by obtaining droplet size-velocity distributions in the immediate downstream of spray and applied as boundary conditions for CFD calculations. For example, Ye *et al.*(2002) considered the interactions between air and droplets just after exiting a spray gun and demonstrated that a complete air flow field between nozzle and the target surface could be simulated by applying air inlet conditions at the nozzle and the initial droplet conditions necessary for the simulation could be prescribed very close to the nozzle. This achievement was important because it enabled a determination of the shape of the spray cone and the effects of paint inlet condition on the film thickness on the work piece. Fogliati *et al.(2006)* also predicted paint droplet trajectories and deposition distribution on rectangular target plates using CFD.

2.4.3 High Volume Low Pressure (HVLP) Devices

HVLP guns were originally developed in response to environmental regulations passed

by California's South Coast Air Quality Management District (SCAQMD) in the mid-80s (Fettis, 1995). Although they have commonalities with conventional air spray devices, HVLP devices have higher volume of air-to-volume ratios of paint and propel paint toward surfaces at a lower air pressure than do conventional air spray devices. Consequently, a higher proportion of paint will reach the target surface with reduced overspray. In practice, a regulator is utilized during HVLP painting to decrease the air pressure. Darroch (1997) introduced two types of HVLPs, including an air conversion spray gun and a HVLP turbine driven system. The HVLP air conversion sprayer was similar to a conventional air sprayer with inlet air pressure near 0.24 MPa to 0.4 MPa; air was routed through the handle of the spray gun and its outlet pressure was reduced to less than 0.07 MPa. In the turbine driven system, the controllable-flow air source is a turbine attached to the spraying system instead of compressed air. Generally, the HVLP approach leads to higher TE than conventional air spray devices and produces excellent-quality finishes.

As a drawback, HVLP spraying technology is considered difficult to operate. The low cap pressure of less than 10 *psi* creates spraying difficulties that can lead to insufficient coverage of surfaces and often result in more repeat paint coverages. Also, if paint atomization is insufficient, an uneven finish is produced which forces paint shops to use more paint; this issue can cause the HVLP system to be more time consuming than other spray systems, i.e. production rates can be low.

Recently, a HVLP with low volume-medium pressure spray has shown promise to alleviate some of these issues, including lessened finishing time and increased TE (Shilton et al., 2002).

2.4.4 Airless Pressure Atomizers

Airless, pressure atomizers have higher TE than conventional air applicators and, because of their high fluid pressures, they can be used for wider variety of coating applications (Schmidt and Walzel, 1984). Airless atomization converts the energy of the fluid under pressure into kinetic energy. A turbulent fluid jet with a high flow speed emerges from a nozzle into a stationary atmosphere. As a consequence, shear forces arising from the jet control atomization.

Paint atomization occurs when paint is pushed through a small tip opening having diameters between 0.18-1.2 *mm* at very high fluid pressures between 8.0 to 52 MPa. Several tip openings can be used to attain optimum atomization regimens and droplet size distributions. Also, a combination of very high pressure and elevated temperatures within the spray tip can be used to enhance paint atomization; heating causes lower viscosity of the paint and, consequently, lower pressures are required. Because the very high pressure contributes to precise targeting onto surfaces to be coated, this method is commonly used for paint tasks that otherwise would involve masking. Airless pressure atomizers are also often used for applying anti-chip coatings to sills and lower sections of automobiles.

Because inertial forces are much greater for the spray emanating from airless pressure atomizers, the inertial forces of the droplet are high and paints with wide range of viscosity can be used; other advantages include a final finish which generally has a wet, uniform thickness with excellent adhesion. The high pressure also enables the paint to better penetrate into partially obscured or deeper crevices. As a consequence, airless, pressure atomizers are used mainly for applications that require large amounts

of a coating, like in the automotive undercoating.

Some disadvantages of the airless, pressure sprayer include: the possibility of coarse atomization which can lead to unsophisticated finish qualities; because of the high flow rate, overspray wastage is usually high; because of the high pressure and high flow rate, significant operating hazards are possible in which, if the spray emanating from the nozzle is accidently pointed toward an operator, serious skin penetration and resulting infection could ensue; furthermore, the operating conditions of the spray system causes a high probability of nozzle clogging.

Schmidt and Walzel(1984) stated that, since the inertial forces dominate in comparison to surface forces for airless, pressure applicators, the creation of droplets from ligaments is delayed in its time after emanating from a nozzle relative to that of other applicators. Walzel(1990) showed that the geometry of the airless spray nozzle could be a detrimental influence on the efficiency of conversion of ligaments into droplets. Settles(1997) gave a visual perspective of spray atomization from airless, pressure applicators, thereby providing a basic understanding of ligament destruction and droplet formation phenomena in which the flow pattern was described to be a quasi-two dimensional flow.

Xing *et al.(1999)* studied airless, pressure applicators for non-Newtonian waterborne latex paint sprays for various sizes of droplets and thickener compounds in which a correlation was developed between SMD and orifice diameters; these correlations depended upon surface tension, viscosity, injection densities of the air and coating, and injection pressure differential. They also indicated that increasing the extensional viscosity increased the droplet sizes and broadened the size distribution.

Plesniak *et al.*(2004), based on fitting of experimental data, discussed the TE of airless, pressure spray painting, with the following correlation:

$$TE = a + b\,SMR - c(SMR)^2 + dD_{32} \tag{2-1}$$

in which, a, b , c, and d are the curve fitting coefficients; $SMR = \dot{m}^2 / \rho A$ (the actual spray momentum rate, with $\dot{m}$, ρ and A the paint mass flow rate, paint density, and gun's tip area, respectively); and D_{32} is SMD, calculated as follows:

$$SMD = \frac{\sum D_i^3}{\sum D_i^2} \tag{2-2}$$

Equation (2-2) represents the volume-to-surface area ratio of the spray, and it was concluded that the SMR had the dominant effect on TE. In contrast, the SMD was found to have little effect on TE. Furthermore, the gun traverse speed was found to have little influence on TE whereas the gun to-target angle did have a significant influence on TE.

Ye *et al*. (2013) carried out numerical simulations using CFD and, together with an experimental investigation, investigated some important issues affecting airless, pressure spray painting for ship finishing industries by focusing on droplet integral velocities and sizes was using Laser-Doppler Anemometry (LDA) and Spraytec Fraunhofer type particle sizers. By examining these parameters close to the spray nozzle, and then using numerical simulations and correlations to examine droplet transportation and deposition, it was found that, with increasing distance between the gun and the substrate, a resultant reduction occurred in both TE and uniformity of the paint film thickness on the substrate.

2.4.5 Air Assisted, Airless Applicators

Various combinations of conventional applicators were introduced in the 1970s that took advantage of the strengths of conventional air spray guns; these innovations lowered paint usage and were shown to be compliant with EPA regulations of that timeframe (Fettis, 1995). One of these developments was the air-assisted, airless sprayer; it combined the best features of HVLP that gave high TE along with the best features of airless, pressure applicators that gave increased production rates.

In air-assisted, airless applicators, the paint is partially atomized using a specially-designed fluid nozzle tip similar to those used in airless, pressure guns. First, pressurization of the paint is provided by an airless pump, thereby enabling viscous and/or dense paints to be sprayed that cannot be sprayed using HVLP. Second, atomization is complemented by injecting a small amount of air from a face and/or the horns of an air nozzle. Liquid paint pressures ranges between 4.8 and 6.2 MPa, and the assisted air pressure ranges between 0.10 and 0.20 MPa. The finish quality provided by these applicators is sufficiently smooth and production rates could be considered to be in the medium range. In general, this sprayer is mainly used during stationary and portable painting applications (Trostle, 2012).

2.4.6 Rotary Bell Atomizers

The development of rotary bell atomizers, also called “paint bells” or “bell applicators”, was an important innovation in paint applicators, especially for those needed in high production rate environments (Toda, 2013). Bell applicators are also preferred for their superior TE, spray pattern consistency and low air consumption in comparison to

conventional applicators. The original rotary bells had rather poor atomization performance and, as a consequence, were used at first only for primer coating. To improve atomization, Ransburg (Toda, 2013) introduced the mini-bell in 1975 which had a better rotation performance than the earlier bell designs but still had inferior atomization performance compared to conventional air guns; furthermore, the early bell designs were prone to creating undesirable air bubbles on coated surfaces under certain operating conditions. Subsequently, grooved mini-bell and metallic bell atomizers were developed that eliminated these problems; these bells are used now not only for top coating but also for metallic applications (Toda, 2013).

Typical bell applicators consist of four major components:

- The valve module, which consists of the passages for: paint, solvent and compressed air, and the valves to control their flow into the system; paint delivery, cleaning and purging with solvent; and, management of compressed air to the valves, turbine and shaping air shroud.

- A rotating surface, which might be a vanned disk, a flat disk or a cup; the most widely used ones are the spinning disk and rotary cup in which the disk or cup is affixed to the shaft of the turbine. The paint is injected into the center at the rear of the disc, and forms a film on the disk surface due to centrifugal forces which also pull the paint film towards the edges where it breaks into atomized droplets.

- The turbine, which is a high speed air motor that rotates the bell cup at speeds ranging between 10,000 rpm to 70,000 rpm, depending on the cup diameter, desired atomization and physical properties of the paint.

- The shaping air shroud, or shaping air ring, which consists of small passages or pinholes from which air flows to the front of the atomizer and outside of the bell cup diameter; it controls the size of the spray pattern. In general, as more air flows through the shroud the atomized paint will be shaped into a smaller deposition pattern. As shown in Figure 14 and generally, two primary and secondary shaping air rings are incorporated for breaking ligaments in two successive stages.

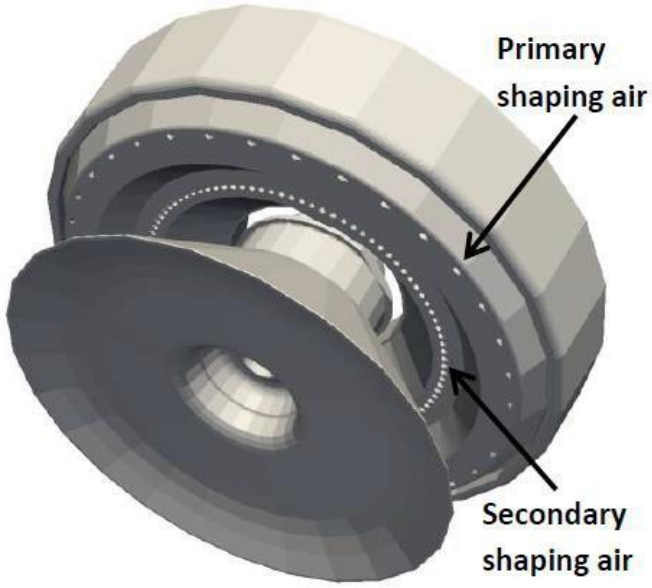

Figure. 14. A typical rotary atomizer (Martinez, 2011)

Rotating atomization has similarities with airless atomization. The atomization energy for rotary bells is provided by the high-speed rotation and the centrifugal forces associated with it. Accordingly, droplet diameters depend mainly on the rotating speed and the diameter of the atomizer. Generally, the mechanisms of atomization depends on the disk geometry, rotational speeds, liquid flow rates and liquid properties; Marshall *et al.(1954)* made substantial contributions to understanding the

physics behind these atomizing mechanisms.

Figure 15 depicts three different mechanisms of droplet formation for a rotary cup atomizer (Dombrowski and Lloyd, 1972). In the sheet formation mechanism, liquid leaves the cup in the form of attenuating sheets that disintegrate in a number of ways depending upon the operating conditions. Under most practical conditions, the disintegration is caused primarily by imposition of aerodynamic waves which grow in amplitude until fragments of sheets are detached. These fragments contract under the action of surface tension into ligaments of liquid which subsequently break into droplets. In a second ligament formation mechanism, liquid flows from a torus around the cup periphery in the form of long curved ligaments which disintegrate into droplets at a distance from the cup. For this case, droplet diameters may not be uniform but are still more uniform than from conventional air spray guns. And finally, in the direct drop formation mechanism, drops can be produced directly from the torus and would give highly uniform droplets.

Frost (1981) investigated the process of ligament formation from a rotating disk with a high angular speed and developed the criteria for ligament occurrence in which an expression for predicting droplet size was obtained. It was pointed out that the resultant mean droplet size is a function of liquid flow rate and bell rotational speed, and that a log normal droplet size distribution could be expected with a standard deviation of 0.1 when the correct flow rates were used. In contrast, a sprayer, like a conventional air spray device that relies on shear forces for droplet formation has a standard deviation of about 0.25 for the droplet size distribution.

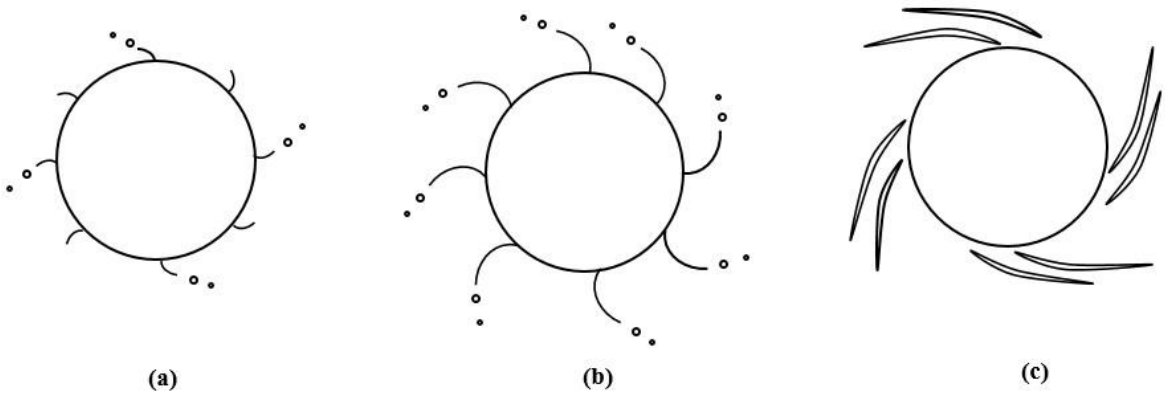

Figure 15. Different mechanisms of liquid disintegration by during rotation of bell cups; (a) direct drop formation, (b) ligament breakup and (c) film breakup.

Kawase and De (1982) were among the first to examine droplet formation mechanisms for non- Newtonian liquids from spinning disks. The suspension and rheological properties of paints were also assessed relative to the atomization mechanism, and a method was presented to calculate the number of ligaments for Newtonian and non-Newtonian fluids. Liu *et al.(2013)* used two mathematical models to predict maximum unstable growth rates, wave lengths, film lengths, break-up times and droplet sizes for the rotating cups at high and low Weber numbers, and obtained film break-up lengths and droplet sizes which were validated during experimentation. More recently, Ahmad and Youssef (2014) offered a comprehensive investigation on the effects of cup and disk geometrical configurations on droplet breakup mechanisms, droplet sizes and velocity fields using four different designs for rotating disks and cups. They compared SMD and mean droplet velocity for various cups and disks with those of droplets produced by a regular flat disk atomizer. Their results showed that their predicted SMD correlation obtained for spinning regular flat disks can be satisfactorily employed to predict the one produced by rotating cup and disk atomizers with different configurations.

In summary, the parameters affecting droplet size distributions from rotary bell atomizers are: 1) inlet liquid properties, of which the most important are viscosities, surface tensions, and rheology; 2) liquid and air inlet flow rates; 3) geometrical configurations of the cup or disk; and, 4) the rotational speeds of the bell. According to published results, the rotational speeds of the bell and the inlet liquid flow rates are most influential because of their importance during droplet formation.

2.4.7 Electrostatic Spray Painting

Electrostatic painting was first introduced in the U.S. by Ransburg in the 1940s (Tilney, 1953). Electrostatic spray painting offered substantial savings in the usage of paint during the painting of manufactured items. During operation, paint droplets are electrically charged at the sprayer tip and the ensuing repelling forces spread the droplets evenly when they exit the needle. Simultaneously, an electric field is established between the spray gun and the target which forces the charged particles to follow equipotential lines of the field to the target. As a result, a very uniform coating of the target surface can be established and the TE is very high. Electrostatic spray painting has grown significantly in recent years, and is now the commonly used for finishing in many industries like agriculture machinery and products, office furniture, microencapsulation, electro- emulsification using fine powders and even ink jet printing. Kelly (1994), and Okuda and Kelly (1996) have summarized the theories and practices of different applications and recent reviews were presented by Hayati *et al*. (1987), Jaworek and Krupa (1999) and Jaworek (2007).

Several types of electrostatic spray, i.e. electro-spraying, techniques are used, including air sprays, airless sprays and rotary sprays. Because of the electric field between the spray gun and the target, metallic paints can coat more than the surface of a target that is visually seen

from the sprayer tip, i.e. it is possible to "wrap" the charged paint particles around geometries like wire-shaped goods and other complex surfaces and assemblies. Reports by Tilney (1953), Straubel (1954), Hines (1966), and several patents (Roger, 1962, Demeter, 1970, Bienduga, 1995) have demonstrated the ease with which paint is atomized and applied to vehicles, housewares and various metal goods.

One issue of concern for electrospray coating is the potential liabilities associated with sparking due to the charged particles, and the possibility of fire and worker injury. Another issue is that the paint will not only coat the targeted surface but also will coat all surrounding, grounded objects like a paint booth ceiling, the conveyor and conveyor protection systems, the spray gun and its handler.

Electrospray techniques are used successfully to paint automobile components, with the most common technique being electrostatic rotary bell applicators (ERBS). Figure 16 illustrates a basic system of ERBS used in automotive paint shops. A surfacer is pumped into the gun using a hollow drive shaft; rotation of the spray cap scatters the surfacer and causes the primary atomization after which electrostatic forces cause additional atomization of the surfacer droplets in a second disintegration/atomization mechanism.

The atomization of paint using rotating bell applicators with electro-spraying has been studied extensively in experimental, theoretical and numerical investigations. Hines (1966) studied atomization during electro-spraying testing at the Scientific Laboratory of Ford Motor Company using single jet sand rotating cups while measuring droplet sizes and mean specific changes. His experiments resulted in a qualitative understanding of the influence of various operating parameters on the properties of the resultant coatings. Bell and Hochberg (1981) undertook the first major effort to investigate ERBS application

for metallic paints by simulating automotive production conditions and obtained a power law relationship for mean droplet size as a function of bell voltage, rotational speed, and liquid flow rate and viscosity. Ellwood and Braslaw (1998) numerically simulated an external ERBS by modeling two-phase, electrostatic flow and postulated that an electric field not only controlled the trajectories of droplets but also enhanced deposition mechanisms. Furthermore, they concluded that the droplet charge-to-mass ratios played a significant role in the atomization and deposition processes.

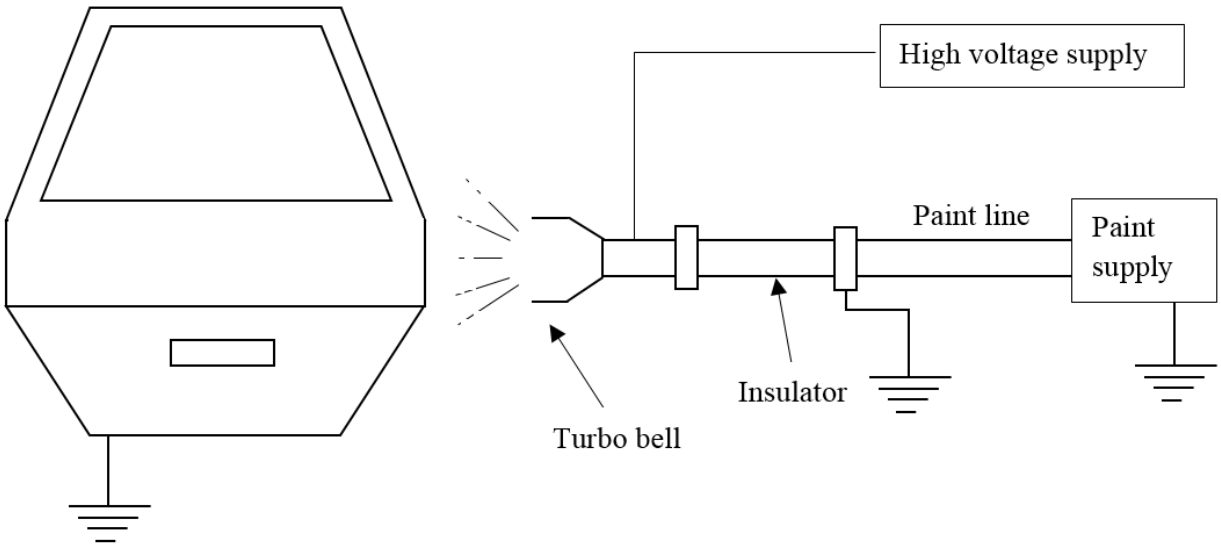

Figure 16. Electrostatic spray painting (Fettis, 2008)

Im(1999) and Im et al.(Im et al., 2001, Im et al., 2004) reviewed technological challenges and research issues for ERBS, and then described spray atomization through visualization, droplet size and velocity measurement of a water-borne paint spray under a range of operating parameters including liquid flow rates, shaping air flow rates, bell rotational speeds and high voltage settings. Their results showed that the bell speed dominated atomization, but high voltage and flow rate settings significantly modified spray transport, including: droplet sizes decreased with increased bell speeds and finer-

sized droplets decreased the spray cone width; increased liquid flow rates widened the spray cone shape whereas higher shaping air flow rates narrowed the spray cone width; and higher electric field voltages caused the spray to become more dense and uniform in the cone core region. The code they developed used the Euler-Lagrange approach to simulate electrostatic and drag forces acting on the droplets, but effects of the droplets on air, and droplet breakup and coalescence were not assessed.

Research has also been performed to examine the effects of ERBS bell designs on TE and the quality of coatings. For example, Domnick (2010) examined the changes in droplet size distributions and deposition processes for designs having different bell geometries with smooth, straight serrations and cross-wise serrations as the diameters, bell speeds, liquid flow rates and bell edge velocities were varied. Both of the serrated bells at high bell rotational speeds produced bimodal droplet size distributions having decreased droplet size maximums in comparison to when no serrations were present.

Few studies have been done so far on dynamic targets, i.e. where relative motion between the spray gun and the target exists; such relative motion can affect the deposition processes substantially. For a dynamic target, in which the target surface moves in a constant velocity, the boundary layer on a target surface differs from that of a static or stationary target. Mark et al. (2013) developed a numerical method to solve Navier-Stokes equations considering that the airflow was coupled with the electrostatic field and charged droplets and the target was dynamic. Experimental investigations performed on both plate and car fenders were performed to validate their numerical simulations.

An important issue with the use of ERBS with metallic paints has been suggested to be the resultant dull finishes and apparent color changes that it can produce. Fukuta et al.

(1993), Inkpen and Melcher (1987) and Im et al. (2004) investigated possible factors contributing to color change and dullness and concluded the cause was related to the distortion of the aluminum flakes in transit to the target. To overcome this issue it was postulated that the bell rotational speed should be maintained only in a limited optimal range that produced fine droplets and prevented aluminum flake distortion; simultaneously, the air velocity should be high enough to maintain flake orientation parallel to the substrate. Nevertheless, their values of TE were near 65%, a value much lower than the 90% TE reported (Im, 1999) for normal ERBS operations. Currently, the issue of finding a balance between color and TE for metallic paints still persists for ERBS's.

The objective of the current study is to develop a digital coating method to drastically reduce overspray and conserve painting material and to minimize environmental impact. The digital atomizer can generate mono-dispersed droplets, with significantly reduced overspray. CFD simulation in combination with a paint rheology model is used to estimate the operational performance of the proposed digital atomizer. A volume-of-fluid (VOF) method is used to capture the dynamics of the free boundary between the liquid and air. The VOF approach is chosen due to its robustness and computational efficiency in handling global topological changes which occurs in breakup processes. Effects of involved parameters, including inlet flow rate, actuator frequency and liquid properties on ejected droplets' characteristics, droplet diameter and their successive spacing are studied in detail.

CHAPTER 3

3 Governing Equations and Numerical Simulation

3.1 Introduction

This chapter is devoted to the analysis of breakup phenomena of an ejected filament using numerical method. First, the problem associated to each issue, satellite drop, droplet size and coating applicator will be stated. Then, the governing equations of forced liquid jets and their characteristics are reviewed. By non-dimensionalizing the governing equations, driving parameters are obtained. Numerical simulation of liquid jet disintegration using a Volume-of-Fluid (VOF) interface tracking method is detailed. A brief review of the interface-capturing scheme employed in the present study is provided. Then for each issue, the capability of the interface tracking model is validated by the experimental results obtained in the literature. Finally, parametric study on the influence of influential factors driving the phenomena is reported.

3.2 Problem statement

3.2.1 Satellite droplet issue

The physical system considered in the current study is same as the inkjet prototype studied in (Castrejón-Pita et al., 2011). In this study a large-scale DOD generator capable of producing droplets with diameters ranging from 250 μm up to 4 mm and is designed to resemble the fluid mechanical conditions relevant to a typical commercial inkjet print-head. Figure 17 shows a brief schematic of the experimental setup. Injection process is carried

out by pressure pulsating provided by a loudspeaker actuator. The injection system consists of two liquid chambers, one inside the print-head above the nozzle, and another larger one that is open to the atmosphere. The largest one is for two intents: one to feed liquid into the print-head and two, to control the meniscus position at the nozzle tip. By controlling the height of the smaller container, one can easily grasp the meniscus from dripping. Figure 18 shows the dimensions of the print-head. The nozzle is machined out of a 3 mm PMMA sheet with precision of 50 μm with a diameter of 2 mm.

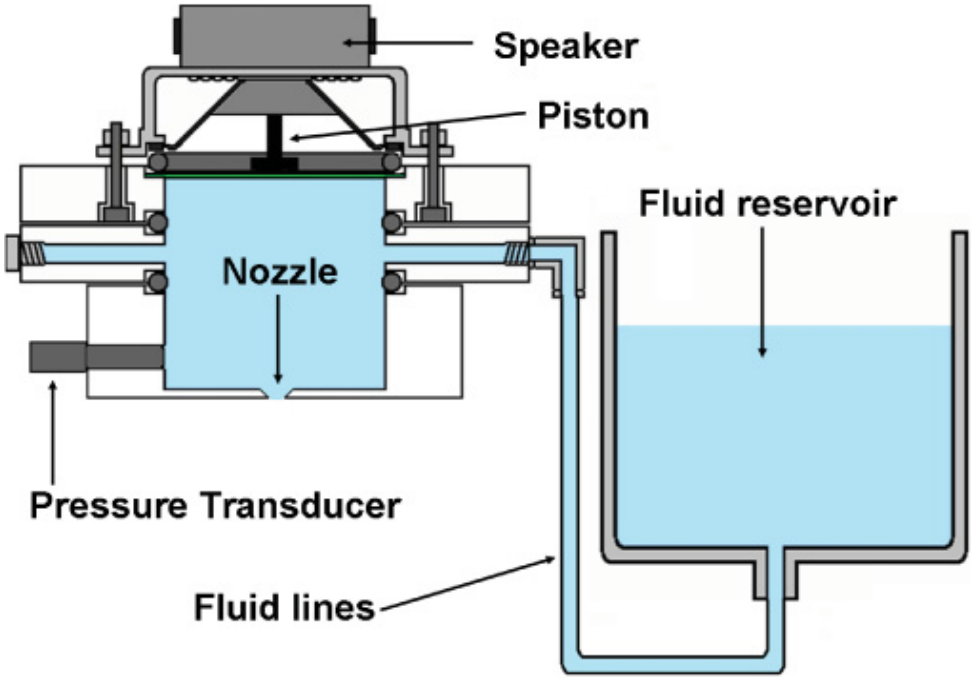

Figure 17. Schematic of the experimental setup of DoD generator utilized in (Castrejón-Pita et al., 2011)

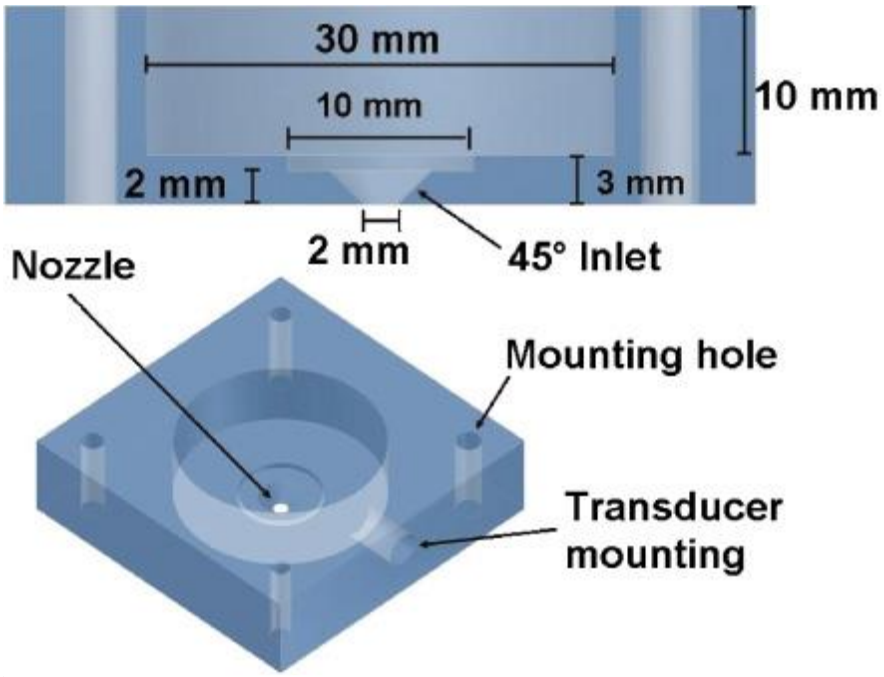

Figure 18. Perspex print-head design parameters in Castrejón-Pita et al. (2011)

Figure 19 presents the schematic of a large scale model inkjet with the detailed geometry of the nozzle and print-head, and the model structure to simulate performance of a nozzle radius of 1 *mm*. Worthy to note that our current study focuses on DOD formation by modeling a conjectured velocity waveform at the print-head inlet. The inlet velocity for the numerical simulation has the same profile as (Castrejón-Pita et al., 2011) and with it, a transient flow rate is imposed at the inlet to play the role of piezoelectric push-pull operation. A no-slip condition was imposed on the wall inside the print-head, and a static contact angle on the wall is assumed as 10^{o} in order to pin the contact line at the edge of the nozzle outlet (Castrejón-Pita et al., 2011).

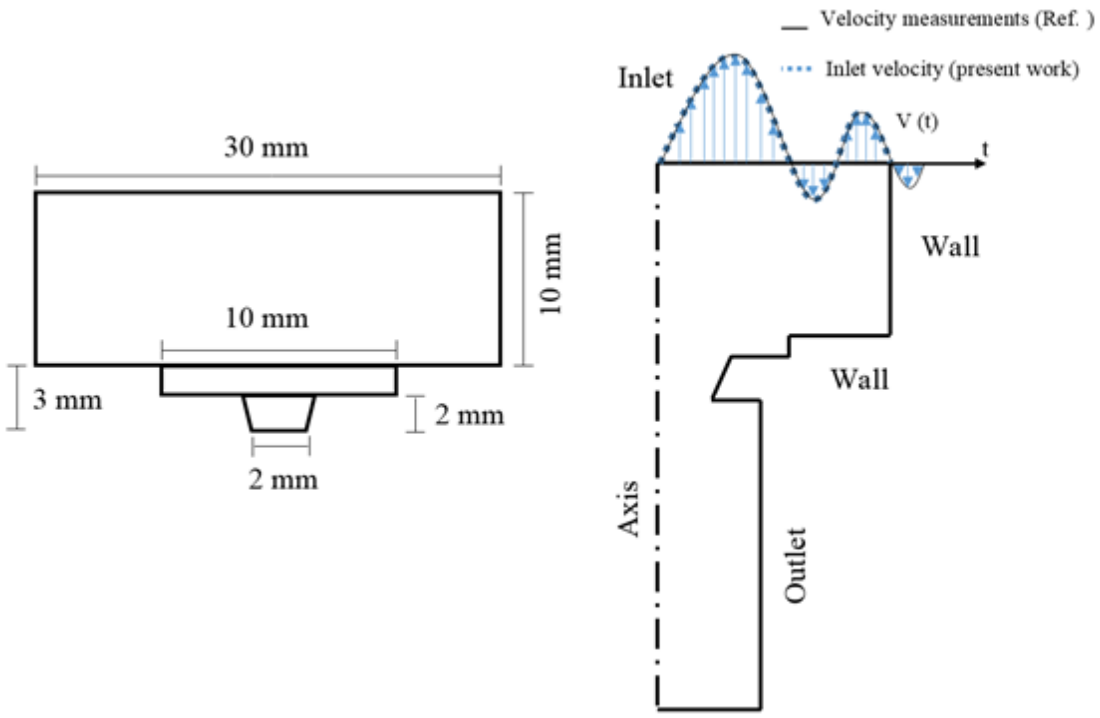

Figure 19. Left: schematic of the large scale inkjet used in (Castrejón-Pita et al., 2011), right: schematic of the current model employed to simulate the large scale inkjet print-head.

We treat the problem as 2-D symmetry and compute only a symmetric half of the domain. The problem statement for droplet size issue is similar, however, the main focus will be toward finding a way to drastically lower the droplet size without changing the geometry of the print-head.

3.2.2 Coating Application

Figure 20 shows a 3-D schematic of the atomizer employed in the current study. It depicts the liquid nozzle and the co-flow air nozzle. Besides, there is a piezoelectric actuator capable of pulsating the paint liquid at high frequencies up to 150 kHz. This actuator with a sinusoidal wavelength signal pushes the paint into the liquid nozzle which is then carried

out by air flow to be delivered by carbody. This periodic procedure leads to generation of mono-dispersed distribution of droplets. Considering a fixed spray geometry, controlling parameters in the present study are the liquid inlet flow velocity and the frequency imposed by the actuator to the inlet paint liquid. The liquid nozzle diameter is chosen to be 50 micron, and the air velocity is 10 m/s.

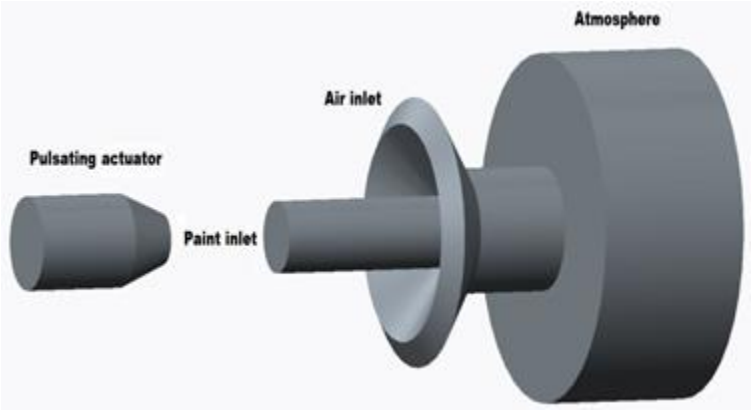

Figure 20**.** Schematic of the atomizer coupled with a pulsating actuator.

The atomizer is modelled in ANSYS FLUENT. The problem is considered symmetric, as such a 2-D symmetry approach is used in which only a symmetric half of the domain is computed. The domain is meshed using ANSYS meshing capability. For the boundary and regions close to the axis, where the rate of fluid property variation is high, finer grid sizes are used, which is about one micron in size. The number of gird cells is chosen to make sure that property differences in adjacent cells are captured in the simulation. Some of the main assumptions are; the internal liquid and air flows are laminar: this assumption stems from the fact that *Re* number for inlet liquid and for inlet air are 100-800 and 20-150 respectively; the flow phenomena can be considered axisymmetric: holding the first assumption to eliminate swirls and eddies in the flow filed, and

considering this fact that during Rayleigh type regime, axisymmetric waves as well as axisymmetric breakup are the dominant mechanisms of atomization, leading to having a 2-D axisymmetric flow; both liquid and air are treated to be incompressible flows: this assumption is due to small Mach number which is less than 0.5; the liquid transport properties, except viscosity, are known and constant; external air flow around the atomizer is neglected and the atomization takes place in a stagnate atmosphere: this assumption is just a simplification; boundary layer at the target surface is not considered: this assumption is just a simplification; evaporation of the liquid during atomization process in neglected: this assumption is just a simplification.

3.3 Numerical Method

3.3.1 Satellite droplet issue

Liquid jet breakup phenomena can be classified as a multi-phase processes involving liquid and gas flows. Describing the breakup can be represented through unsteady-state Navier-Stokes equations in their conservation forms, in which mass and momentum conservation can be written as follows (two dimensional):

$$\frac{\partial \rho}{\partial t} + \nabla.(\rho \vec{V}) = 0 \tag{3-1}$$

$$\frac{\partial (\rho \vec{V})}{\partial t} + \nabla.(\rho \vec{V} \vec{V}) = -\nabla p + \nabla.\left[\mu(\nabla \vec{V} + \nabla \vec{V}^{T})\right] + \rho \vec{g} + \vec{F}_{\sigma} \tag{3-2}$$

where $\vec{V}=(u,v)$, p is the pressure, $\vec{g}$ is the gravitational acceleration, μ is the viscosity, and $\vec{F}_\sigma$ is the surface tension force per volume. These two equations are valid for both flow filed and interface regions.

In the current study, a VOF model (Yang et al., 2013, Poozesh et al., 2015a) is employed to simulate two immiscible phases of air and liquid by solving a single set of momentum equations and tracking the volume fraction of a particular phase in each cell throughout the model domain. VOF as an interface-capturing technique employs the volume fraction as an indicator function to specify involved phases. The interface is a transition area where the fluid is a weighted mixture of the involved phases. The volume fraction indicator operator is given as:

$$\alpha=\begin{cases}1 & \text{For regions inside the representative phase}\\ 0<\alpha<1 & \text{For interface region}\\ 0 & \text{For regions outside of the representative phase}\end{cases}$$

So $D\alpha/Dt=0$ and, the continuity equation across the interface becomes

$$\frac{\partial\alpha}{\partial t}+\frac{\partial}{x_i}(V\alpha)=0 \tag{3-3}$$

Eq. (3-3) is solved for the volume fraction of one or more phases and to track the interface between them. For a representative phase *q*, the transport equation at the interface, equation (3-3) gives us the following:

$$\sum_q\frac{1}{\rho_q}\left[\frac{\partial}{\partial t}(\alpha_q\rho_q)+\nabla.(\alpha_q\rho_q\vec{V}_q)\right]=\sum_q\frac{1}{\rho_q}\sum_{p=1}^{n}(\dot{m}_{pq}-\dot{m}_{qp}) \tag{3-4}$$

where $\dot{m}_{pq}$ is the mass transfer from phase p to phase q, and $\dot{m}_{qp}$ is the mass transfer from phase q to phase p. The volume fraction of the primary-phase, which in this study was air, will be obtained based on the following equation:

$$\sum_{q=1}^{n} \alpha_q = 1 \tag{3-5}$$

where α is the volume fraction, and q describes the phases in the system.

Eq. (3) is solved by explicit time discretization as following:

$$\frac{\alpha_q^{n+1}\rho_q^{n+1} - \alpha_q^n \rho_q^n}{\Delta t} V + \sum_f (\alpha_{q,f}^n \rho_q \vec{U}_f^n) = V\left[\sum_{p=1}^{n} (\dot{m}_{pq} - \dot{m}_{qp})\right] \tag{3-6}$$

where $n+1$ is the index for the current time step and n is the index for a previous time step, $\alpha_{q,f}$ is phase value of the q^{th} volume fraction computed from a compressive scheme, V is the volume of cell, and U_f is the volume flux through the face, based on normal velocity.

The surface stress tensor due to surface tension is represented as:

$$T = \sigma(I - \hat{n} \otimes \hat{n})|\vec{n}|$$

where I is the unit tensor, σ is the surface tension coefficient, $\otimes$ is the tensor product of two vectors, and

$$\hat{n} = \frac{\vec{n}}{|\vec{n}|} \quad \text{and} \quad \vec{n} = \nabla \alpha$$

and the surface tension force is represented as:

$$\vec{F}_{\sigma} = \nabla.T$$

The volume fraction of secondary phase is obtain via Eq. (3-5) and Eq. (3-6) can be used to obtain the primarily phase's volume fraction.

In the VOF model, a single momentum equation is solved throughout the domain, and the resulting velocity field is the same at the interphase. The foregoing momentum Eq. (3-2) is dependent on the volume fraction of the two phases through the properties of ρ and μ; in each control volume, the volume fractions of all phases sum to unity. The fields for all variables and properties are shared by the two phases and are volume-averaged values, if the volume fraction of each of the phases is known at each location. Thus, depending upon the volume fraction values, the physical properties in each cell are purely representative of one of the phases or of a mixture of the phases, and values of properties or desired variables in each cell will be determined based on their respective volume fraction. For instance, if the volume fraction is shown by α, the density in each cell is given by:

$$\rho = \alpha_g \rho_g + (1-\alpha_g)\rho_l \tag{3-7}$$

where the subscripts *g* and *l* represent gas and liquid phases, respectively. Generally, for an *n*-phase system all of these properties can be represented by:

$$\vartheta = \sum \alpha_q \vartheta_q \tag{3-8}$$

in which *q* is a chosen phase and ϑ is a representative property. Hence, the number of equations is *4n+1* equations and the number of unknowns is *5n*. Because *n-1* additional

equations are needed to calculate the unknowns, it is possible to apply constraints on the pressure that all involved phases share the same pressure field, such that:

$$p_q = p, \quad \forall q \in [1, n] \tag{3-9}$$

The pressure implicit with splitting of operators (PISO) scheme along with two additional corrections, including neighbor correction and skewness correction were used for the pressure-velocity coupling. Simultaneously, a pressure staggering option scheme and second-order upwind scheme were employed for interpolating the pressure and momentum equations, respectively. Then, a geo-reconstruct scheme was utilized to reconstruct the interface. Finally, a variable time-stepping method, in which the time step is calculated for a fixed value of the Courant number (0.2), was used for reducing calculation times.

To have a better understanding of the important parameters influencing breakup phenomena, momentum equation needs to be non-dimensionalized. Considering Eq.(3-2), and substituting obtained expression for the surface tension force and then nondimensionalizing it based on a length scale (e.g., nozzle radius, *R*), and a velocity scale (e.g., scaled velocity, *U*), we can write:

$$\vec{x}^* = \frac{\vec{x}}{R},\ \vec{V}^* = \frac{\vec{V}}{U},\ t^* = \frac{t}{R/U} \quad and \quad p^* = \frac{p}{\rho U^2}.$$

$$\frac{U^2}{R}\left[\frac{\partial(\vec{V}^*)}{\partial t^*} + \nabla.(\vec{V}^*\vec{V}^*)\right] = -\frac{U^2}{R}\nabla p^* + \frac{U\mu}{\rho R^2}\nabla.\left[\nabla\vec{V}^* + \nabla(\vec{V}^*)^T\right] + \frac{\sigma}{\rho R^2}\nabla.\left[(I - \hat{n}\otimes\hat{n})|\vec{n}|\right]$$

So,

$$\frac{\partial(\vec{V}^*)}{\partial t^*} + \nabla.(\vec{V}^*\vec{V}^*) = -\nabla p^* + \frac{1}{\mathrm{Re}}\nabla.\left[\nabla\vec{V}^* + \nabla(\vec{V}^*)^T\right] + \frac{1}{We}\nabla.\left[(I - \hat{n}\otimes\hat{n})|\vec{n}|\right]$$

This shows that by assuming an incompressible flow for a typical inkjet print-head, the breakup phenomena is controlled by two dimensionless parameters, *Re* and *We* numbers.

In general, jet breakup of a liquid filament may arise because of a strangulation of the filament by surface tension which acts as a driving cause, while the inertia and viscos forces act as retarding causes to suppress filament breakup (Delhaye et al., 2013). Accordingly, two independent pi-numbers describing this competitive nature were identified (Emori et al., 2008) and included W*e*, which can be represented by a ratio of the inertial force-divided by the-surface tension force, and *Re*, which can be represented by a ratio of the inertia force-divided by the-viscous force. Another pi-number, the *Oh* number, was derived from a combination of *We* and *Re*, where $Oh = We^{1/2}/Re$. Previous research outcomes have discussed these three dimensionless numbers (Emori et al., 2008), or pi-numbers. For the benefit to past studies, all three pi-numbers are calculated, as following:

$$We = \frac{\rho U^2 R}{\sigma} \quad , \quad \mathrm{Re} = \frac{\rho U R}{\mu} \qquad and \quad Oh = \frac{\mu}{\sqrt{\rho R \sigma}} \tag{3-10}$$

where *R* is the nozzle radius *(m)*, *V* is the velocity scale of the droplet ejection process (*m-s*$^{-1}$) which will be determined later, σ is the surface tension (*N-m*$^{-1}$) of liquid drop surrounded by air, and ρ is the density (*kg-m*$^{-3}$) of the ejected liquid. Since *Oh*, *We* and *Re* numbers are interdependent, e.g. $Oh = \sqrt{We} / \mathrm{Re}$, liquid filament break up may be described while employing either *We* and *Oh*, or *Re* and *We*, numbers.

It is important to note that recent studies (Castrejón-Pita et al., 2012a, Hoath et al., 2013) have sought to find a boundary between the operating regimes for satellite formation, and have considered two non-dimensional numbers, the aspect ratios l / R', where R' is the

radius of the cylindrical filament, and *Oh*. However, the process of DOD formation is dependent on liquid properties, print-head geometry and the input driving signal (Dong et al., 2006). Hence, the current study uses the radius of the nozzle to characterize print-head geometry and the velocity of the droplet as the input driving signal, and enables the following to be stated:

$$l = fn(\rho, \sigma, \mu, U, R), R' = fn(\rho, \sigma, \mu, U, R) \tag{3-11}$$

Using a previously discussed scaling analysis technique(Emori et al., 2008) with two separate characteristic lengths l and R', and using ρ, V and R as the repeating parameters, the following is derived:

$$l / R = fn(We, \mathrm{Re}), \quad R' / R = fn(We, \mathrm{Re})$$

and

$$l / R' = fn(We, \mathrm{Re}) \tag{3-12}$$

Therefore, the aspect ratio is a function of the two fundamental numbers, *We* and *Re*, both of which depend on the liquid properties and nozzle size as well as the droplet velocity. Although the three pi-numbers *Oh*, *Re* and *We* were introduced as a way to characterize the DOD formation process, their interdependency requires to the use of either (*Re* and *We)* or (*Oh* and *We)* numbers to delineate the boundaries between the two regimes.

3.3.2 Droplet size

For the purpose of examining different operational conditions, a time-periodic Hagen-Poiseuille flow boundary condition was axially imposed at the print-head inlet as the inflow boundary condition, where

$$u = [1 - (\frac{2r}{D})^2]u_m \sin(ft) \tag{3-13}$$

The symbols *u, f, D* represent the axial component of the velocity, the temporal frequency of the imposed flow rate and the print-head inlet diameter, respectively. For droplet size issue, the liquid properties are fixed; so *Oh* number is constant. In order to take into account the effects of velocity modulation at the print-head inlet, also defined were:

$$We = \frac{\rho u_m^2 R}{\sigma} \quad and \quad \Omega = f\sqrt{\rho R^3/\sigma}$$

where Ω is a non-dimensional temporal frequency, scaled with capillary time $\sqrt{\rho R^3/\sigma}$, (Chen and Basaran, 2002).

3.3.3 Coating application

- **Power Law for Paint Non-Newtonian Viscosity**

Power law model is one of the most widely used constitutive equations for the simulation of transport process of shear rate dependent viscosity fluids. Non-Newtonian paint will be modeled according to the following power law for the non-Newtonian viscosity:

$$\eta_{\min} < \eta = k\dot{\gamma}^{n-1}H(T) < \eta_{\max} \tag{3-14}$$

In which k is a measure of the average viscosity of the fluid (the consistency index); and n is a measure of the deviation of the fluid from Newtonian (the power-law index); $\eta_{\min}$ and $\eta_{\max}$ are, respectively, the upper and lower limiting values of the fluid viscosity. The value of n determines the class of the fluid, which for our case of water borne (WB) paint is less than 1. In order to get the input parameters for WB two data sets, provided by a client company and with data measured at UK (Figure 21) were used in the CFD simulation. From this data, k and n will be 5.6 and 0.44 respectively.

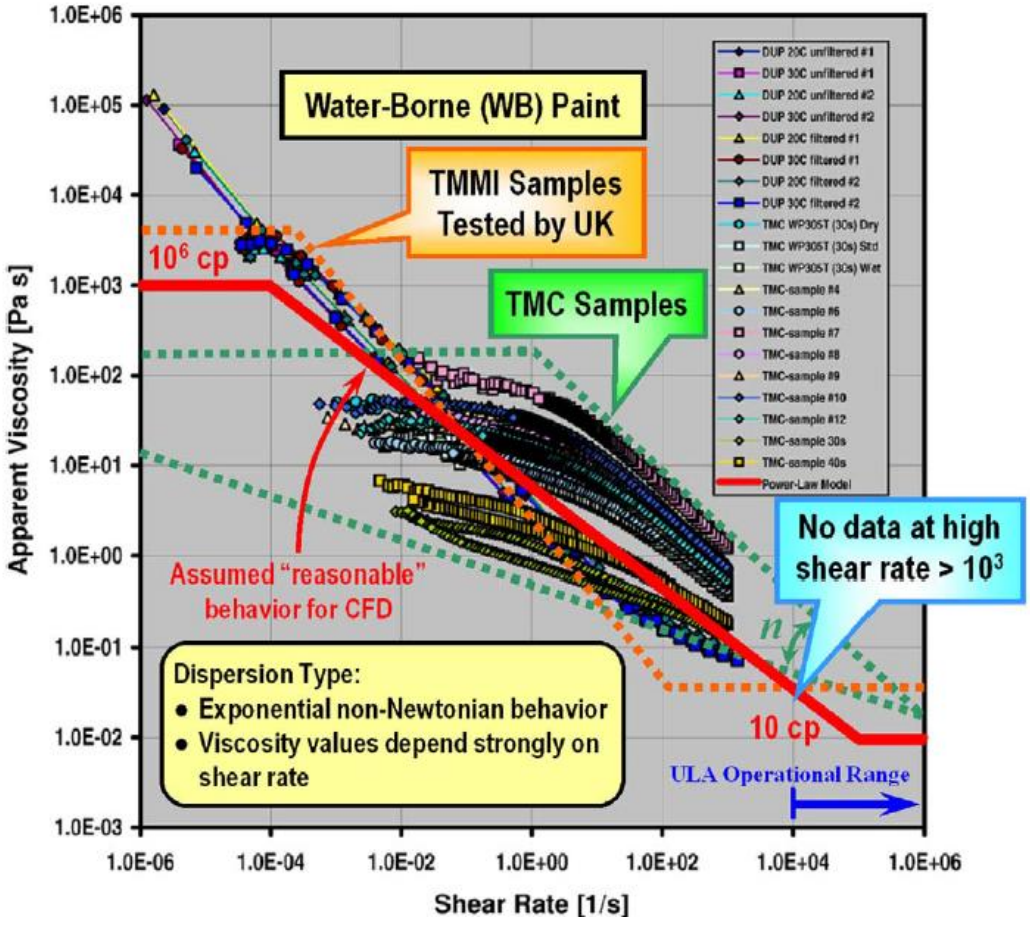

Figure 21. Water-borne paint viscosity vs. shear rate data. Two set of data are presented: (1) data provided by TMC, and (2) Samples provided by TMMI w/data measured at UK (Salazar and Saito, 2008)

3.4 Validation of the current numerical simulation

The computational domain is divided into three parts: the ink chamber, the nozzle, and the area outside of the nozzle. To achieve a uniform distribution of the discretization errors, finer grid sizes are chosen that adopt a small grid spacing in regions such as near the nozzle, the immediate solid walls, and the trajectory of the flight drops of which the derivatives of the variables change erratically and large discretization errors are expected. The number of gird cells is chosen to make sure that property differences in adjacent cells are captured in the simulation. Figure 22 presents the grid size independency test proving that the variations of droplet axial position by choosing 39483 elements are negligible. For our simulation, we employed the following values: a glycerol-water mixture with the density, viscosity, and surface tension of 1222 kg-m-3, 0.1 kg-$m^{-1}s^{-1}$, and 0.064 N-m^{-1}, respectively.

Figure 22 shows that the current numerical simulation is in reasonably good agreement (with maximum relative error of 7%) with Castrejon-Pita *et al.*'s experimental results. There is a problem, however, with the Lagrangian simulation presented in (Castrejón-Pita et al., 2011) which is alleviated in the current numerical simulation. The negative inflow after 15 *ms* up to pinch-off to occur about 20 *ms* may locally affect the tail of the liquid thread by pulling the tail toward the nozzle and thus leading to a decrease in the forward momentum of tail tip (Castrejón-Pita et al., 2011). In the numerical simulations, this negative inflow is neglected, so it creates an overestimated forward momentum which in turn, might result in overestimated forward momentum of droplet after the tail was fully absorbed into the head, and consequently results in slightly overestimated falling velocity compared to the experiment. However, by considering gravity in the experiments as

another participating force, which is more important after droplet pinching off, the numerical simulation, on the other hand, must create an underestimation for the droplet axial position. Therefore the numerical results of droplet axial position shall get closer to the corresponding experimental results and finally cross it at some point. Thus the observed deviating trend (Castrejón-Pita et al., 2011) is not in accord with physical common sense of droplet behavior. This can be because of missing grid independency test which guarantees the result accuracy. As can be seen from Figure 10, the current numerical simulation is favorably showing the trend. Figure 23 schematically compares between the current numerical simulation and the experimental results (Castrejón-Pita et al., 2011) for droplet shapes at five different time periods after the liquid filament ejection, t=21 *ms* and 20 *ms* for experimental and the present work, respectively. The single-flash photograph is on the left and the simulation plot is on the right. There is a close correspondence between the drop shapes computed in the simulation and those observed in the experiment. Worthy to note that there are also flash timing errors in the experimental results which might hinder us to have precise timing for droplet shapes. Qualitative droplet shape comparisons for single flash images obtained from the experiments and the ones obtained from Lagrangian method (Castrejón-Pita et al., 2011) show a maximum error of 4*ms* between the nearest matches. However in the current numerical simulation, the maximum error between the corresponding matches is less than 1*ms*.

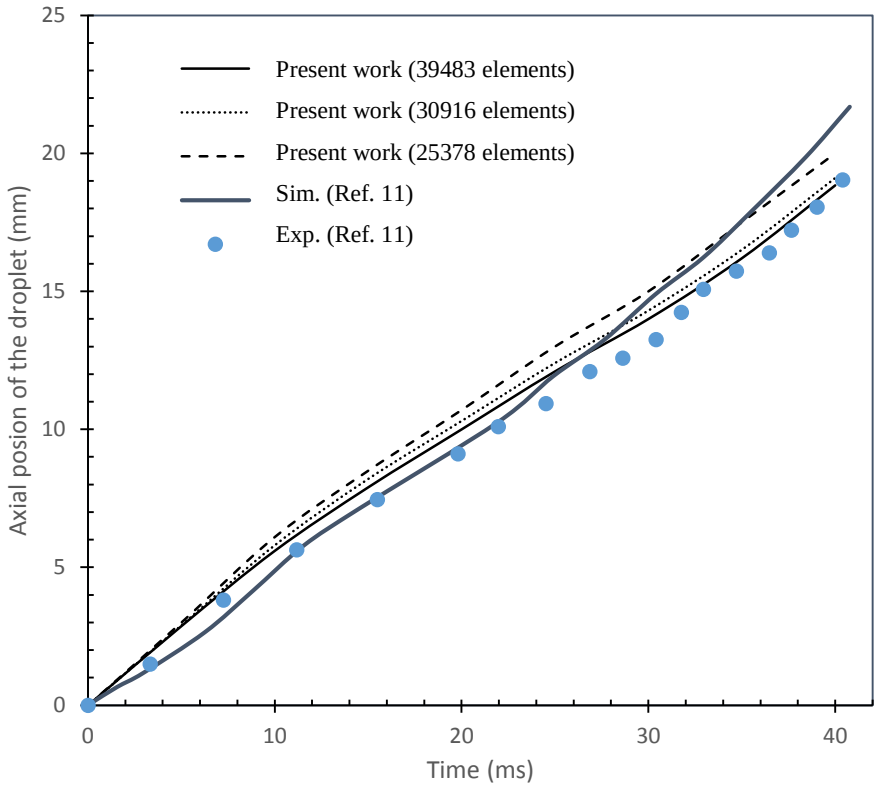

Figure 22. Grid independency test and validating the current numerical simulation

(a) (b) (c) (d) (e)

Figure 23. Experimental results of filament evolution (Castrejón-Pita et al., 2011) alongside their corresponding current numerical simulation results; frames are separated by 3 ms, starting at 21 ms and 20 ms after ejection, (a), for experimental and present work, respectively.

This validation task can be used for both satellite and droplet size issue. To verify present numerical simulation for coating purposes, a comparison to the analytical equation for size of droplets formed during the breakup of cylindrical liquid jets based on instability analysis is made. Teng *et al*. (Teng et al., 1995) obtained the following equation for liquid-in-liquid or liquid-in-gas systems

$$\frac{d}{d_0} = \left(\frac{3\pi}{\sqrt{2}}\right)^{1/3}\left[1+\frac{3\mu}{\sqrt{d_0\rho\sigma}}\right]^{1/6} \tag{3-15}$$

where d and d_0 are droplet mean diameter and needle diameter, respectively. And μ, ρ and σ are respectively viscosity, density and surface tension of the atomized fluid. This equation applies to low-velocity Newtonian or non-Newtonian fluids flowing through a low viscosity gas. As can be seen from Table 2, a good agreement between the numerical simulation results and droplet size obtained from equation (3-15) exists.

Table 2. Comparison between current numerical simulation with water as liquid and air as the carrier, and analytical equation given by (Teng et al., 1995) .

Needle diameter	Droplet size		Error
	NS	Teng *et al.* (1995)	
80	137.3	151.51	0.094
50	84.8	94.85	0.106
30	56.40	57.04	0.011
20	41.95	38.11	0.101

3.5 Closure

In this chapter, first, for each issue, the problem was clearly stated and specified. Governing equations in combination with the initial and boundary conditions were given. Based on characteristic scales, then, the equations were non-dimensionilized and driving parameters were obtained. Numerical simulations of the fluid motion, governing equations, the Navier-Stokes equations, were discussed. Grid independency test was carried out to make sure the results are not dependent on the number of taken grids. To track the events of liquid evolution into a gas domain, Volume-of-Fluid based interface capturing scheme was considered. The numerical simulation results were validated using results from a large-scaled inkjet prototype reported in the literature for satellite and droplet size issues; and analytical results given in the literature for coating applicator, respectively.

CHAPTER 4

4 Results and Discussion

4.1 Introduction

In this chapter, results obtained from the numerical simulations on given issues are presented and discussed. For each defined problem, jetting performance is evaluated under various conditions. These conditions are changed either by changing input modulation configurations or liquid properties.

4.2 Results for satellite droplet issue

Liquid droplet formation processes were studied under a wide range of jetting conditions through an assessment of *Oh, We* and *Re* numbers. Figure 24, which displays the time evolution of the axial tip position for four different values of *We* and *Oh*, in which all the curves have an identical slope up to 10 *ms*. This slope points to the actual ejection speed of the droplet to be 0.6 *m/s* for all four cases depicted in Figure 24, as determined by the magnitude of the actuation pulse which gives a velocity scale for characterizing inertial effects. Then, the 0.6 m/s ejection speed was used for calculating the *We* number.

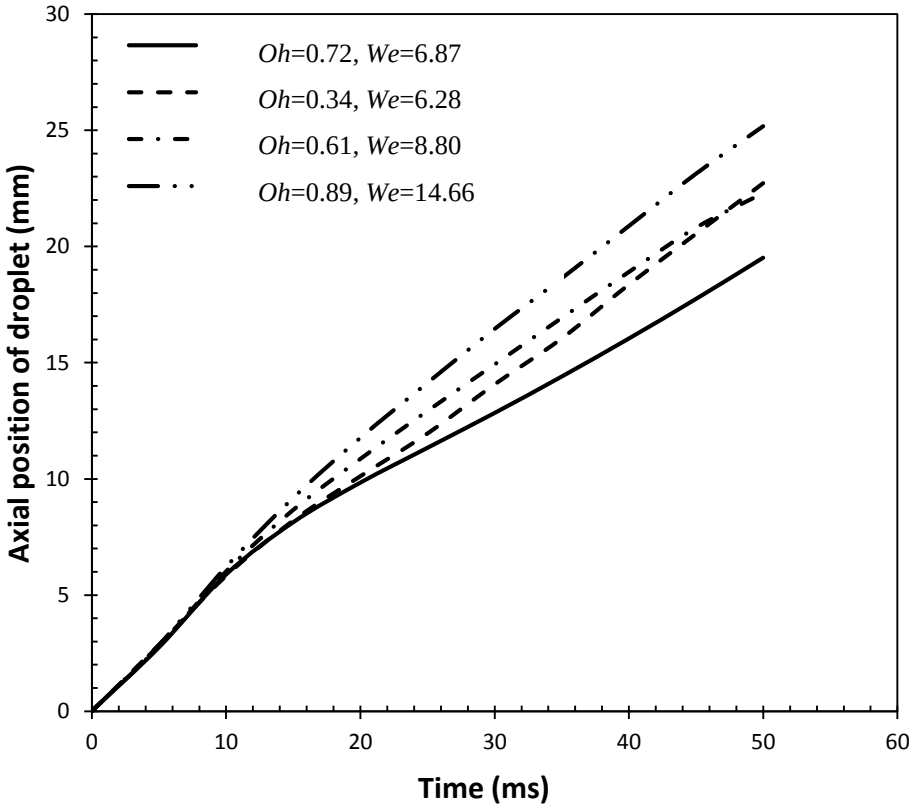

Figure. 24. Axial position of the droplet over time for different *Oh* and *We* numbers.

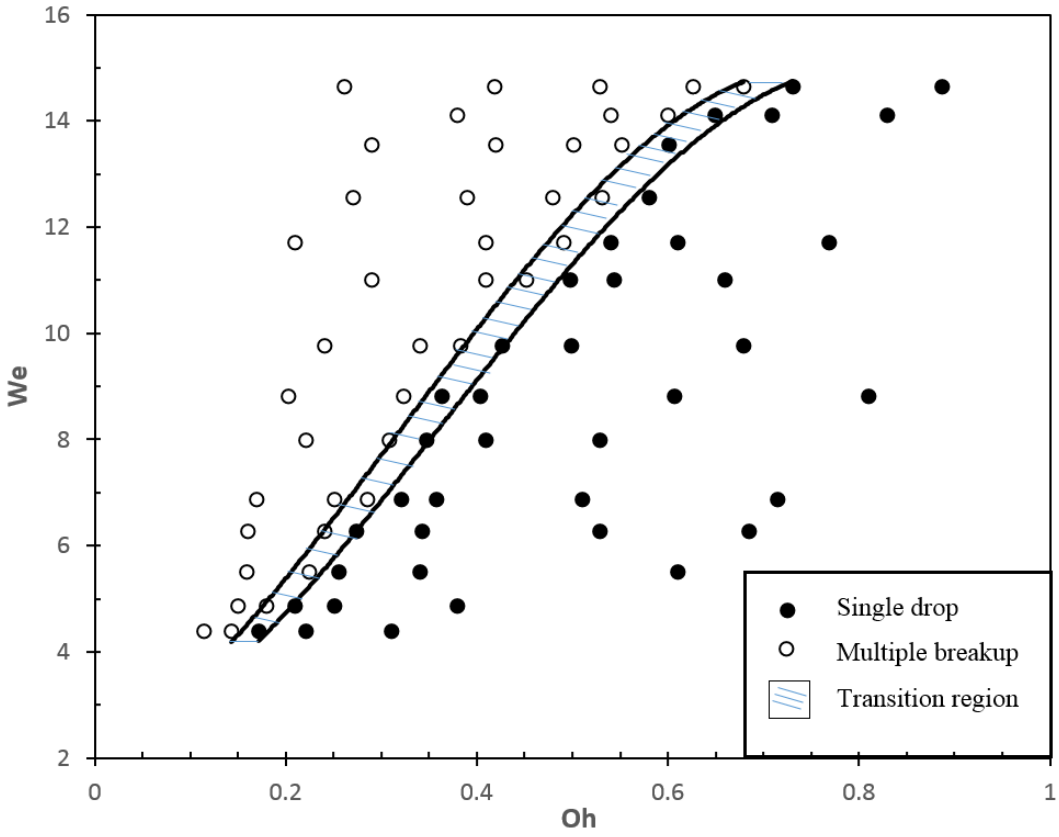

Figure 25. Criteria for single and multiple break-up based on *We* and *Oh* numbers; the solid line represents a distinction line between the two modes.

Figure 25 shows the simulation results for different jetting conditions, plotted as a function of *We* and *Oh* numbers; data are shown for $0.1 \le Oh \le 1.0$, a range which is applicable to DOD inkjet printing and typical commercial printers. The solid circles represent the generation of single droplets and the open circles denote the generation of droplets having multiple satellite droplets. The boundary between these two regimes is shown in shaded area of Figure 25, and may be called the transition region; it is a region rather than a line and represents the uncertainties within the precision of the numerical simulation or the errors related to judging whether a specified filament breaks up or not. Outside of the transition region one can be sure if filaments break up or not.

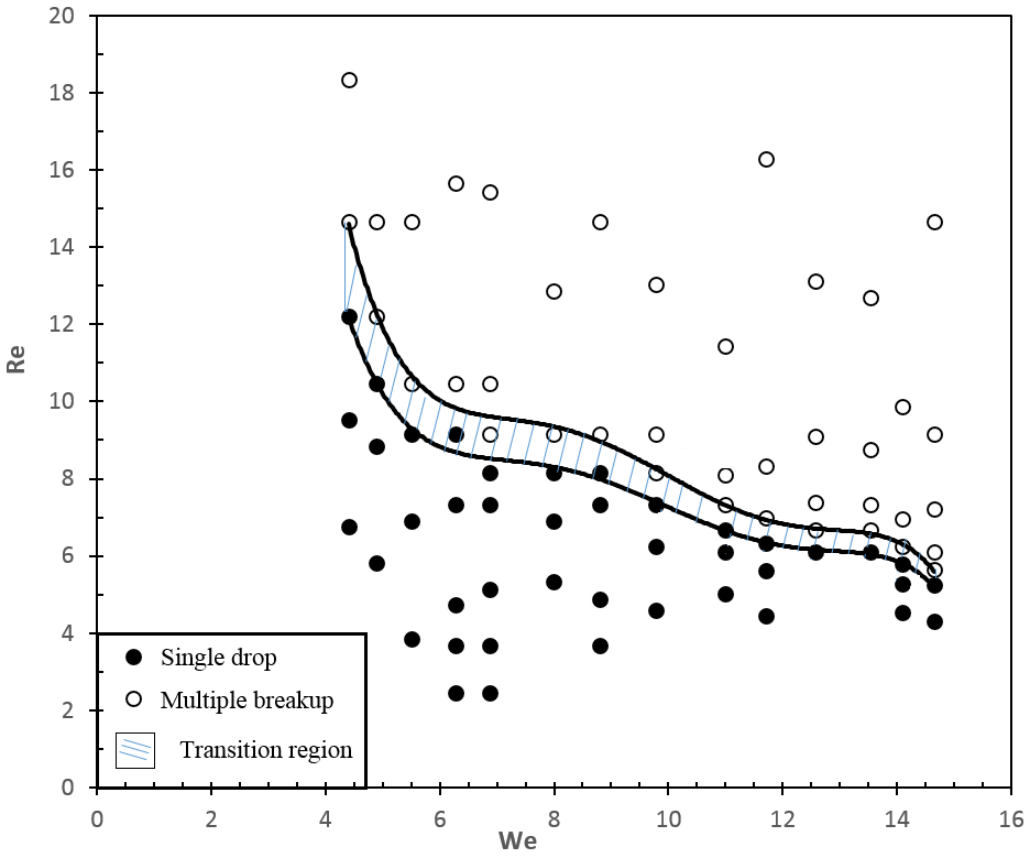

Figure 26. Criteria for single and multiple break-up based on *Re* and *We* numbers.

The information in Figure 26 shows that at a specified *We* number an increase in the *Oh* number is required to transition from breakup producing droplets with satellites to single droplets; in other words, higher fluid viscosities delay liquid ligament breakup and droplet formation. It also suggests that avoiding breakup for a long liquid thread with low surface tension would require an increase in liquid viscosity. The (*We and Oh)* number plot can be converted to a (*Re* and *We)* number plot, as shown in Figure 26; it also displays a transition region that separates single droplet and droplet with satellite regimes.

Experimentally, it is difficult and time-consuming to precisely measure droplet parameters such as initial speed and the initial relative speed of opposite ends of a liquid filament, and

the diameter and length of a liquid filament. However, Hoath *et al.*(2013) successfully acquired such data and used it to describe a simple criterion for droplet breakup based on the non-dimensional number *Oh* and the liquid filament aspect ratio. Their study has important implications but may not be strictly applicable to real ink jet operation because liquid jets that were studied only had small initial relative speeds between their two ends; furthermore, their analyses required very high precision photography to capture the ejected filament physical features, an expensive and time-consuming process.

In contrast, the significance of the current study is to propose and demonstrate a simulation method which provided excellent precision along with close replication of experimental data already available. The results of this simulation demonstrated specific criteria are required to transition between single and multiple droplet modes as described by either (*Oh* and *We)* or (*Re* and *We)* couplets, all of which were only dependent on the ejected liquid properties and the velocity waveform at the print-head inlet.

4.3 Results for droplet size issue

Liquid droplet formation processes were studied under a wide range of jetting conditions through an assessment of *We* and Ω numbers. Figure 27 shows a time history of the pressure contours and flow streamlines. Only the region closest to the nozzle tip is depicted and different stages of droplet ejection were simulated under the action of a variable pressure applied to a liquid reservoir. At t=0.0012 s, the liquid would experience an inflow from a nozzle because, for example, an applied voltage to a piezo activator would cause the liquid at the orifice of a nozzle to pull inward toward the liquid reservoir. As a consequence, a valley would be created on the liquid surface at the nozzle orifice. At other

times in the pressure sequencing when a positive pressure is applied, for example at t = 0.0023 and 0.0034 s, liquid would be ejected from the nozzle because of creating a high pressure region at liquid surface by applying an appropriate voltage to the piezoelectric activator. At t=0.0052 s, another negative inflow separates produced filament from the main liquid column. Ink refilling task as well as accelerating released filament is then carried out at t=0.0065 s. In order to returning the main liquid column to its initial position the time then elapses till the second injection process occurs. This time necessary for a liquid jet to recoil into the liquid chamber and, thereby, to prevent creation of a satellite droplet is called the relaxation time, t_r, which is variable but in this study was chosen to be 15% of the total period time.

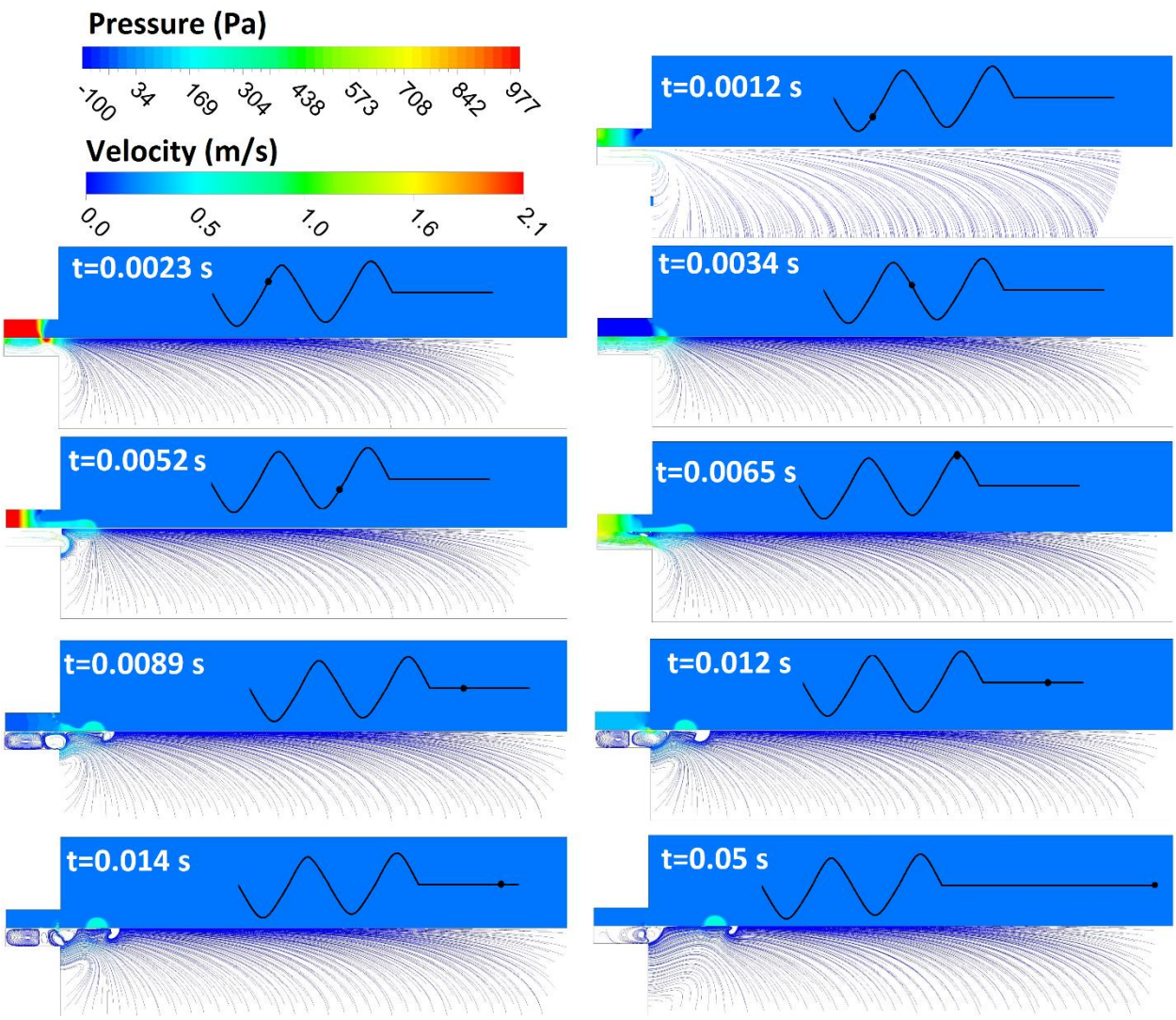

Figure 27. Time evolution of pressure contours and streamlines for nozzle with V_m=*0.11* ms^{-1} and f=*20*s^{-1}.

Figures 28 and 29 present results for two *We* numbers, one of which is moderately low at 40 and the other moderately high at 140.4. and different Ωs. When Ω=0.02 and Ω=0.04, the main droplets had the highest volumes were accompanied by satellite droplets. As Ω was increased to greater than about 0.05, satellite droplets were eliminated and droplet sizes decreased. However, an increase in Ω also decreased the duration of liquid inflow to the reservoir and, as a result, any droplet expelled from the nozzle had low energy and

would not travel very far from the nozzle tip. Hence, for $\Omega \geq 0.12$, no droplet was ejected from the nozzle; rather, only disordered oscillations occurred on the liquid surface at the nozzle outlet.

Figure 29 represents the same type of data depicted in Figure 28 but when *We* = 140.4; Interestingly, the droplet ejection process became more complex and showed many changes as the value of Ω was increased. At low Ω, as also shown in Figure 5, the main droplets were accompanied by satellite droplets and increasing the frequency to $\Omega = 0.24$ caused the formation of pure, independent droplets. Such independent droplets were also formed when $\Omega = 0.43$ and 0.51, whereas Ω values between 0.24-to-0.43 and 0.43-to-0.51 caused satellite droplet formation; the droplet sizes also decreased as Ω was increased when either independent droplets or satellites were formed. Unlike for the conditions used for Figure 28, at relatively high frequencies when Ω was greater than 0.43, and for the first cycle, no droplet was produced because the inertial force of the liquid was not enough to overcome viscous and surface tension forces and the produced filament was re-absorbed by the bulk liquid. However, in subsequent cycles the inertial force was sufficient to release a tiny drop with a proper velocity. At $\Omega=0.6$, no droplets were formed and the bulk liquid surface oscillations observed during the *We* = 40 cycle in Figure 5 was repeated.

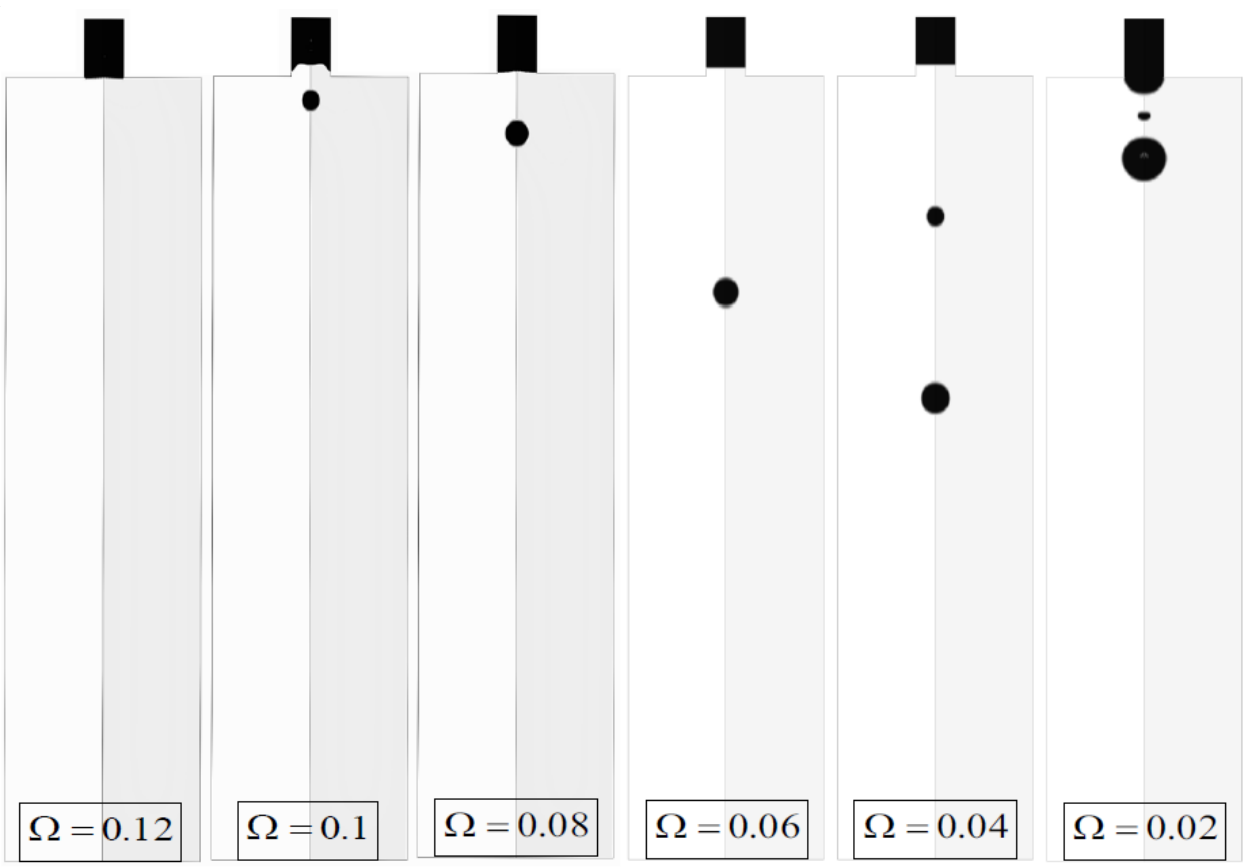

Figure 28. Injection process for different frequencies in We = 40 at $\hat{t} = 10.1$

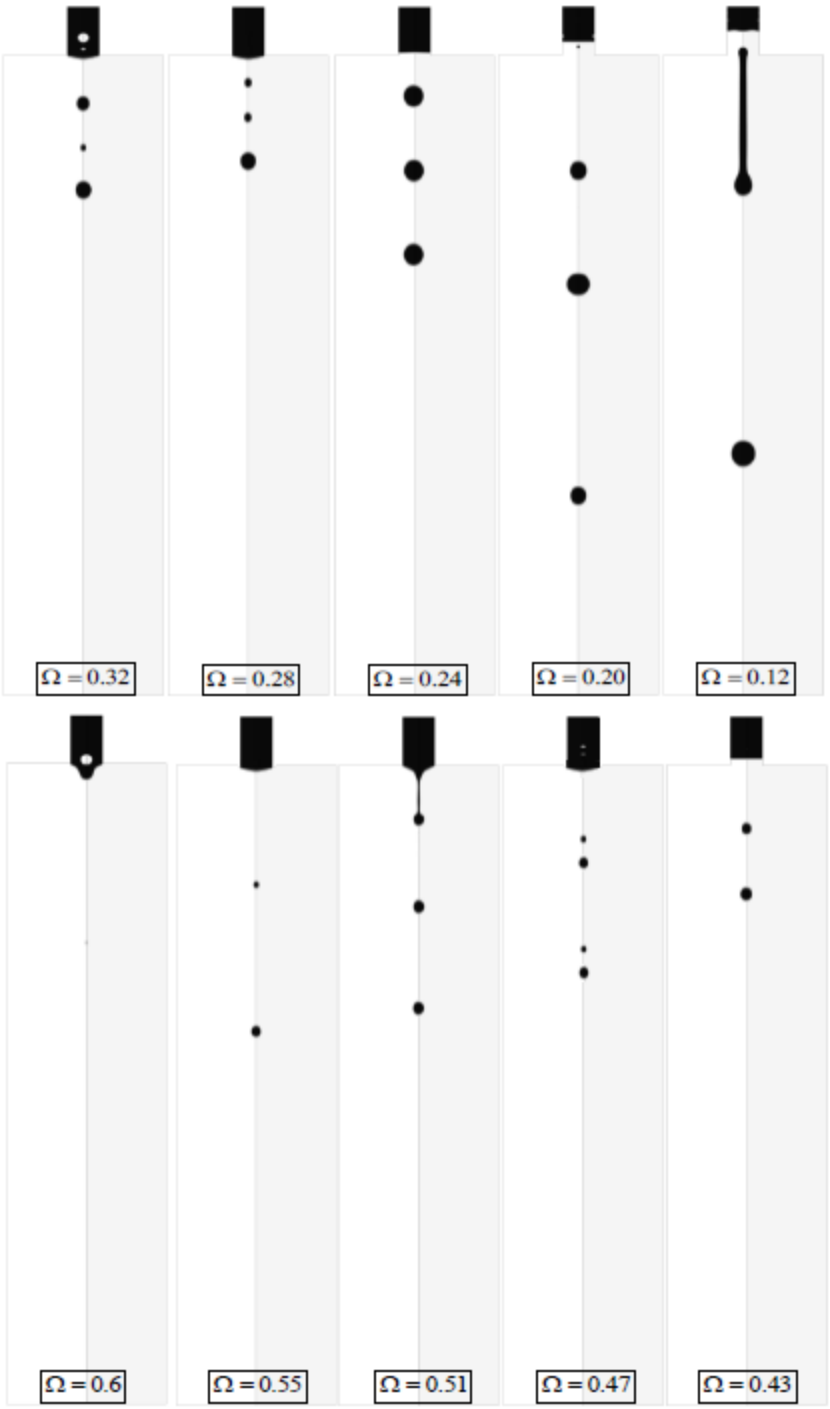

Figure 29. Injection process for different frequencies in We=140.4 at $\hat{t} = 10.1$.

In order to examine the formation process of each studied case with specified *We* and Ω over time, the mass flow rate per droplet cycle was calculated by using the equation

$\dot{M} = \int \rho u dA$ to examine the repeatability of droplet formation and flow past a fixed plane positioned 6 *mm* below the nozzle tip as both *We* and Ω were varied. Figure 30 shows the results of this test for the case when *We* =140.4; it also displays droplet mass flow rate with time. Filaments with larger leading and trailing masses were released from the nozzle when $f=50\ s^{-1}$, and they contained different shapes during each droplet ejection cycle. As observed in Figure 6 at Ω=0.2, resultant droplets are also varied in size. According to Figure 7, modulation with $f=60\ s^{-1}$represents the injection case resulting in a chain of same size droplets in every cycle from the beginning. When $f=130\ s^{-1}$, no droplets were ejected during the first three cycles, however after these initial cycles, the high pressure zone at the circular surface of the liquid gained enough inertia to form an independent droplet without satellites. The droplet formation continued evenly with time after the fourth cycle for the two later cases.

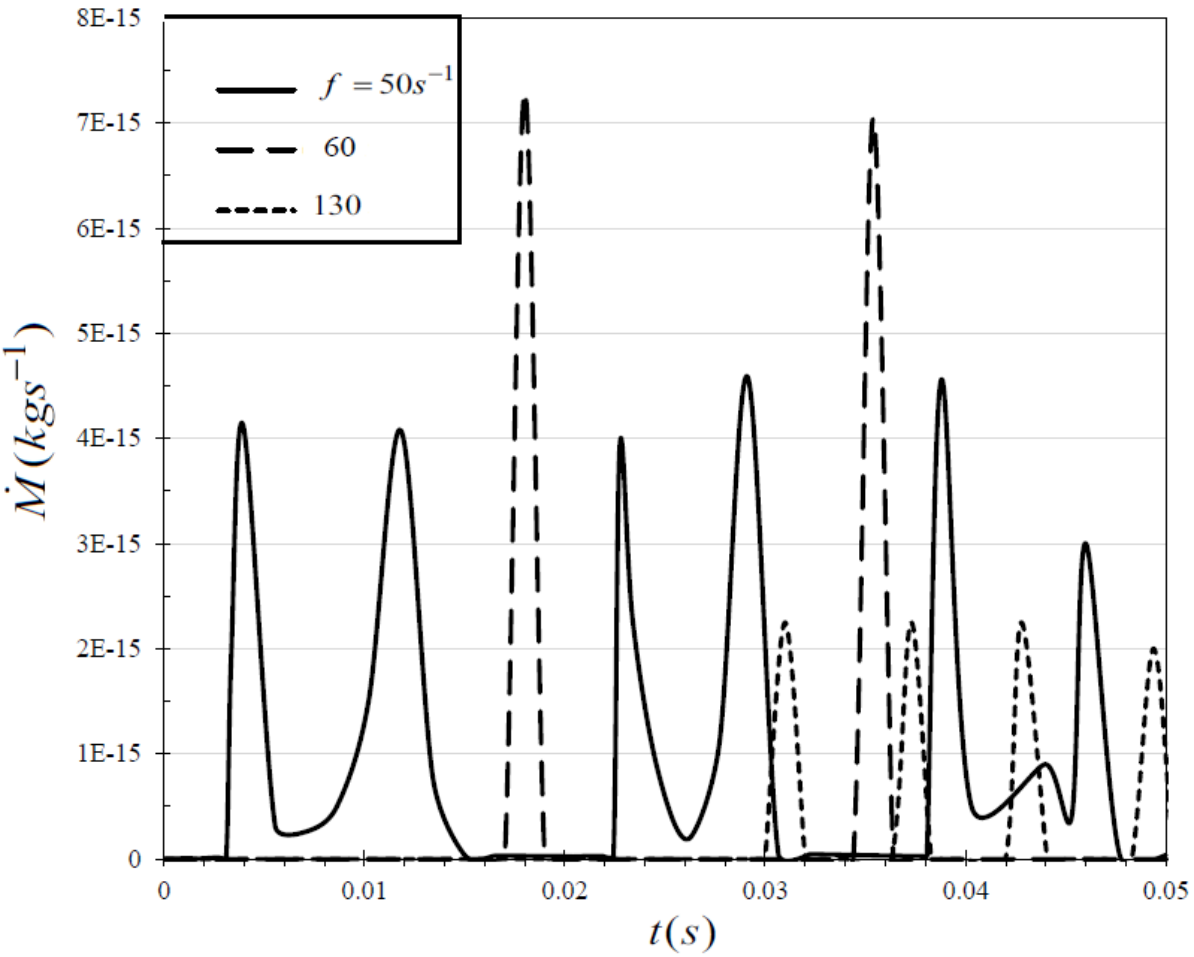

Figure 30. Repeatability of mass flow rates when *We*=140.4 and at different ejection frequencies.

Droplet ejection was simulated over wide ranges of *We* and Ω numbers to assess whether it would be possible to define regimes in which independent droplets were or were not produced. As a consequence, six general regimes were identified, as depicted in Figure 31 and discussed below; Figure 32 displays the broad array of conditions simulated.

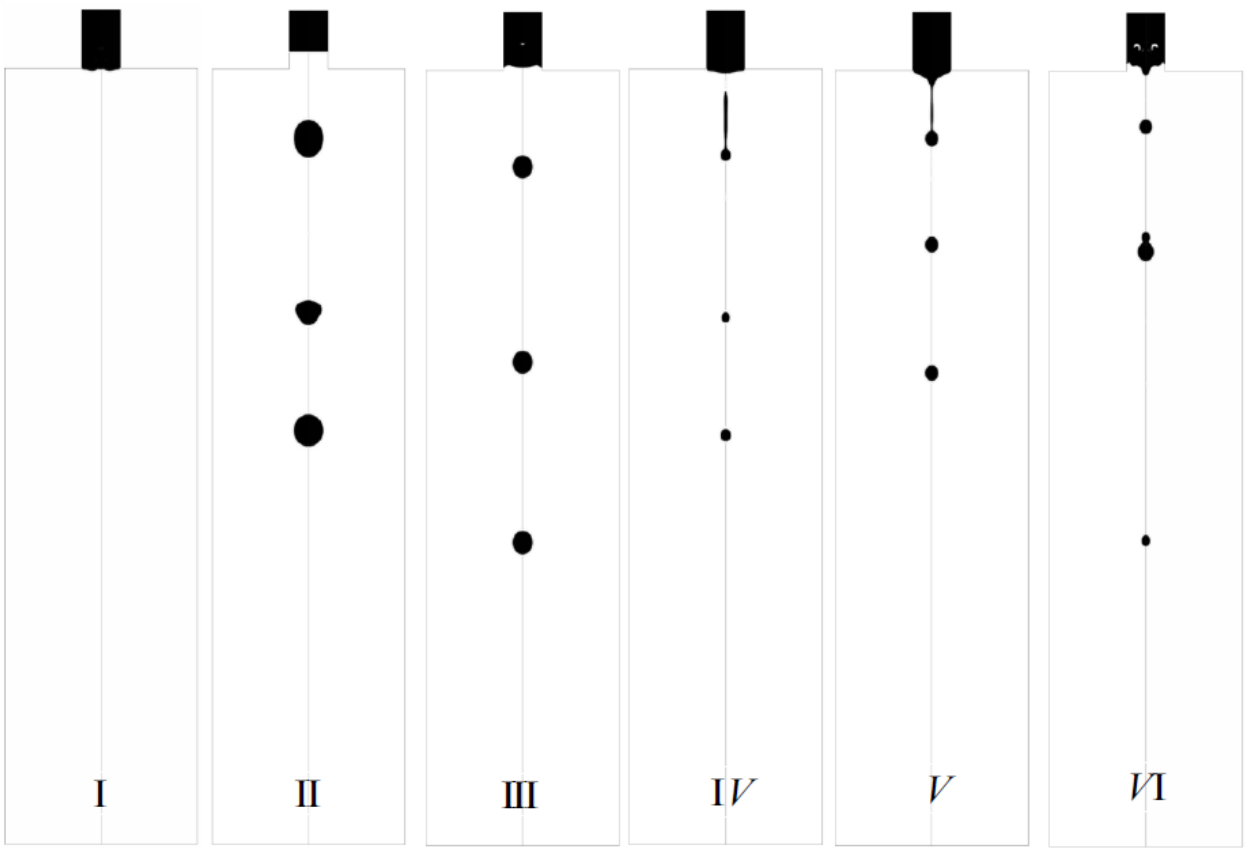

Figure 31. Observed regimes of droplet formation under different jetting conditions.

- **Regime I**

At small *We* or high Ω number, inertial forces were not large enough to push liquid out of the nozzle. In other words, in this regime the viscous forces dominated capillary forces and the liquid failed to eject from the nozzle because the more dominant viscous force dissipated the inertial force that was required to eject the fluid from the nozzle. Duineveld et al (2002) and Xu and Basaran (2007) also reported that droplet formation would not occur when *We* was low or the frequency was high.

- **Regime II**

In this regime, droplets about the size of the nozzle are formed along with satellite droplets, and primarily occurred when the frequency was low relative to *We*. This regime is depicted by triangles in Figure 32.

- **Regime III**

This regime gave independent droplets that were approximately one-half the diameter of nozzle and satellites were eliminated if appropriate *We* and Ω values were employed. As seen in Figure 32, this regime almost can be represented by a linear relationship between the *We* and Ω values.

- **Regime IV**

During the first one-to-three cycles in this regime, no droplet formation occurred. This is because of the changes in meniscus height after each cycle. As also pointed out by (Tran et al., 2009), the initial meniscus shape is a determinant factor in injection process. After the first cycle (s), protruded meniscus (rather than the flat one observed in lower frequencies) is more likely to produce a filament out of the nozzle. Besides, in this regime, satellite droplets were always formed after the initial cycle(s).

- **Regime V**

Independent and very small droplets without satellites were formed in the regime; these droplets were smaller than those produced in Regime III. The droplet sizes were changed by increasing the frequency such that the each thin filament would coalesce into tiny independent droplets.

- **Regime VI**

In regime VI, satellite droplets were formed although the sizes of the primary droplets were always smaller than the nozzle diameter. It was interesting to note that when *We* was greater than 190, no border between regimes IV and VI was evident.

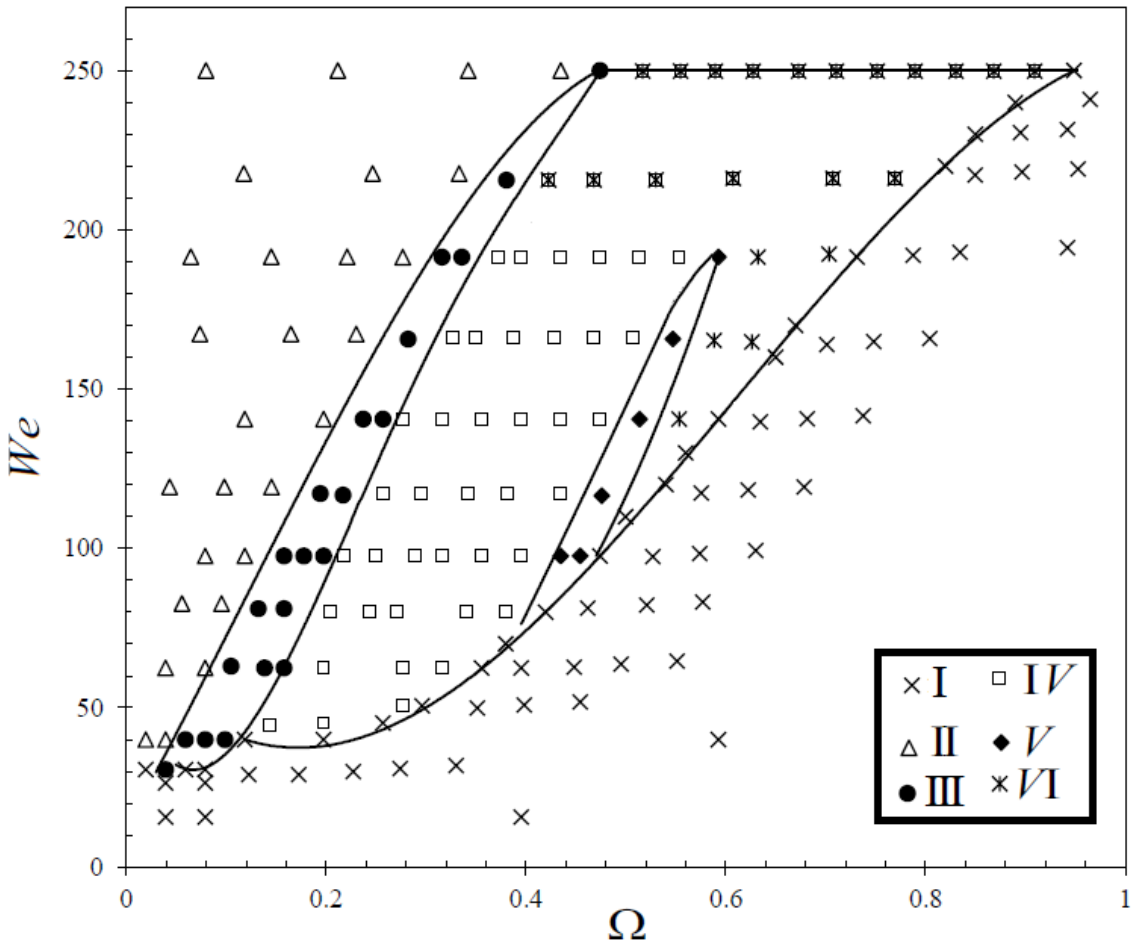

Figure 32. Regimes map based on two non-dimensional parameters, *We* and Ω.

Thus, the data in Figures 31 and 32 demonstrate that the most favorable regimes for independent droplet formation with no satellites were III and V, and could be mapped by plotting the non-dimensional *We* and Ω numbers. Besides having independent droplets with no satellites, it is also important to examine how size of the droplets could be

controlled. This assessment was accomplished by examining Eq. (3-13) which shows that the instantaneous flow rate at the inflow boundary is dependent on $(v_m D^2\pi/8)sin(ft)$. Integrating this dependency over time gives the volume of the liquid that would pass the inlet boundary as $v_m D^2\pi/(8f)\ (1-cos(ft))$; in other words, the maximum volume of liquid that can be expelled from the nozzle will vary with v_m/f. Thus, if the *We* numbers are the same in both regimes III and V, regime V would give smaller droplets (Figure 33).

Figure 33 shows Ω plotted as a function of *We* for regime III and V; it also displays the non-dimensional droplet sizes, defined as the ratio of the nozzle diameter divided by the droplet radii, *D/2R*, plotted as a function of *We* for regimes III and V. In regime III, values of *We* between ~20-60 produced a steep reduction in droplet sizes as the value of *We* was increased whereas any further increase in *We* did not affect droplet sizes. In contrast, within regime V the droplet sizes decreased with increasing *We* values between ~100-200. Importantly, the minimum droplet size within regime III was found to be about 40% of the nozzle diameter, whereas in regime V the minimum droplet size was about 18 % of the nozzle diameter.

Favorable operational conditions with their corresponding injecting performance are shown in Figures 34 and 35 for regimes III and V, respectively. Worthwhile to note that the ranges of *We* and Ω values are checked to be feasible for actual inkjet print-heads (Castrejón-Pita et al., 2008).

Potential benefits of this new method, and the obtained optimized operational conditions could be ensued for very delicate and precise applications with ultra-narrow nozzles that are susceptible to clogging or increased hydraulic resistance. With this method, without

changing the nozzle geometry, one could lower droplet size up to 5 times smaller than the regular droplet size generated from regular input waveforms.

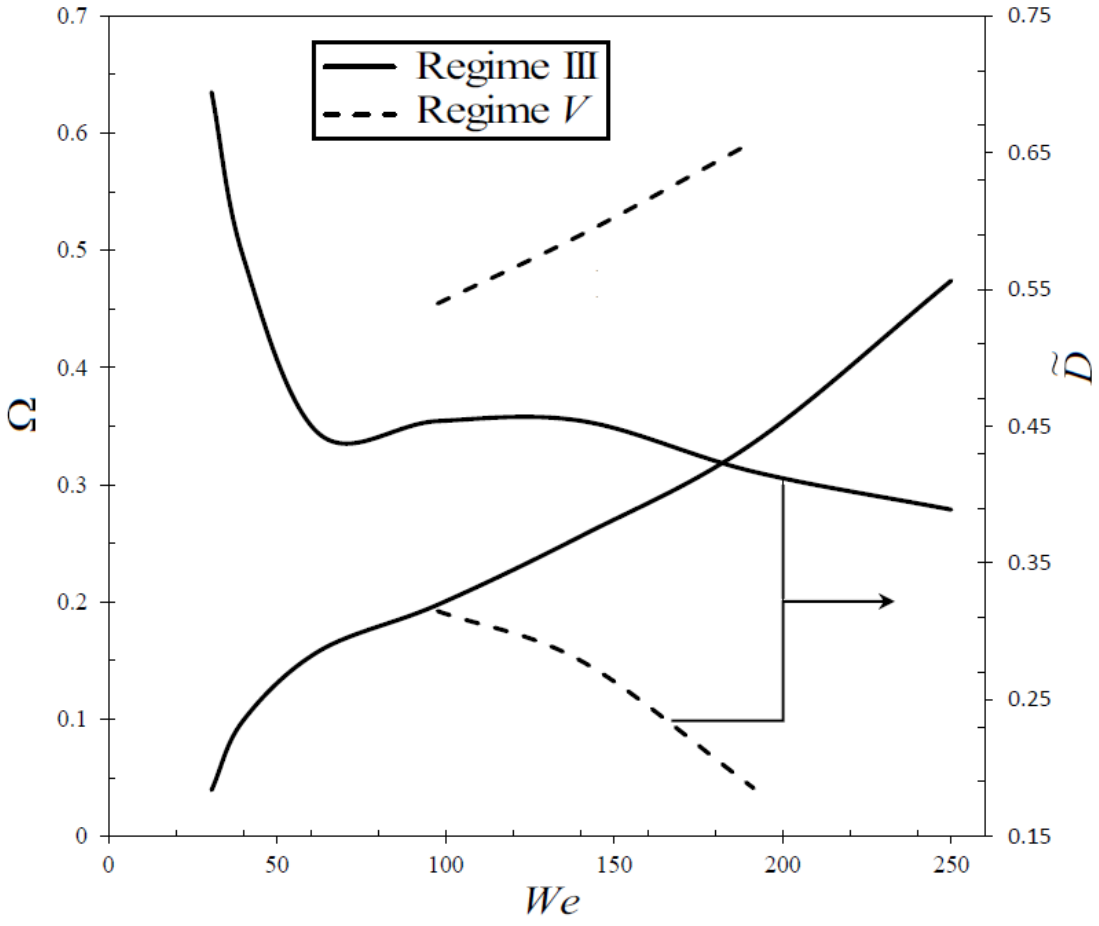

Figure 33. Non-dimensional droplet size, $\tilde{D}$ and frequency Ω as functions of We for regime III and V.

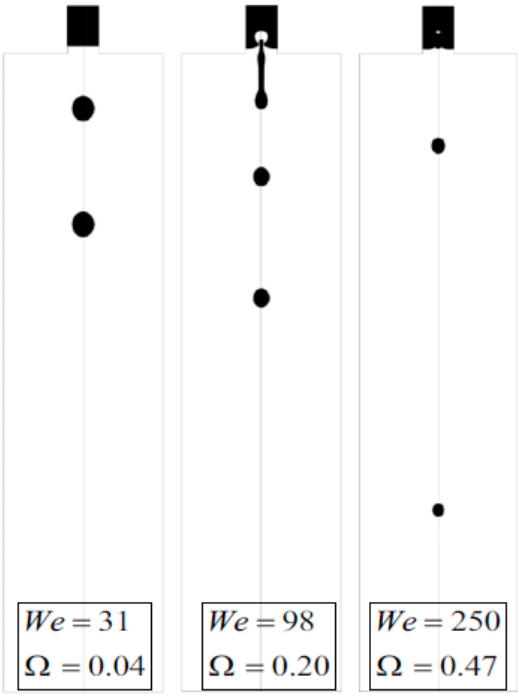

Figure 34. Favorable operational conditions for regime III.

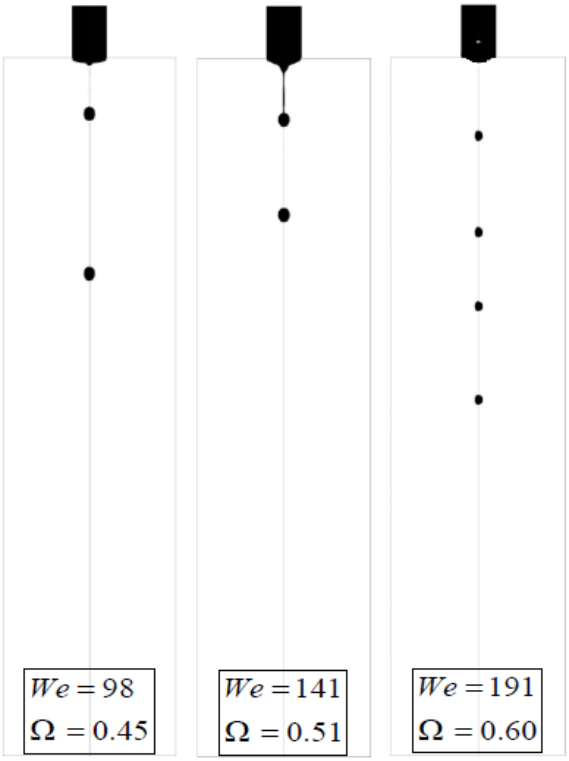

Figure 35. Favorable operational conditions for regime V.

4.4 Results for coating applicator

This section is devoted to study a novel application of the inkjet printing technology in coating industry. As a reminder, current spray technology is suffering from low TE and non-uniform deposition. Inkjet technology as a digital fabrication technology, under the right conditions, can lend to producing a chain of drops with uniform size and uniform successive spacing. Hereby, this technology can mitigate both low TE by depositing all of the ejected droplets on the target and deposition non-uniformity by providing droplets with uniform properties.

In the first stage, a prototype based on inkjet printing technology with coating capabilities is designed as a CAD 3D model. The assembly of the proposed sprayer is depicted in Figure 36. In this figure, the left hand side model shows the standard view of the model package and the right hand side shows the front view depicting the interfaces of various components.

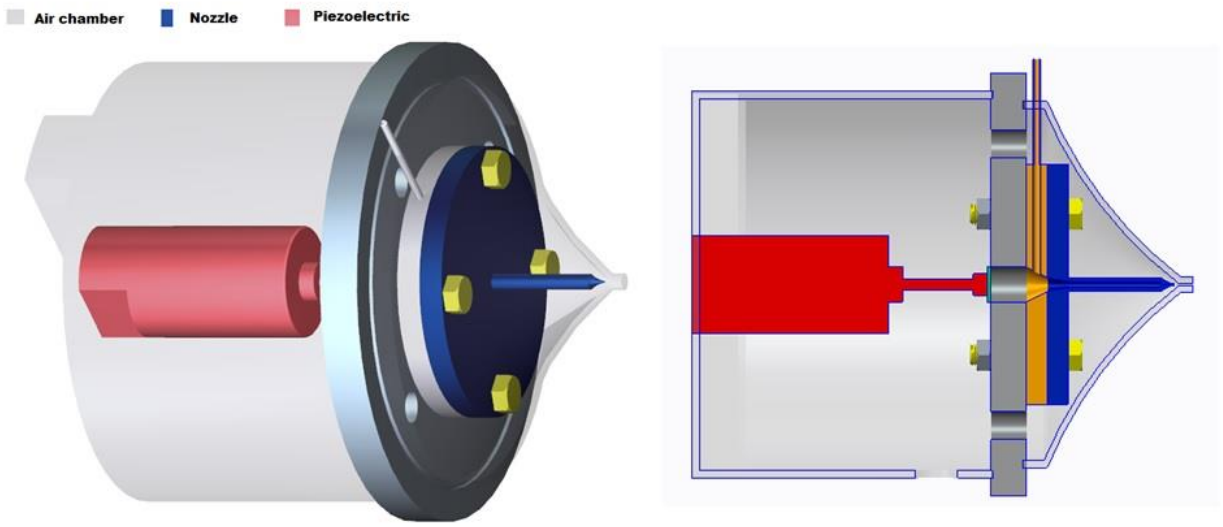

Figure 36. 3D CAD model designed in PTC Creo software.

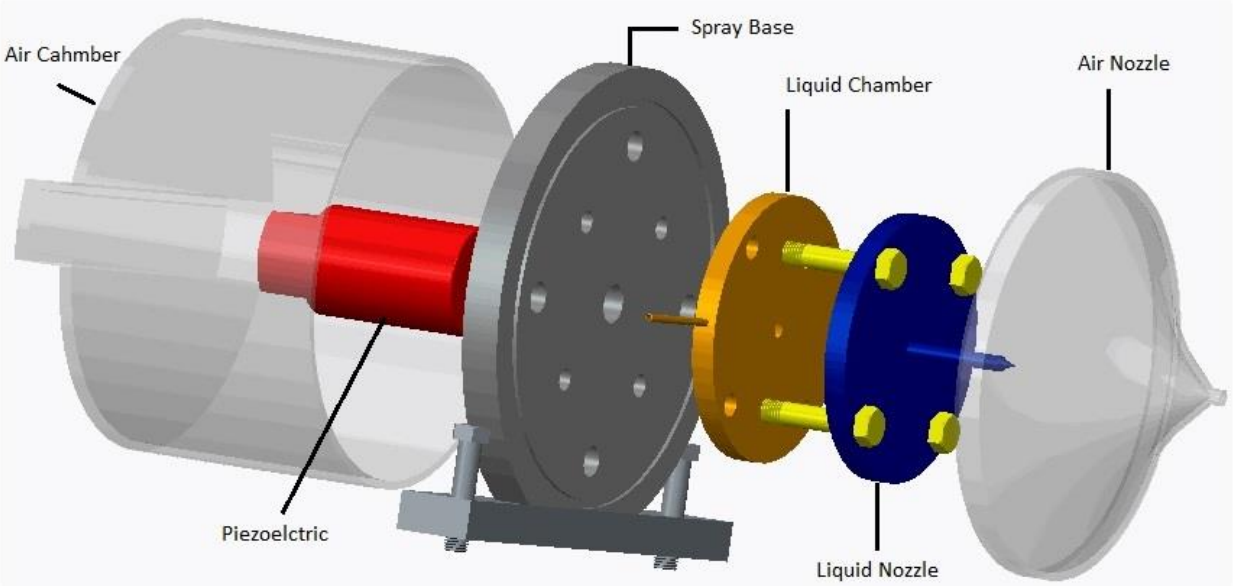

Figure 37. 3D designed CAD model with the components.

The designed sprayer consists of an air chamber which surrounds a piezoelectric transducer and a spray base which connects all the parts to create a compact sprayer. The liquid chamber directs the liquid through the liquid nozzle; the air is supplied from an air chamber after crossing through the spray base holes and then flows into the air nozzle and co-flow with the droplets released form the liquid nozzle. Figure 37 shows the main components of the new sprayer.

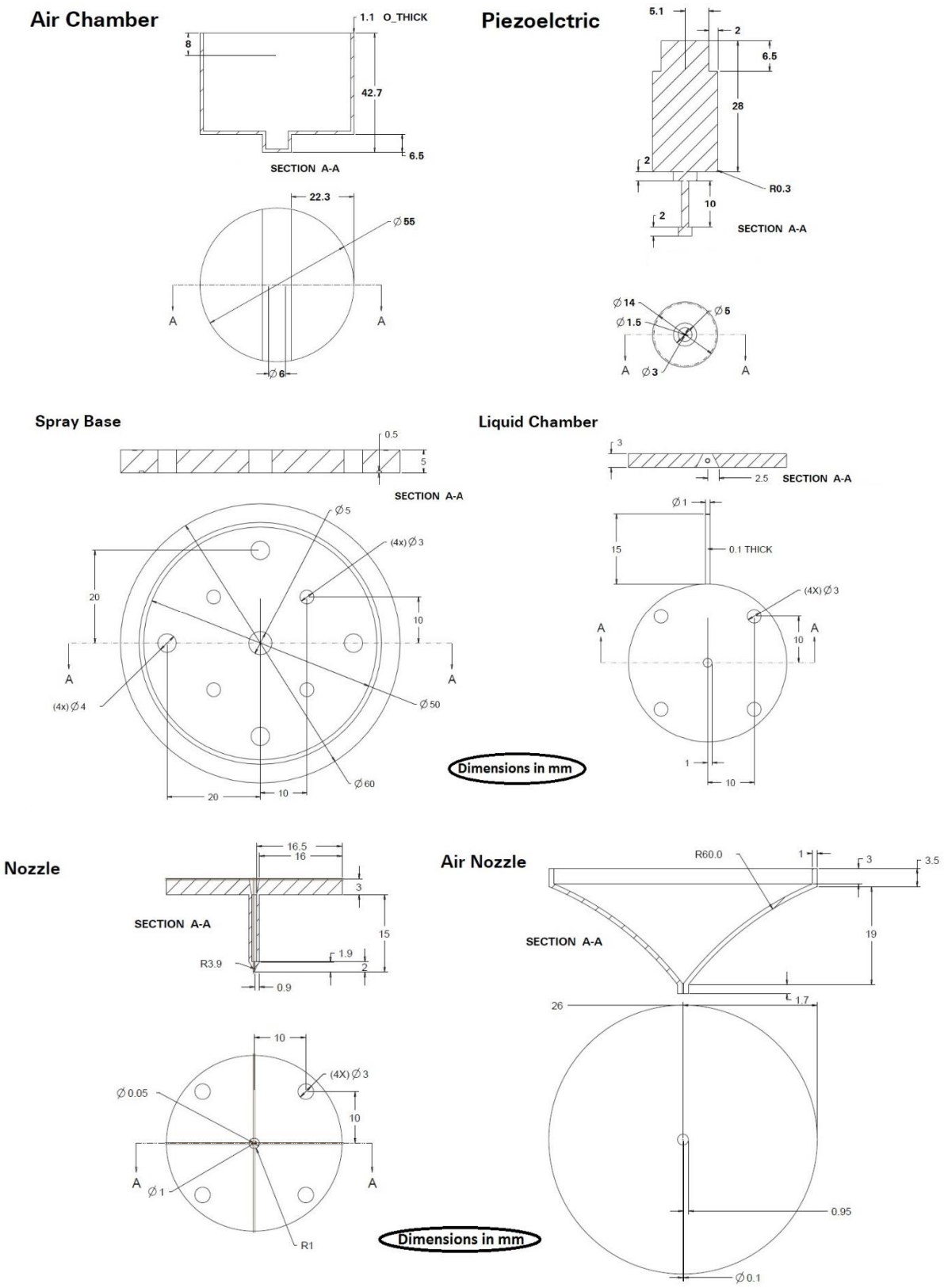

Figure 38. Components' Dimensions of the 3D designed CAD model.

Figure 38 depicts the dimensions of the sprayer components. It is worthy to note that the chosen piezoelectric transducer for the current application is PA8 with a M3 thread end and a maximum frequency of 40 kHz with a corresponding head motion up to 8 microns; also, the blocking force is 850 *N*. This type of piezoelectric transducer is used mainly in microinjection applications. As Figure 39 shows, the liquid nozzle diameter was chosen to be 0.1 *mm*.

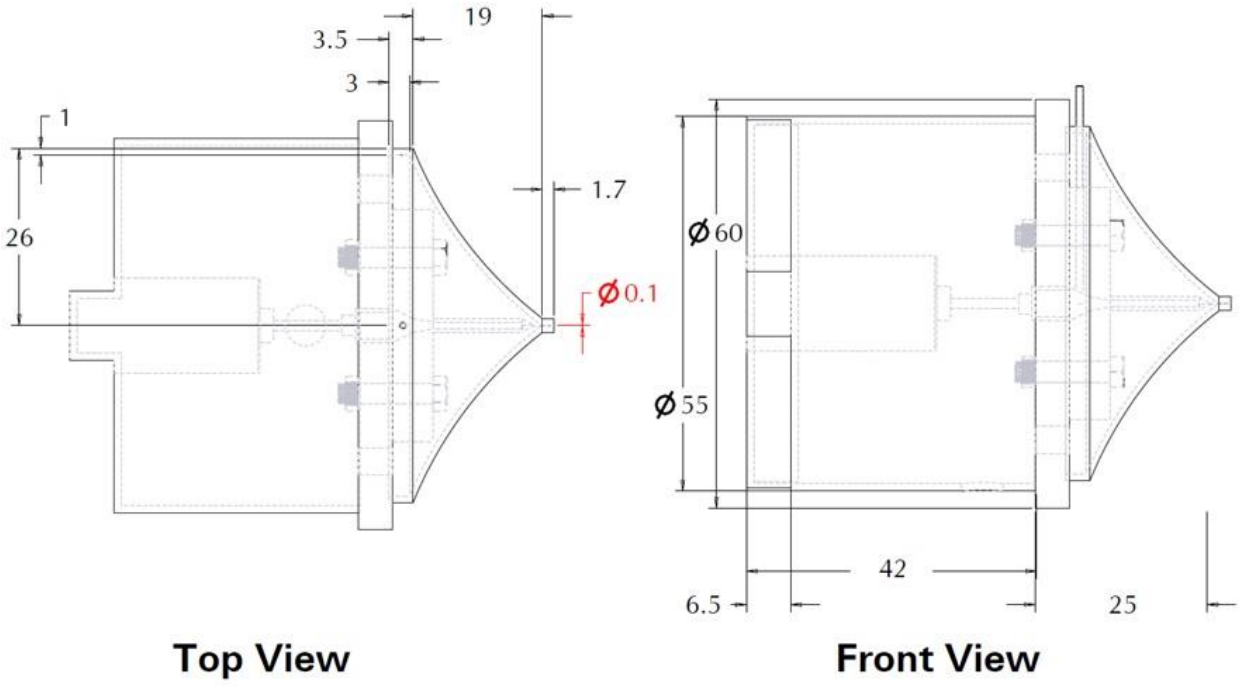

Figure 39. Dimensions of the 3D designed CAD assembly model.

A numerical simulation based on CFD was employed to test the prototype sprayer's atomization performance. Figure 40 illustrates the section of the prototype that is to be simulated; it represents the area from the membrane (marked with green) to the end of the sprayer where the droplets are released into the atmosphere. Figure 40 also shows the model with its boundary labels incorporated for the numerical simulation. A moving wall

was used as the model of the piezoelectric head, which has a reciprocal motion with controllable displacement and frequency. The liquid is supplied through liquid inlet, and then it is pushed through the liquid nozzle exit where it is co-flowed with the air. Finally, the ejected droplets will be pushed to the outlet atmosphere.

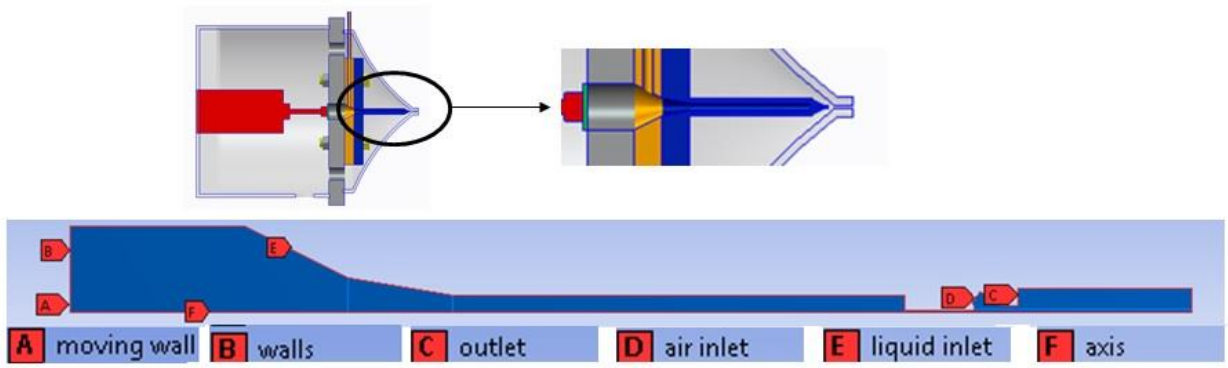

Figure 40. Simulated section in prototype (up) and the corresponding employed model for numerical simulation purpose with the boundary labels.

The motion of the piezoelectric was simulated using a dynamic mesh model to move the boundaries of a cell zone relative to other boundaries of the zone, and to adjust the mesh accordingly. In this model, the nodes that define the cells in the domain are updated as a function of time, and hence the dynamic mesh solutions are inherently unsteady. With respect to dynamic meshes, the integral form of the conservation equation describing the fluid motion for a general scalar, ϕ, on an arbitrary control volume, V, whose boundary is moving can be written as:

$$\frac{d}{dt}\int_V \rho\phi dV + \int_{\partial V} \rho\phi(\vec{u}-\vec{u}_g).d\vec{A} = \int_{\partial V} \Gamma\nabla\phi.d\vec{A} + \int_V S_\phi dV \qquad (4\text{-}1)$$

where $\vec{u}$ is the fluid velocity vector, $\vec{u}_g$ is the mesh velocity of the moving grid, Γ is the diffusion coefficient and S_ϕ is the source term of ϕ. Equation (4-1) is the generic transport equation and applies to all applicable model equations, including those of continuity and momentum. In order to simulate a periodic motion impressed by the piezoelectric transducer, a user-defined function is implemented to characterize $\vec{u}_g$.

After modelling the problem and meshing it, a suitable solution method (discussed before) was employed to solve the fluid flow within the simulated sprayer domain. The controlling parameters were air flow pressure and piezoelectric characteristics of head displacement and frequency. It is important to note that in currently used paint sprayers, air atomizes the ejected liquid, whereas in the current application air is used only to carry the droplets to a target. Thus, a suitable air pressure which can direct droplets in a straight line without breaking them must be chosen and employed.

Figure 41 shows the air volume fraction of the sprayer for different air pressures in which the red color represents the air phase and blue color represents the liquid phase; colors between these extremes represents interfaces. The simulation is carried out for water as the ejected liquid, and a piezoelectric displacement and frequency of $0.17\,\mu m$ and 12 *kHz*, respectively. Because the droplets were most uniform in size without satellite droplets when the air pressure was 0.5 *Psi*, it was used for the rest of the study. It was the maximum pressure that wouldn't break the droplets. Hence, in the remainder of this part of the investigation, the controlling variables of displacement and frequency for the piezoelectric transducer were studied.

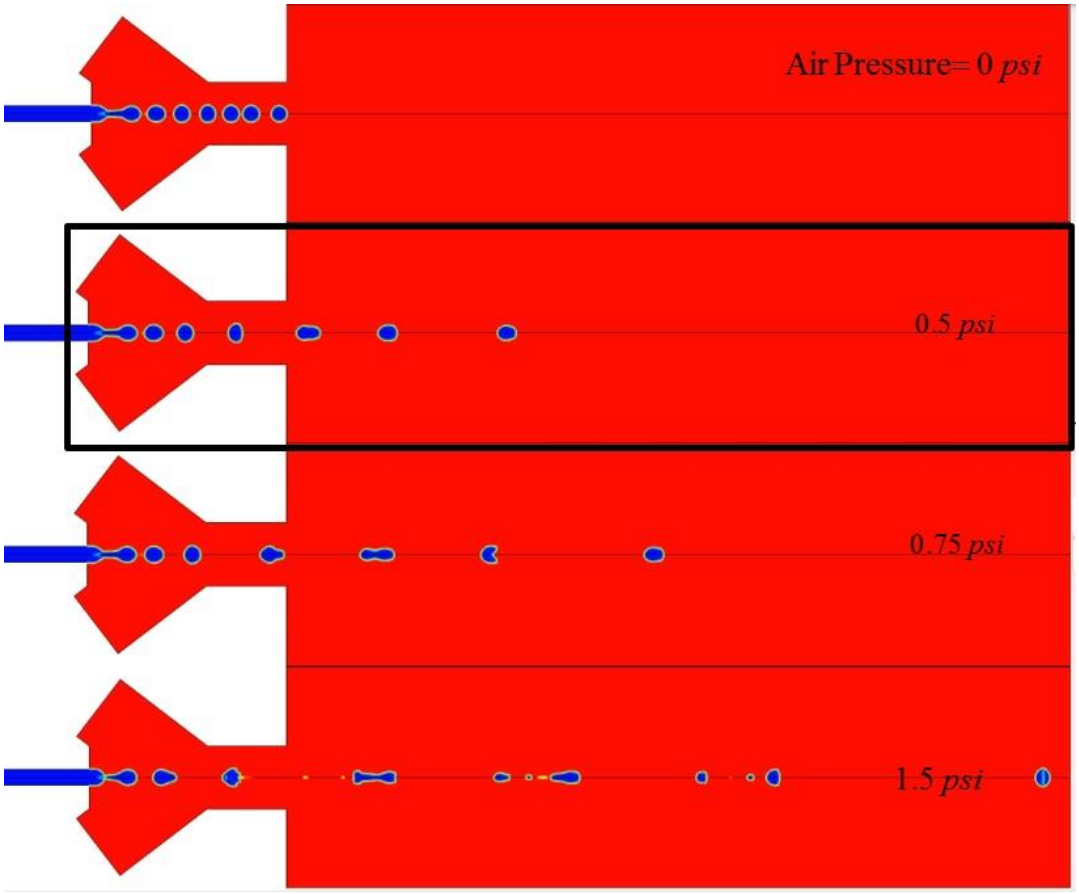

Figure 41. Finding suitable air pressure.

Figures 42-44 show the air volume fraction for different piezoelectric displacements, *d*, and for several values of the piezoelectric frequencies, *f*. When $d = 0.15\,\mu m$ and low frequencies such as below 12 *kHz*, no droplets were ejected because the energy transferred from the piezoelectric plate was not enough to push the droplets through the nozzle. In contrast, as is shown in the figures, filaments of liquid were ejected from the nozzle when the frequency was increased. However, coalescence of the ejected droplets very near the liquid nozzle was occurring as the frequency was increased, a condition which is unfavorable for producing uniform droplets; it retards the droplets flow and creates non-uniform chains of droplets with varying sizes and inter-droplet spacing.

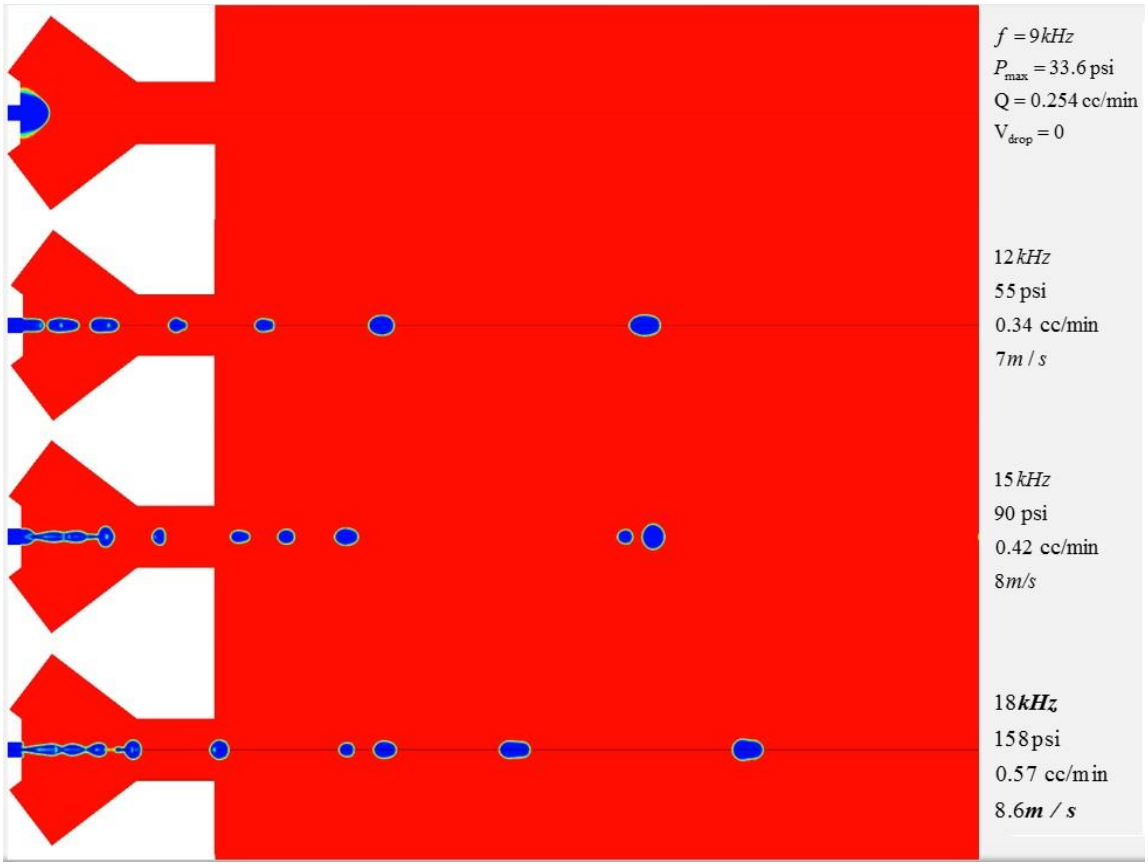

Figure 42. Effects of piezo frequency on atomization performance for piezo displacement, $d = 0.15\,\mu m$.

As shown in Figure 43, ejection of uniform droplets and inter-droplet spacings occurred whenthe piezoelectric head displacement was greater than 0.15 µm and when the head frequency was at specific values. Furthermore, Figure 44 shows that droplet mean velocities increased while the spacing between the droplets decreased as the head frequency was increased, a situation which agrees with intuition; at the increased head frequencies, droplet ejection was also more erratic and the droplets were more susceptible to coalescence.

Hence, numerical simulation was capable of showing the proposed sprayer could produce mono-dispersed droplets with controllable size and spacing, as is needed for its application in coatings. The influence of two independent piezoelectric characteristics, i.e. maximum head displacement and frequency, on droplet breakup could be investigated intensively, and favorable displacements and frequencies could be identified.

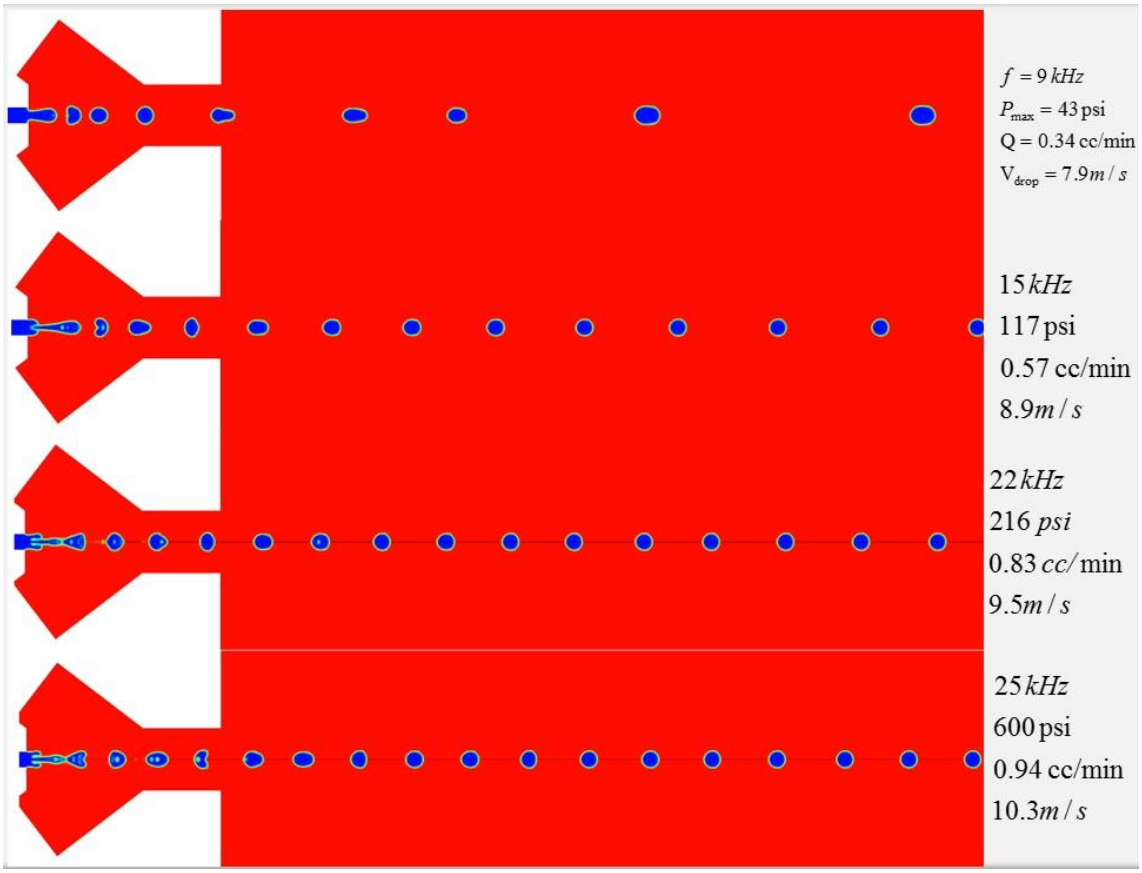

Figure 43. Effects of piezo frequency on atomization performance for piezo displacement, $d = 0.20\,\mu m$.

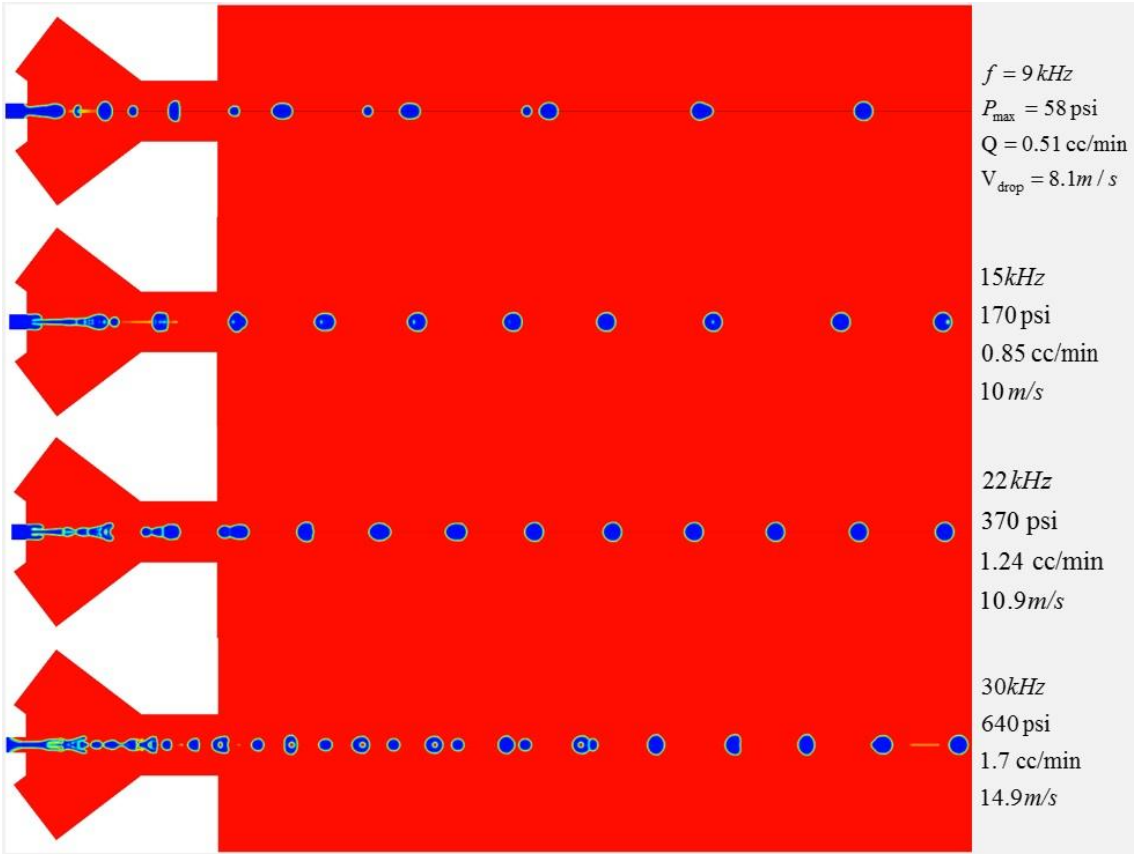

Figure 44. Effects of piezo frequency on atomization performance for piezo displacement, $d = 0.30\,\mu m$

- Effects of viscosity

Figure 45 shows that changing the viscosity of the liquid affected droplet ejection and sizes when $d = 0.30\,\mu m$ and *f*=12 kH at t=0.001 s; as the liquid viscosity was increased to 50 times that of water, droplet break up did not occur In contrast, Figure 46 displays results when t was increased to t = 0.02 s; here, when the liquid viscosities were 20-50 times greater than that of water, droplet breakup would occur but at relatively large distances or breakup lengths from the nozzle.

To assess whether droplets could be formed and then retain their sizes for the 5 cm distances required in coating applications, numerical simulations were performed using liquid characteristics that would be identical to the paint viscosity model described in equation (3-14). Figure 47 displays some results from these simulations, and illustrates the contours of air volume fraction, pressure and velocity under favorable operational conditions. Although the droplet spacing was not perfectly homogenous, the data depict that favorable operational conditions existed in which the droplets maintained their trajectory and spacing very well even after traveling 5 cm in distance.

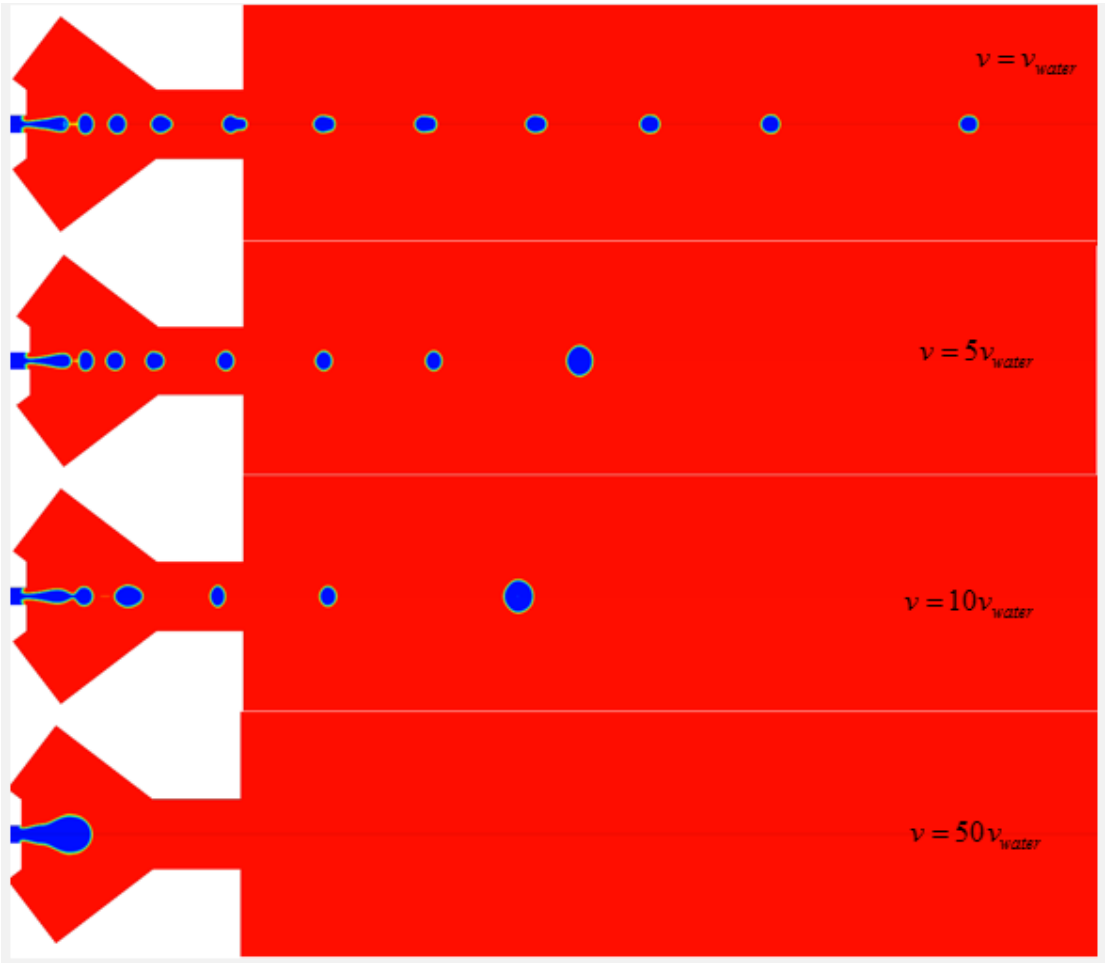

Figure 45. Effect of viscosity on the jetting performance for $d = 0.30\ \mu m$ and f=12 kH at t=0.001 s.

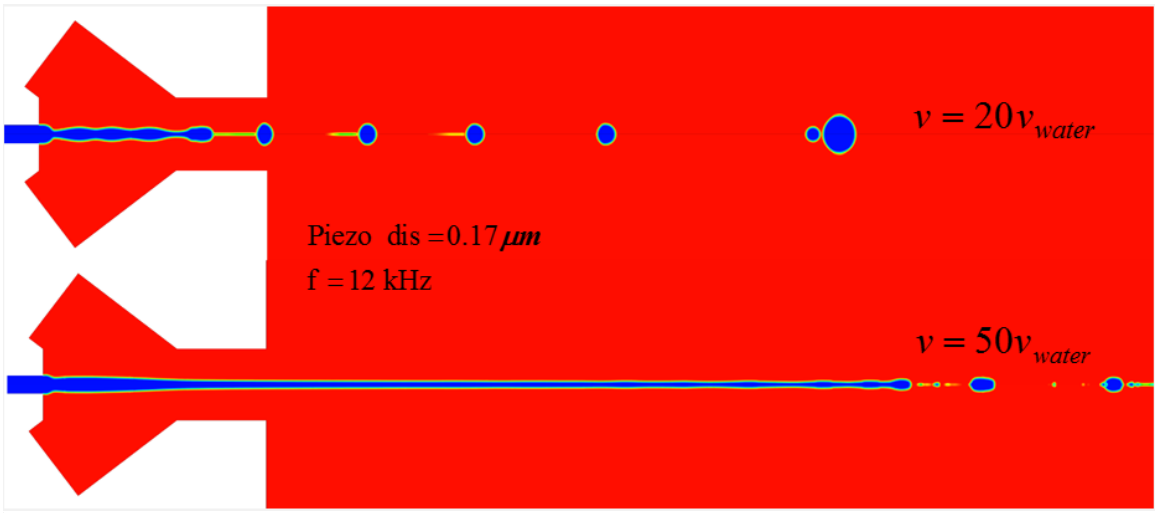

Figure 46. Effect of viscosity on the jetting performance for $d = 0.30\ \mu m$ and f=12 kH at t=0.01 s.

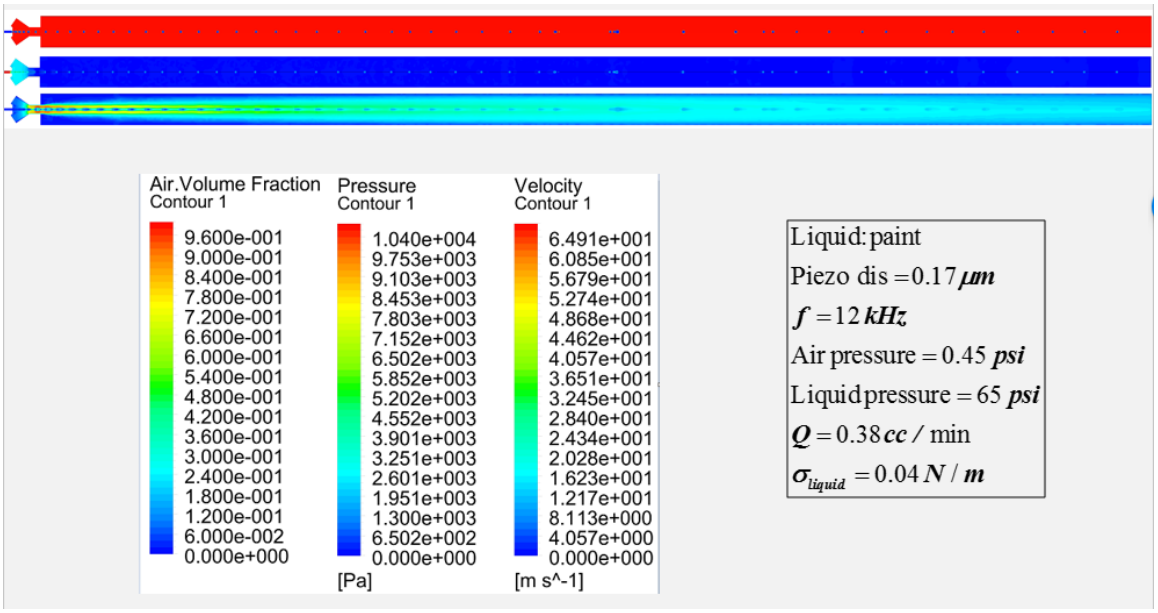

Figure 47. Air volume fraction, pressure and velocity contours for paint model in favorable operational conditions.

4.5 Summary of Numerical Results

This section summarizes the numerical results for solutions to the most important inkjet issues, including satellite formation and droplet size; it also summarizes the results of numerically testing the new prototype sprayer that was based on inkjet technology.

- ✓ For the formation of satellites, a volume of fluid (VOF) numerical study was presented in which new pi number-based criteria were discussed that identified two different operational regimes for a DOD print-head system. Liquid filament break-up behavior was predicted using a combination of the two pi-numbers, We - Ohs or Re- We. These were determined to be dependent only on the ejected liquid properties and the velocity waveform at the print-head inlet.
- ✓ For droplet sizes, a new approach to reduce droplet sizes without changing nozzle sizes was introduced and tested numerically, and anin-depth evaluation of relevant parameters that included *We* and Ω numbers were accomplished. For a given liquid, six distinct flow regimes were determined to affect droplet sizes. The use of specific regimes were shown to enable the specification of operational conditions that controlled and minimized droplet sizes to less than 20% of the nozzle orifice diameter with up to 150 times smaller droplet volumes from nozzle orifices.
- ✓ A new sprayer prototype based on inkjet printing principles was introduced and tested numerically. The ultimate objective was to develop the knowledge for establishing a digital coating method that could drastically reduce overspray, conserve paint material, minimize environmental impact and coat hard to reach areas in a uniform manner. Spray injection performance was numerically tested under different operational conditions and optimal conditions were identified.

CHAPTER 5

5 CONCLUSIONS AND FUTURE RECOMMENDATIONS

5.1 Conclusions

5.1.1 On satellite droplet formation

The present study was dedicated to find a boundary line between single and multiple breakup regimes of liquid filaments ejected from a inkjet printer head.. A numerical simulation based on the volume-of-fluid (VOF) model was employed to investigate droplet formation dynamics from a DOD print-head prototype. Grid independency and comparisons with literature results were accomplished to provide a firm, quantitative and qualitative, justification, of the numerical simulations. Filament behavior and the transition between the two single and multiple breakup regimes were determined using only two non-dimensional parameters that reflected the competition between driving and retarding forces by using either a combination of Oh and We numbers or We and Re numbers.

5.1.2 On generating small drops

For DOD inkjet technology, the capacity to reduce inkjet droplet sizes without changing the size of the nozzle orifice would beneficially impact coating, processing and maintenance attributes. This study applied numerical simulations based on computational fluid dynamics and an in-depth assessment of relevant parameters associated with producing liquid droplets to examine droplet size dependencies, and then compared the outcomes with published data. For a given liquid, six distinct flow regimes were determined to affect droplet sizes, the critical characterization of which could be effectively assessed by using two non-dimensional parameters, including the Weber number, *We*, and

a newly-defined, non-dimensional temporal frequency number, Ω. The use of specific regimes were shown to enable specification of operational conditions that could control and minimize droplet sizes to less than 20% of the nozzle orifice diameter; under these conditions, up to 150 times smaller droplet volumes would emanate from nozzle orifices. As a consequence, this new method is proposed to potentially useful for lowering droplet sizes while maintaining desired droplet quality for deposition on and coating of surfaces.

5.1.3 Coating applicator

A comprehensive review was given of current issues that need to be solved in automotive painting and the influential parameters of importance for each issue. The deposition transfer efficiency, or TE, and finish quality were identified as common factors that have been the primary focus of paint sprayer research. An alternative spray technology based on inkjet printing was developed and tested numerically to prove its potential for generating mono-dispersed droplet sizes. The influences of parameters, including liquid properties, piezoelectric frequency and head displacement, on jetting performance were investigated. A prototype sprayer was numerically modelled for jetting water-borne paint along a 5*cm* path into free atmosphere.

5.1.4 Contribution of this dissertation

This study focused on numerical simulations while carefully considering liquid properties and the actuation driving waveforms. As a consequence of this research, a new path to lowering droplet sizes from prescribed inkjet nozzles was discovered. The potential benefits of this new approach lie in using the optimized operational conditions for applications demanding ultra-small droplets from of fixed-size orifices; without changing the nozzle geometry, it would be possible to decrease droplet sizes by up to 5 times smaller

than those generated from regular input waveforms. Finally in this study a digital coating approach was developed to drastically reduce overspray and conserve paint material, to minimize environmental impact, to coat hard to reach areas uniformly and to enhance the painting experience.

5.2 Future work

During the current study on satellite formation, the input waveform was fixed. Additional studies should be accomplished with an emphasis on changing the input waveforms and then simulating the effects of these changes. The influences of liquid properties were examined but the large variety of available paint types with widely different properties could not be inclusively included; hence, a wider variety of liquid properties should be examined. Also important was the effect of the *Oh* number on droplet sizes and the regime map; According to the literature (Chen et al., 2002), increasing the *Oh* number while maintaining other parameters fixed, would elongate the ejected filaments from an orifice which could lead to smaller droplets; this possibility should be investigated. Finally, for confirmation of the simulation results, it is always of importance to design, build and actually test prototypes; it is also necessary that the parameters measured during these experimental tests are done so in the most capable and quantitative manner.

References

Ahmed, M. & Youssef, M. S. 2014. Influence of spinning cup and disk atomizer configurations on droplet size and velocity characteristics. *CHEMICAL ENGINEERING SCIENCE,* 107**,** 149-157.

Alloo, R. P., Saito, K. & Salazar, A. J. 2005. Control system for controlling the scrubbing of particles from an airflow. Google Patents.

Ambravaneswaran, B., Wilkes, E. D. & Basaran, O. A. 2002. Drop formation from a capillary tube: Comparison of one-dimensional and two-dimensional analyses and occurrence of satellite drops. *Physics of Fluids (1994-present),* 14**,** 2606-2621.

Andrade, R. D., Skurtys, O. & Osorio, F. A. 2012. Atomizing Spray Systems for Application of Edible Coatings. *Comprehensive Reviews in Food Science and Food Safety,* 11**,** 323-337.

Basaran, O. A. 2002. Small-scale free surface flows with breakup: Drop formation and emerging applications. *AIChE Journal,* 48**,** 1842-1848.

Bell Jr, G. C. a. J. H. Mechanics of Electrostatic Atomization Transport and Deposition of Coatings. Proc. 7th International Conference in Organic Science and Technology, 1981 Athens, Greece.

Bernardini, G. L., Rampy, B. A., Howell, G. A., Hayes, D. J. & Frederickson, C. J. 1991. Applications of piezoelectric fluid jetting devices to neuroscience research. *Journal of neuroscience methods,* 38**,** 81-88.

Bienduga, T. J. 1995. Apparatus for electrostatic spray painting. Google Patents.

Brennan, T. M. 1999. Method and apparatus for conducting an array of chemical reactions on a support surface. Google Patents.

Brenner, M. P., Eggers, J., Joseph, K., Nagel, S. R. & Shi, X. 1997. Breakdown of scaling in droplet fission at high Reynolds number. *Physics of Fluids (1994-present),* 9**,** 1573-1590.

Brosseau, L. M., Fang, C., Snyder, C. & Cohen, B. 1992. Particle size distribution of automobile paint sprays. *Applied Occupational and Environmental Hygiene,* 7**,** 607-612.

Burr, R. F., Tence, D. A., Le, H. P., Adams, R. L. & Mutton, J. C. 1996. Method and apparatus for producing dot size modulated ink jet printing. Google Patents.

Castrejón-Pita, A. A., Castrejón-Pita, J. R. & Hutchings, I. M. 2012a. Breakup of Liquid Filaments. *Physical Review Letters,* 108**,** 074506.

Castrejón-Pita, A. A., Castrejón-Pita, J. R. & Martin, G. D. 2012b. A novel method to produce small droplets from large nozzles. *Review of Scientific Instruments,* 83**,** 115105.

Castrejón-Pita, J., Martin, G., Hoath, S. & Hutchings, I. 2008. A simple large-scale droplet generator for studies of inkjet printing. *Review of Scientific Instruments,* 79**,** 075108.

Castrejón-Pita, J. R., Morrison, N. F., Harlen, O. G., Martin, G. D. & Hutchings, I. M. 2011. Experiments and Lagrangian simulations on the formation of droplets in drop-on-demand mode. *Physical Review E,* 83**,** 036306.

Chen, A. U. & Basaran, O. A. 2002. A new method for significantly reducing drop radius without reducing nozzle radius in drop-on-demand drop production. *Physics of Fluids (1994-present),* 14**,** L1-L4.

Chen, A. U., Notz, P. K. & Basaran, O. A. 2002. Computational and experimental analysis of pinch-off and scaling. *Physical review letters,* 88**,** 174501.

Chuang, M. Y. 2009. Medicine injection into skin with heater chip. Google Patents.

Corbeels, P., Senser, D. W. & Lefebvre, A. H. 1992. Atomization characteristics of a highspeed rotary-bell paint applicator. *Atomization and Sprays,* 2.

Corber, P. A. 2010. *The performance of a pressure atomizer with a flow obstruction upstream of the nozzle.* Library and Archives Canada = Bibliothèque et Archives Canada.

Darroch, J. B. 1997. The HVLP revolution: The basics of buying HVLP spray equipment. *FDM,* 69**,** 100-106.

De Laplace, P. S. 1806. *Sur l'action capillaire*.
Delhaye, J. M., Coutris, N., Herran, L., Congress, A. I. M. E. & Exposition, I. 2013. Drop-on-demand: A scale analysis. *ASME Int Mech Eng Congress Expos Proc ASME International Mechanical Engineering Congress and Exposition, Proceedings (IMECE),* 8 C.
Demeter, J. 1970. Electrostatic spray gun. Google Patents.
Dombrowski, N. & Lloyd, T. L. 1972. The spread of liquid on a rotating vane. *CES</cja:jid> Chemical Engineering Science,* 27**,** 1003-1012.
Domnick, J. Effect of bell geometry in high-speed rotary bell atomization. 23rd Annual Conference on Liquid Atomization and Spray Systems, 2010. 69.
Domnick, J., Scheibe, A. & Ye, Q. 2005. The Simulation of the Electrostatic Spray Painting Process with High-Speed Rotary Bell Atomizers. Part I: Direct Charging. *PARTICLE AND PARTICLE SYSTEMS CHARACTERIZATION,* 22**,** 141-150.
Dong, H., Carr, W. W. & Morris, J. F. 2006. An experimental study of drop-on-demand drop formation. *Physics of Fluids (1994-present),* 18**,** 072102.
Duineveld, P. C., De Kok, M. M., Buechel, M., Sempel, A., Mutsaers, K. A., Van De Weijer, P., Camps, I. G., Van De Biggelaar, T., Rubingh, J.-E. J. & Haskal, E. I. Ink-jet printing of polymer light-emitting devices. International Symposium on Optical Science and Technology, 2002. International Society for Optics and Photonics, 59-67.
Edgerton, H., Hauser, E. & Tucker, W. 1937. Studies in drop formation as revealed by the high-speed motion camera. *Journal of Physical Chemistry,* 41**,** 1017-1028.
Eggers, J. & Dupont, T. F. 1994. Drop formation in a one-dimensional approximation of the Navier–Stokes equation. *Journal of fluid mechanics,* 262**,** 205-221.
Ellwood, K. R. J. & Braslaw, J. 1998. A finite-element model for an electrostatic bell sprayer. *ELSTAT</cja:jid> Journal of Electrostatics,* 45**,** 1-23.
Emori, R., Saito, K. & Sekimoto, K. 2008. Scale Models in Engineering (Mokei Jikken no Riron to Ohyou), (ISBN 4-7655-3252-6 C3053). *Tokyo, Japan: Gihodo. Second print in*.
Fettis, G. 1995. *Automotive paints and coatings,* Weinheim; New York, VCH.
Flynn, M. 2000. On the use of computational fluid dynamics in the prediction and control of exposure to airborne contaminantsan illustration using spray painting. *The Annals of Occupational Hygiene,* 44**,** 191-202.
Flynn, M. R. & Sills, E. D. 2001. Numerical Simulation of Human Exposure to Aerosols Generated During Compressed Air Spray-Painting in Cross-Flow Ventilated Booths. *J. Fluids Eng. Journal of Fluids Engineering,* 123**,** 64.
Fogliati, M., Fontana, D., Garbero, M., Vanni, M., Baldi, G. & Donde, R. 2006. CFD simulation of paint deposition in an air spray process. *JCT research,* 3**,** 117-125.
Fromm, J. 1981. *A numerical study of drop-on-demand ink jets,* Yorktown Heights, NY [u.a.], IBM Corp.
Frost, A. 1981. Rotary atomization in the ligament formation mode. *Journal of Agricultural Engineering Research Journal of Agricultural Engineering Research,* 26**,** 63-78.
Fuchikami, N., Ishioka, S. & Kiyono, K. 1999. Simulation of a dripping faucet. *Journal of the Physical Society of Japan,* 68**,** 1185-1196.
Fukuta, K. & Et Al. 1993. New Rotary Bell for Metallic Paint Application. *METAL FINISHING - NEW JERSEY-,* 91**,** 39.
Gan, H., Shan, X., Eriksson, T., Lok, B. & Lam, Y. 2009. Reduction of droplet volume by controlling actuating waveforms in inkjet printing for micro-pattern formation. *Journal of micromechanics and microengineering,* 19**,** 055010.
Greer Jr, L. R. & Tryon, J. A. 2001. Airless system for spraying coating material. Google Patents.
Gueyffier, D., Li, J., Nadim, A., Scardovelli, R. & Zaleski, S. 1999. Volume-of-fluid interface tracking with smoothed surface stress methods for three-dimensional flows. *Journal of Computational Physics,* 152**,** 423-456.

Haruch, J. 2001. Air atomizing nozzle assembly with improved air cap. Google Patents.
Hauser, E., Edgerton, H., Holt, B. & Cox Jr, J. 1936. The Application of the High-speed Motion Picture Camera to Research on the Surface Tension of Liquids. *The Journal of Physical Chemistry,* 40**,** 973-988.
Hayati, I., Bailey, A. I. & Tadros, T. F. 1987. Investigations into the mechanisms of electrohydrodynamic spraying of liquids:I. Effect of electric field and the environment on pendant drops and factors affecting the formation of stable jets and atomization. *YJCIS</cja:jid> Journal of Colloid And Interface Science,* 117**,** 205-221.
Henderson, D. M., Pritchard, W. G. & Smolka, L. B. 1997. On the pinch-off of a pendant drop of viscous fluid. *Physics of Fluids (1994-present),* 9**,** 3188-3200.
Hicks, P. 1995. *Drop Transport in Air Sprays.* Ph. D. thesis, Purdue University, W. Lafayette, IN.
Hicks, P. G. & Senser, D. W. 1995. Simulation of Paint Transfer in an Air Spray Process. *J. Fluids Eng. Journal of Fluids Engineering,* 117**,** 713.
Hines, R. L. 1966. Electrostatic Atomization and Spray Painting. *J. Appl. Phys. Journal of Applied Physics,* 37**,** 2730.
Hoath, S. D., Jung, S. & Hutchings, I. M. 2013. A simple criterion for filament break-up in drop-on-demand inkjet printing. *Physics of Fluids (1994-present),* 25**,** 021701.
Hon, S. F., Kwok, K. W., Li, H. L. & Ng, H. Y. 2010. Self-focused acoustic ejectors for viscous liquids. *Review of Scientific Instruments,* 81**,** 065102.
Im, K.-S. 1999. *An experimental and numerical study of the spray transfer processes in an electrostaic rotating bell sprayer.* Ph. D, Wayne State University.
Im, K.-S., Lai, M.-C., Liu, Y., Sankagiri, N., Loch, T. & Nivi, H. 2001. Visualization and Measurement of Automotive Electrostatic Rotary-Bell Paint Spray Transfer Processes. *J. Fluids Eng. Journal of Fluids Engineering,* 123**,** 237.
Im, K.-S., Lai, M.-C., Yu, S.-T. J. & Matheson, R. R. 2004. Simulation of Spray Transfer Processes in Electrostatic Rotary Bell Sprayer. *J. Fluids Eng. Journal of Fluids Engineering,* 126**,** 449.
Inkpen, S. L. & Melcher, J. R. 1987. Dominant mechanisms for color differences in the mechanical and the electrostatic spraying of metallic paints. *Ind. Eng. Chem. Res. Industrial & Engineering Chemistry Research,* 26**,** 1645-1653.
Jaworek, A. 2007. Micro- and nanoparticle production by electrospraying. *Powder Technology,* 176**,** 18-35.
Jaworek, A. & Krupa, A. 1999. Jet and drops formation in electrohydrodynamic spraying of liquids. A systematic approach. *Experiments in fluids.,* 27**,** 43.
Kawase, Y. & De, A. 1982. Ligament-type disintegration of non-Newtonian fluid in spinning disk atomization. *Journal of Non-Newtonian Fluid Mechanics Journal of Non-Newtonian Fluid Mechanics,* 10**,** 367-371.
Kelly, A. 1994. On the statistical, quantum and practical mechanics of electrostatic atomization. *Journal of Aerosol Science,* 25**,** 1159-1177.
Kim, E. & Baek, J. 2012. Numerical study on the effects of non-dimensional parameters on drop-on-demand droplet formation dynamics and printability range in the up-scaled model. *Physics of Fluids (1994-present),* 24**,** 082103.
Kim, K. & Marshall, W. 1971. Drop‐size distributions from pneumatic atomizers. *AIChE Journal,* 17**,** 575-584.
Kimura, J., Kawana, Y. & Kuriyama, T. 1989. An immobilized enzyme membrane fabrication method using an ink jet nozzle. *Biosensors,* 4**,** 41-52.
Kumar, R. & Lakshmi Prasod, K. S. 1971. Studies on Pneumatic Atomization. *Ind. Eng. Chem. Proc. Des. Dev. Industrial & Engineering Chemistry Process Design and Development,* 10**,** 357-365.
Kwok, K.-C. 1991. *A fundamental study of air spray painting.* PhD, University of Minnesota.

Laurell, T., Wallman, L. & Nilsson, J. 1999. Design and development of a silicon microfabricated flow-through dispenser for on-line picolitre sample handling. *Journal of Micromechanics and Microengineering,* 9**,** 369.
Lee, I., Kim, D. & Koo, J. 2012. Liquid jet breakup structure and transfer efficiency of a two-stage air-blast injector. *Atomiz. Sprays Atomization and Sprays,* 22**,** 561-579.
Lefebvre, A. H. 1989. *Atomization and sprays,* New York, Taylor & Francis.
Liu, J. X., Yu, Q. B. & Qin, Q. 2013. Numerical study on film disintegration by centrifugal atomisation using rotating cup. *Powder Metallurgy Powder Metallurgy,* 56**,** 288-294.
Lloyd, W. J. & Taub, H. H. Ink jet printing. Output hardcopy devices, 1988. Academic Press Professional, Inc., 311-370.
Mansour, N. N. & Lundgren, T. S. 1990. Satellite formation in capillary jet breakup. *Physics of Fluids A: Fluid Dynamics (1989-1993),* 2**,** 1141-1144.
Mark, A., Andersson, B., Tafuri, S., Engstrom, K., Edelvik, F., Carlson, J. S. & Sorod, H. 2013. Simulation of electrostatic rotary bell spray painting in automotive paint shops. *Atomiz. Sprays Atomization and Sprays,* 23**,** 25-45.
Marshall, W. R. 1954. *Atomization and spray drying,* [New York, American Institute of Chemical Engineers.
Martinez, L. A. 2011. *Automotive Rotary-Bell Spray Painting Modelling and Simulation.* Master, University of Gothenburg.
Masters, K. 1979. *Spray drying handbook,* London; New York, G. Godwin ; Halsted Press.
Morikita, H. & Taylor, A. M. 1998. Application of shadow Doppler velocimetry to paint spray: potential and limitations in sizing optically inhomogeneous droplets. *Measurement Science and Technology,* 9**,** 221.
Movahednejad, E., Ommi, F. & Hosseinalipour, S. M. 2010. Prediction of droplet size and velocity distribution in droplet formation region of liquid spray. *Entropy Entropy,* 12**,** 1484-1498.
Notz, P. K. & Basaran, O. A. 2004. Dynamics and breakup of a contracting liquid filament. *Journal of Fluid Mechanics,* 512**,** 223-256.
Notz, P. K., Chen, A. U. & Basaran, O. A. 2001. Satellite drops: Unexpected dynamics and change of scaling during pinch-off. *Physics of Fluids (1994-present),* 13**,** 549-552.
Nukiyama, S. & Tanasawa, Y. 1939. An experiment on atomisation of liquid the effect of the properties of liquid on the size of drops. *Transactions of the Society of Mechanical Engineers (JSME Journal),* 18**,** 8.
Nukiyama, S. & Tanasawa, Y. 1940. An experiment on atomisation of liquid the atomisation pattern of liquid by means of air stream. *Transactions of the Society of Mechanical Engineers (JSME Journal),* 22**,** 9.
Okuda, H. & Kelly, A. J. 1996. Electrostatic atomization—Experiment, theory and industrial applications. *Physics of Plasmas (1994-present),* 3**,** 2191-2196.
Perçin, G., Atalar, A., Degertekin, F. L. & Khuri-Yakub, B. T. 1998. Micromachined two-dimensional array piezoelectrically actuated transducers. *Applied physics letters,* 72**,** 1397-1399.
Peregrine, D., Shoker, G. & Symon, A. 1990. The bifurcation of liquid bridges. *Journal of Fluid Mechanics,* 212**,** 25-39.
Plateau, M. 1856. XXXVII. On the recent theories of the constitution of jets of liquid issuing from circular orifices. *The London, Edinburgh, and Dublin Philosophical Magazine and Journal of Science,* 12**,** 286-297.
Plesniak, M., Sojka, P. & Singh, A. 2004. Transfer efficiency for airless painting systems. *Journal of Coatings Technology and Research,* 1**,** 137-145.
Poozesh, S., Akafuah, N. & Saito, K. 2015a. NO formation analysis of turbulent non-premixed coaxial methane/air diffusion flame. *International Journal of Environmental Science and Technology***,** 1-6.

Poozesh, S., Akafuah, N. & Saito, K. 2015b. Numerical Simulation of a Coating Sprayer Capable of Producing Controllable Paint Droplets. *SAE Technical Paper*.
Rizkalla, A. & Lefebvre, A. 1975. The influence of air and liquid properties on airblast atomization. *Journal of Fluids Engineering,* 97**,** 316-320.
Roger, P. M. A. 1962. Rotating heads for electrostatic atomizing and spraying apparatus. Google Patents.
Rune, E. 1951. Measuring instrument of the recording type. Google Patents.
Sakai, S. Dynamics of piezoelectric inkjet printing systems. NIP & Digital Fabrication Conference, 2000. Society for Imaging Science and Technology, 15-20.
Salazar, A. J. & Saito, K. 2008. Novel automative spray painting systems: Computational fluid dynamics study of ultrasonic ligament atomizer. *IAES Final Report, project sponsored by Toyaota Motor Corporation*
Savart, F. 1833. Mémoire sur la constitution des veines liquides lancées par des orifices circulaires en mince paroi. *Ann. Chim. Phys,* 53**,** 1833.
Schick, R. 2006. Spray technology reference guide: Understanding drop size, Spray analysis and research services. Spray Drying Systems Co.
Schmidt, P. & Walzel, P. 1984. Zerstäuben von Flüssigkeiten. *PIUZ Physik in unserer Zeit,* 15**,** 113-120.
Schonhorn, H. 1967. Surface Tension-Viscosity Relationship for Liquids. *J. Chem. Eng. Data Journal of Chemical & Engineering Data,* 12**,** 524-525.
Schulkes, R. 1994. The evolution and bifurcation of a pendant drop. *Journal of Fluid Mechanics,* 278**,** 83-100.
Schulkes, R. M. S. M. 1996. The contraction of liquid filaments. *Journal of Fluid Mechanics,* 309**,** 277-300.
Settles, G. S. A flow visualization study of airless spray painting. ILASS-Americas 10th Annual Conference on Liquid Atomization and Spray Systems, 1997. 18-21.
Shi, X., Brenner, M. P. & Nagel, S. R. 1994. A cascade of structure in a drop falling from a faucet. *SCIENCE-NEW YORK THEN WASHINGTON-***,** 219-219.
Shilton, M. G., Miles, P., Robinson, G. W. & Robinson, J. V. 2002. Spray gun with common control of fluid and air valve. Google Patents.
Shim, Y. S., Choi, G. M. & Kim, D. J. 2008. Numerical modeling of hollow-cone fuel atomization, vaporization and wall impingement processes under high ambient temperatures. *International Journal of Automotive Technology,* 9**,** 267-275.
Straubel, H. 1954. The electrostatic atomization of liquids. *Z. Angew. Physik,* 6**,** 264.
Strutt, J. W. & Rayleigh, L. 1878. On the instability of jets. *Proc. London Math. Soc,* 10**,** 4-13.
Sziele, D., Brüggemann, O., Döring, M., Freitag, R. & Schügerl, K. 1994. Adaptation of a microdrop injector to sampling in capillary electrophoresis. *Journal of Chromatography A,* 669**,** 254-258.
Teng, H., Kinoshita, C. M. & Masutani, S. M. 1995. Prediction of droplet size from the breakup of cylindrical liquid jets. *International Journal of Multiphase Flow,* 21**,** 129-136.
Tilney, R. 1953. Electrostatic coating processes. *British Journal of Applied Physics,* 4**,** S51-S54.
Toda, K. 2013. What Is Spray Coating? . *In:* Toda, K., Salazar, A. J. & Saito, K. (eds.) *Automotive painting technology: a Monozukuri-Hitozukuri perspective*. Dordrecht; New York: Springer Science + Business Media.
Tran, S. B. Q., Byun, D., Nguyen, V. D. & Kang, T. S. 2009. Liquid meniscus oscillation and drop ejection by ac voltage, pulsed dc voltage, and superimposing dc to ac voltages. *Physical Review E,* 80**,** 026318.
Trostle, J. 2012. Best Application Technology. *JCT Coatings Tech,* 9**,** 68-75.
Walzel, P. 1990. Zerstäuben von Flüssigkeiten. *CITE Chemie Ingenieur Technik,* 62**,** 983-994.
Weber, C. 1931. Zum zerfall eines flüssigkeitsstrahles. *ZAMM ‐ Journal of Applied Mathematics and Mechanics/Zeitschrift für Angewandte Mathematik und Mechanik,* 11**,** 136-154.

Wijshoff, H. 2010. The dynamics of the piezo inkjet printhead operation. *Physics Reports,* 491**,** 77-177.
Wilkes, E. D., Phillips, S. D. & Basaran, O. A. 1999. Computational and experimental analysis of dynamics of drop formation. *Physics of Fluids (1994-present),* 11**,** 3577-3598.
Xing, L.-L., Edward Glass, J. & Fernando, R. 1999. Parameters influencing the spray behavior of waterborne coatings. *Journal of Coatings Technology,* 71**,** 37-50.
Xu, Q. & Basaran, O. A. 2007. Computational analysis of drop-on-demand drop formation. *Physics of Fluids (1994-present),* 19**,** 102111.
Yang, F., Zhou, S., Zhang, C. & Wang, G. 2013. Mixing of initially stratified miscible fluids in an eccentric stirred tank: Detached eddy simulation and volume of fluid study. *Korean Journal of Chemical Engineering,* 30**,** 1843-1854.
Ye, Q., Domnick, J. & Khalifa, E. 2002. Simulation of the spray coating process using a pneumatic atomizer. *Zaragoza,* 9**,** 11.
Ye, Q., Shen, B., Tiedje, O. & Domnick, J. 2013. Investigations of Spray Painting Processes Using an Airless Spray Gun. *Journal of Energy and Power Engineering,* 7**,** 74.
Young, T. 1805. An essay on the cohesion of fluids. *Philosophical Transactions of the Royal Society of London***,** 65-87.
Yousefifard, M., Ghadimi, P. & Nowruzi, H. 2015. Numerical investigation of the effects of chamber backpressure on HFO spray characteristics. *International Journal of Automotive Technology,* 16**,** 339-349.
Zhang, D. & Stone, H. 1997. Drop formation in viscous flows at a vertical capillary tube. *Physics of Fluids (1994-present),* 9**,** 2234-2242.
Zhang, X. 1999. Dynamics of growth and breakup of viscous pendant drops into air. *Journal of colloid and interface science,* 212**,** 107-122.
Zhang, X. & Basaran, O. A. 1995. An experimental study of dynamics of drop formation. *Physics of Fluids (1994-present),* 7**,** 1184-1203.

Vita

Sadegh Poozesh

Born in Kohkilouye province, Iran

Education:

September 2006-September 2010 Isfahan University of Technology, Isfahan, Iran.

B.S. Mechanical Engineering

September 2010-June 2012 Amirkabir University of Technology, Tehran, Iran.

M.S. Mechanical Engineering/Fluid mechanics

Publications

Journals:

Poozesh, S. *, Akafuah, N., & Saito, K. (2015). Numerical Simulation of a Coating Sprayer Capable of Producing Controllable Paint Droplets (No. 2015-01-0737). SAE Technical Paper.

Poozesh, S. *, N. Akafuah, and K. Saito. "NO formation analysis of turbulent non- premixed coaxial methane/air diffusion flame." International Journal of Environmental Science and Technology (2015): 1-6.

Poozesh, S. *, N. Akafuah, and K. Saito. "New Criteria for Filament Breakup in Droplet- on-Demand Inkjet Printing Using Volume of Fluid (VOF) Method" The Korean journal of chemical engineering" Accepted.

Sadegh Poozesh*, Nelson Akafuah and Kozo Saito, "Review on the Effects of Spray Coating Technology on Transfer Efficiency and Finished Painted Surface Quality", International journal of automotive engineering, submitted.

Sadegh Poozesh*, Nelson Akafuah and Kozo Saito, "Comprehensive Examination of a New Mechanism to Produce Small Droplets in Droplet-On-Demand Inkjet Technology", Applied Physics A, under review.

Presentations/Proceedings:

Sadegh Poozesh*, Tianxiang Li, Kozo Saito; "Numerical Study on Quasi-Steady-State Spherical Carbon Particle Gasification With and Without Thermal Radiation". The 9th U. S. National Combustion institute Meeting. Cincinnati, OH. May 2015.